HEAT TRANSFER FROM A SPHERE TO LIQUID SODIUM DURING FORCED CONVECTION

By

LARRY CLAUDE WITTE

Bachelor of Science
Arlington State College
Arlington, Texas
1963

Master of Science
Oklahoma State University
Stillwater, Oklahoma
1965

Submitted to the Faculty of the Graduate College
of the Oklahoma State University
in partial fulfillment of the requirements
for the degree of
DOCTOR OF PHILOSOPHY
May, 1967

HEAT TRANSFER FROM A SPHERE TO LIQUID SODIUM

DURING FORCED CONVECTION

Thesis Approved:

Donald R. Haworth
Thesis Adviser

Louis Boxer, Jr.

Ladislaus J. Fila

John Blackshear

Lee Hasnsberger

A. N. Durham
Dean of the Graduate College

ACKNOWLEDGEMENTS

The author wishes to express his gratitude to all who have given him assistance and encouragement during the course of this investigation.

My sincere appreciation goes to Dr. D. R. Haworth who served most capably as thesis advisor. Prof. L. J. Fila and Dr. J. B. West provided many helpful suggestions regarding the interpretation of the data obtained in this study.

The author expresses his gratitude to the staff of the Chemical Engineering Division of the Argonne National Laboratory for their assistance in the thesis work. In particular I am indebted to Dr. L. Baker, Jr. for his direction of the thesis project. My appreciation is expressed to M. B. Silverman and J. Pavlik who provided technical assistance in the experimental portion of the study. To H. Edfeldt and R. Flegel the author expresses gratitude for the fabrication of much of the experimental equipment.

To the Associated Midwest Universities goes my appreciation for financial assistance during thesis work.

Finally, I thank my wife, LaVerne, for her patience and understanding during these years of graduate study.

TABLE OF CONTENTS

LIST OF TABLES

LIST OF FIGURES

CHAPTER I

INTRODUCTION

Nuclear power reactor technology has progressed to the point where large reactors can be operated near metropolitan areas. An important part of the development of reactor technology has been the development of knowledge related to the consequences of severe accidents, both hypothetical and actual accidents. The design of each reactor is accompanied by extensive analyses of many minor and some major accidents. The detailed analyses of major accidents makes it possible to show that the probability of experiencing such an accident is extremely low and moreover, that the consequences of such an occurrence would not constitute an undue public safety hazard. In effect, an accident analysis is meaningful only if the course of the hypothetical accidents and the individual accident steps have a sound scientific basis.

A destructive power excursion is one of the hypothetical accidents which must be considered in the safety analysis of a power reactor. This is particularly true for the case of liquid-metal-cooled, fast reactors where, because of very short neutron lifetimes, there is little or no time for external control mechanisms to terminate an excursion. One of the important questions in assessing the consequences of a destructive excursion concerns the rate of vapor generation which occurs when molten or fragmented core material contacts the liquid metal

coolant. Sudden coolant boiling may result not only in damaging pressure pulses but may also affect the magnitude of the nuclear energy release through the agency of sodium void reactivity feedback. Thus, the neutronic behavior as well as the mechanical behavior of the reactor core depends upon the rate of heat transfer and vapor generation occasioned by contact between overheated core fragments and the coolant.

Fast power reactors presently under development utilize liquid sodium as the coolant. Sodium is especially attractive as a heat transfer medium because of its high thermal conductivity and its high boiling point. The high boiling point (1620°F) makes operation under high pressure unnecessary.

This investigation is a fundamental study of the heat transfer from moving spherical particles to liquid sodium. The spherical particle simulates an extremely hot core fragment which might be discharged into the coolant of a sodium-cooled fast reactor during a destructive nuclear excursion. The basic mechanism of heat transfer from the spherical particles to the liquid was of primary interest in this investigation.

Both theoretical and experimental studies of this problem were performed under this study. Neither theoretical nor experimental data for heat transfer rates from extremely hot particles moving through a liquid metal such as sodium were currently available. A theory was developed assuming that film boiling was the basic mechanism for heat transfer from the spherical particles to liquid sodium. However, alternate mechanisms such as superheating of the sodium were considered and compared with experimental data in order to establish the actual

heat transfer mechanism.

Heat transfer rates from a 1/2-inch diameter tantalum sphere to liquid sodium were measured as the sphere moved through a sodium pool. These data were obtained using a transient quenching technique similar to the method used by Merte and Clark (1)* to obtain basic heat transfer data from spherical bodies to liquid nitrogen. Sphere temperatures up to 3600°F were attained. Measurements were made in liquid sodium at 572°F (300°C) and 842°F (450°C). The velocity of the sphere was varied from 3.48 ft/sec to 14.06 ft/sec. All measurements were made at atmospheric pressure. These experimental data were compared to heat transfer rates computed from the theories developed in this study.

* Numbers in parentheses denote references in the bibliography.

CHAPTER II

LITERATURE SURVEY

Boiling in liquids is one of the phenomena of nature which has, no doubt, been observed by man since the discovery of fire. However, only relatively recently has there been any attempt to inquire into the basic mechanisms of this phenomenon.

In recent years, the field of boiling heat transfer has received much attention. It was recognized that boiling was a very efficient way to remove large quantities of energy from surfaces surrounded by liquids. In the nucleate boiling regime, it is possible to achieve high heat fluxes with relatively low surface temperatures. Higher surface temperatures are required to achieve high heat fluxes in the film boiling regime.

Film boiling, which is characterized by the esistence of a vapor film completely enclosing the heated surface, as well as nucleate boiling, has been known for many years. Nucleate boiling is that type of boiling in which vapor is formed at discrete locations on the heated surface called nucleation sites. As early as 1756, the German scientist, Leidenfrost, (2) observed and reported a phenomenon whereby a liquid and a heated surface were separated by a vapor film. This phenomenon is still referred to as the Leidenfrost phenomenon. Also, Boutigny in 1843 in work related to boiler explosions referred to this phenomenon and called it the "spheroidal" state of water "(3)".

Pilling and Lynch in 1920 (4) reported the apparent differences in heat transfer rates between nucleate and film boiling in experiments in which metal samples were quenched in water and various other fluids. Mosciki and Broder (5) in 1926 heated wires of several different metals electrically. They observed that there was a definite temperature limit for each liquid in which the metal wires were submerged, above which the liquid would not wet the metal surface. This, of course, was the phenomenon of film boiling.

In 1934, Nukiyama (6) performed boiling experiments with an electrically heated platinum wire in water. He was successful in obtaining two distinct regimes of boiling behavior, nucleate and film boiling. Nukiyama also postulated that there was a transition region of boiling which connected these two regimes but was unable to attain it with the electrically heated wire. Nukiyama also obtained "burnout" data. Burnout refers to the point where maximum heat flux occurs just prior to transition to film boiling. The term "burnout" is used because many materials will actually melt at this heat flux as the boiling undergoes transition from nucleate to film boiling. As transition occurs, a continuous vapor film is formed over the heated surface. The thermal conductivity of the vapor as compared to the liquid is quite low, and the surface temperature must increase to support the heat flux. If this temperature is above the melting temperature of the material, then the material melts or "burns out". A more appropriate term for this maximum is the "critical" heat flux.

In the following pages, an attempt has been made to summarize the

more recent literature concerning nucleate and film boiling, with particular emphasis on their application to systems using liquid metals.

Nucleate Boiling

The nucleate boiling regime has resisted attempts to treat it in a theoretical manner. It is a very complex physical phenomenon, and although it has been extensively investigated, there are still widely varying theories concerning the basic mechanism of nucleate boiling.

McAdams et. al. (7) studied surface boiling of water in forced convection in a stainless steel annulus. The water was degassed and distilled. The effect of bulk velocity was shown to be small in the nucleate boiling regime. It was also found that for a given pressure, the driving potential for heat transfer in the forced convection boiling regime is the temperature difference, $\Delta T_{sat} = T_W - T_{sat}$ where T_W is wall temperature and T_{sat} is saturation temperature. If heat flux data is plotted versus ΔT_{sat}, velocity has no effect on the heat flux in the nucleate boiling regime. It was also observed that the critical heat flux could be increased by increased subcooling in the fluid. Kreith and Summerfield (8) confirmed this finding with similar data.

Rohsenow and Clark (9) analyzed a series of motion pictures taken by McAdams, et. al. in forced convection subcooled boiling. The number of bubble sites per unit area was estimated, and the bubble radius-time relation was found. The quantity of heat required to form a bubble of mean radius r''_m was then calculated. In this manner, the fraction of

total heat which left the heated surface which was carried by the "latent heat" of the bubbles could be estimated. It was found that the energy carried by latent heat represents a very small fraction of the total energy transfer. Rohsenow and Clark proposed that the high heat fluxes were caused by violent agitation of the liquid near the heated surface resulting from the motion of the bubbles being generated there.

Forster and Grief (10) proposed a slightly different mechanism for nucleate boiling. They postulated that the formation of bubbles "pumps" superheated fluid from the heated wall and the collapse or departure of bubbles brings colder fluid into contact with the heated surface. This is called the vapor-liquid exchange theory. Calculations were performed which showed that this mechanism is more than adequate to account for observed heat fluxes in nucleate boiling experiments. This theory also accounts for the apparent insensitivity of boiling heat flux to subcooling.

Recent work by Mesler and Moore (11) and Rallis and Jawurek (12) indicate that latent heat transport is significant in saturated nucleate boiling. Mesler and Moore made temperature measurements on a heated surface with micro-thermocouples capable of high response. It was noted that during nucleate boiling, the surface experienced a regular rapid drop in temperature followed by a smaller rapid rise and then a gradual reattainment of the initial temperature. They calculated that 70 to 90 percent of the total heat transfer could be attributed to this temperature drop. Hendricks and Sharp (13) combined the same type of temperature measurements made by Mesler and Moore with an optical

system and showed that the temperature drop in the surface occurred when the perimeter of a bubble passed over the thermocouple junction. Hendricks and Sharp then reached the same conclusion as postulated by Mesler and Moore that evaporation was causing the rapid temperature drop, and that latent heat transport is indeed important in the nucleate boiling regime.

Vliet and Leppert (14, 15) investigated forced convection nucleate boiling in both saturated and subcooled water flowing normal to a circular cylinder. They observed that, in nearly saturated water, nucleation first began on the rear half of the cylinder and spread to the forward portion of the cylinder as the heat flux is increased. The vapor bubbles which form on the forward portion of the cylinder grow and move around the cylinder. The bubbles separate from the cylinder somewhat downstream of the 90-degree position. As the heat flux is increased further, the two-phase mixture in the cylinder wake increases in vapor percentage until a vapor cavity forms behind the cylinder. Liquid, however, is still supplied to the downstream portion of the cylinder. It apparently moves into the region through breaks in the cavity wall and between individual bubbles.

Vliet and Leppert postulated two reasons for this type of flow behavior. The first was that, as heat flux increases, the amount of vapor contained in the cylinder wake is sufficient to allow the liquid flowing around the cylinder to continue in a tangential direction at the 90-degree position. The second concerns the relative densities of the liquid and vapor in the two-phase mixture moving around the surface of the cylinder. As the mixture reaches the 90-degree position

on the cylinder and tries to follow the surface of the cylinder, an outward force arising from the inward centripetal acceleration acts upon the mixture. Since the liquid is more dense than the vapor, it experiences a greater force and tends to be separated from the vapor. Therefore, upon reaching the 90-degree position on the cylinder, the liquid tends to flow in a tangential direction and the vapor tends to move into the wake region.

At higher heat flux, the amount of liquid entering the vapor cavity is seen to decrease because of more closely packed bubbles. A condition is soon reached where the amount of liquid in the vapor cavity is insufficient to cool the rear portion of the cylinder. The entire cylinder then rapidly overheats and the critical heat flux is reached.

The flow mechanism in highly subcooled water was observed to be quite different, however. Because of the rapid condensation which occurs, there is insufficient vapor to form a vapor cavity. The liquid-vapor boundary layer continues around to practically the 180-degree position on the cylinder. Nucleation fails when irregular and unstable accumulations of vapor occur in this region. The mechanism of nucleation failure may be similar to that in nearly saturated water but the region in which it occurs is much smaller and less well defined.

The combined effect of subcooling and velocity on the peak heat flux was observed to be very large. The peak heat flux from a 1/8-inch outside diameter tube at a fluid velocity of 11.0 ft/sec and a subcooling of 100°F was approximately seven times greater than the peak heat flux

for a 1/8-inch tube at 0.65 ft/sec and subcooling of approximately 12°F.

Film Boiling

The existence of a film boiling regime has been known for many years, e.g., the Leidenfrost phenomenon named after the German scientist who published his observations in 1756. This phenomenon is sometimes called the "spheroidal" state. It was so named by Boutigny in 1843. However, very little research was actually done in the area of film boiling until relatively recently. Work was begun by Bromley and his co-workers (16,17,18). Colburn, in unpublished lecture material referred to the apparent similarity between film boiling and film condensation (19). Bromley (16) investigated this similarity. The resulting equation for the heat transfer coefficient for film boiling around a horizontal cylinder is identical to that given by Nusselt's theory for thin film laminar condensation with the gravity term replaced by the buoyancy term and with a differing constant "(20)". The case considered by Bromley was natural convection film boiling, and the contribution of radiant heat transfer was neglected. Experiments performed by Bromley with six organic liquids indicated that this equation predicted the heat transfer rates from tubes ranging in outside diameter from 0.188 to 0.468 inch. Later experiments by Barker, Banchero, and Boll (21) and experiments by McAdams et. al. (22) indicated that this equation fails to hold for tube diameters less than 0.025 inch and greater than 0.750 inch.

In a subsequent paper, Bromley et. al. (17) included the effects of

velocity upon film boiling. Again radiation was neglected although corrections were made for radiation at the end of the derivation. In flows where forced convection predominates over free convection, it was found that heat transfer coefficient due to conduction alone varied as

$$h_{co} = C \left[\frac{k\rho\lambda' U_\infty}{D\ \Delta T}\right]^{1/2}, \qquad (1)$$

where k is the thermal conductivity, ρ is the density, λ' is the latent heat of vaporization, U_∞ is the bulk velocity of the fluid, D is the tube diameter, and ΔT is the wall temperature minus the saturation temperature. The constant C could in theory be evaluated, but in practice was obtained from experimental data and is given as 2.70. For this case, Bromley gives as the total heat transfer coefficient

$$h = h_{co} + 7/8\ h_r \qquad (2)$$

where h_r is the coefficient due to radiation.

In both of the preceding analyses by Bromley, a linear temperature profile in the vapor film was assumed. This was shown to be valid if an "effective" latent heat of vaporization is used. This quantity is

$$\lambda' = \lambda \left[1 + \frac{0.4\ C_p\ \Delta T}{\lambda}\right], \qquad (3)$$

where C_p is the specific heat capacity of the vapor and was derived by Bromley (23).

In the final paper in the series, Motte and Bromley (18) included the effect of subcooled liquid in the flowing system. The resulting expression for the heat transfer coefficient was quite complex, and the authors state that the equation as such is not exact and should be used for correlation purposes only. Data taken with various organic liquids

point out markedly the increased heat transfer coefficients that can be achieved with large degrees of subcooling.

Ellion (24) performed an investigation very similar to Bromley's investigation (16). Ellion's results agreed well with Bromley's results.

In 1959, McFadden and Grosh (25) performed an analysis for laminar film boiling in the free convection regime which included the effects of inertia and convection in the vapor film which had been neglected by Bromley in his 1950 paper. This was done by using the boundary layer concept with the appropriate boundary conditions. The cases analyzed were the vertical flat plate and the horizontal cylinder. It was shown that through suitable assumptions, the boundary layer equations were identical for these two cases. The analysis also included the effects of variable physical properties and of a nonisothermal wall. The special case of constant properties and an isothermal wall was also calculated. An approximate analysis was also performed for the case where radiation heat transfer is comparable in magnitude to the convection heat transfer. The variable-property analysis agreed quite well with a constant property analysis as long as the fluid is sufficiently far from the critical state.

Chang (26) and Hsu and Westwater (27) performed analysis of film boiling on vertical plates. Hsu and Westwater included the effects of turbulence in their theoretical work.

Bradfield et. al. (28) performed experiments in film boiling from the surface of various hydrodynamic shapes, including a sphere,

in water and liquid nitrogen. The primary object of this program was to test the possibility of drag reduction by the formation of a vapor film around the body. Heat transfer data were taken also, however. Some very interesting photographic observations were made in conjunction with these measurements. It was observed that the effect of motion was to stabilize the liquid-vapor interface (damp the laminar waves present in free convection film boiling) up to a point where transition to turbulence resulted in "froth" flow in the boundary layer. Subcooling in the liquid also had this effect. This can be explained by a reduction in vapor film thickness due to the effects of motion and subcooling in the liquid. It was also noted that for very large degrees of subcooling, the liquid-vapor interface again became unstable and would collapse and a transition to nucleate boiling would apparently occur. The surface temperature at which this happened was observed to have a definite dependence upon the degree of subcooling present in the liquid. In fact, it was noted for their experiments that for subcooling greater than approximately 100°F in water, that it was difficult to maintain a stable vapor film. These observations are in conflict with a theory proposed by Westwater (29) which states that a fluid cannot be in contact with a surface that is above the critical temperature of the fluid and remain in the liquid state. Some of the observed surface temperatures at which apparent transition to nucleate boiling occurred are well above 705°F, the critical temperature of water. Recently, Bradfield (30) has shown that there can be liquid-surface contact in the normally stable film boiling regime.

Berenson (31) analyzed film boiling from a horizontal plane sur-

face. He used strictly hydrodynamic considerations. Berenson was successful in deriving an expression for the heat transfer coefficient that was very similar to the coefficient derived by Bromly for a horizontal cylinder.

Sparrow and Cess (32, 33, 36), Tachibana and Fukui (34) and Koh (35), have performed analyses of the film boiling problem. Sparrow and Cess utilized the boundary layer theory very successfully in achieving solutions to the problem. The horizontal and vertical flat plate were the surfaces which were considered in these studies. Koh also used the boundary layer treatment with success. Tachibana and Fukui performed an analysis on film boiling from a small wire. They used integral techniques to achieve a solution.

Also in 1962, Frederking and Clark (37) published the results of an analysis for natural convection film boiling from a sphere in a saturated liquid. The contribution of thermal radiation to the net heat transfer was neglected. The velocity and shear stress at the liquid-vapor interface were assumed to be zero. Kinetic energy effects and energy convection effects in the vapor film were neglected also. The film thickness was considered small compared to the radius of the sphere. By writing an energy balance at the liquid-vapor interface, an expression for the film thickness as a function of angular position could be written and solved exactly. This immediately leads to heat transfer results, since heat is assumed to be transferred across the vapor film by conduction only, and the neglect of energy convection terms gives a linear temperature profile in the vapor film. A comparison of this theory to data taken in liquid nitrogen shows

some disagreement; however, it should be noted that very little data has been taken from a sphere, and further work should be undertaken to test this theory.

Sparrow (38) studied the effect of thermal radiation upon the film boiling process. The case which was analyzed was a plane, vertical isothermal surface in a saturated liquid. Forced convection motions were not present. Both radiatively participating and nonparticipating vapors were considered in this paper. The conservation equations were put in nondimensional form and solved for each case. A comparison of the nonparticipating vapor solution to the theory of Bromley shows good agreement. The practical value of the solution involving a participating vapor is somewhat limited because very little knowledge of vapor emissivities, particularly for metal vapors, is now available. However, the analysis does indicate that for liquids such as water at relatively low pressure, the effect of a radiatively participating vapor should be negligible.

Merte and Clark (1) have made measurements in saturated liquid nitrogen from a 1-inch diameter copper sphere. Heat transfer data was taken during a quenching process; i.e., the sphere was heated to a desired initial temperature and then inserted into the liquid nitrogen pool. The thermal diffusivity of copper is such that the sphere can be assumed to be at a uniform temperature. This was verified by thermocouples which were installed at various radial locations in the sphere. A comparison of these data, obtained during a transient process, to steady state data shows good agreement. This points out the usefulness of this technique to obtain boiling data in all regimes

in an efficient and rapid manner. A comparison of these data to the theory of Bromley shows considerable disagreement. However, the authors state that these data were taken under turbulent conditions, and Bromley's theory is known to apply only to laminar flow cases.

Very recently Kobayashi (39) has attempted to develop a theory for the prediction of forced convection film boiling around a sphere in a saturated liquid. An approach similar to that used by Bromley for forced convection film boiling around a cylinder was used. Unfortunately, the pressure distribution corresponding to that around a cylinder instead of a sphere was used in the formulation of the problem. This, of course, introduces some error into the results of the theory. The manner in which Kobayashi treats the effect of thermal radiation is also in error. He states that the total heat transfer coefficient in film boiling from a sphere is the direct sum of the coefficient which is calculated by assuming that thermal radiation is negligible and the coefficient which is calculated from radiation considerations. These two heat transfer coefficients are not independent of each other, and cannot be added directly to obtain the total coefficient.

Liquid Metal Boiling

Farmer (40) was among the first investigators to study extensively the boiling of liquid metals. Farmer boiled pure mercury from copper and chromium surfaces. The copper surface gave twice as large a film coefficient as the chromium surface. This apparently could be attributed to differences in wetting characteristics of copper and

chromium by mercury.

Lyon, Faust, and Katz (41) measured boiling heat transfer coefficients for pure mercury, sodium, and for cadmium and also for mercury with 0.1 percent sodium, mercury with 0.02 percent magnesium and a trace of titanium and for sodium-potassium alloy. These fluids were boiled at temperatures ranging from 670°F to 1600°F and at atmospheric pressure. These liquid metals were boiled on the outside of a 3/4-inch diameter single, horizontal, stainless steel tube. A comparison of heat flux measured to mercury and mercury with 0.1 percent sodium at a particular temperature difference showed the effects of additives. Mercury alone did not wet stainless steel, and the heat transfer rates for pure mercury were much lower than those for mercury with traces of sodium. Pure mercury apparently went from the convection heat transfer regime directly into the film boiling regime whereas the mercury plus 0.1 percent sodium wet the surface and experienced nucleate boiling.

Madsen and Bonilla (42) boiled sodium-potassium alloy (44 wt. % K) on a horizontal nickel surface. The boiling surface was heated electrically. The heat transfer rate to the boiling metal was found by the application of a heat balance on the system. Rapid fluctuations in temperature in both heating surface and boiling liquid were observed. These temperature fluctuations were accompanied by distinct "bumps" which were immediately followed by a rapid temperature decrease. It was found that the experimental heat transfer rates could be best correlated with the equation

$$q/A = 134\ (p)^{0.25}(\Delta T)^{1.24},$$

where q/A is the heat flux, p is the pressure in the vapor space above the molten metal pool in absolute millimeters of mercury, and ΔT is the difference between the temperature of the heating surface and the equilibrium temperature for the liquid at the prevailing vapor space pressure in degrees Fahrenheit.

Korneev (43) reported experiments with mercury and magnesium amalgam boiling on horizontal and vertical steel tubes from 0.5 to 0.87 inch in diameter submerged in a pool. Korneev's nucleate boiling data which were compared to the data of Lyon and Bonilla show poor agreement. Korneev's data show ΔT_{sat} one order of magnitude higher for the same heat flux than do the data of Lyon and Bonilla. Korneev also performed experiments with pure mercury in the film boiling regime. His data agree very closely with those of Lyon. Korneev also observed that no appreciable difference in temperature between the top and the bottom of the horizontal tube occurred during film boiling in mercury.

Noyes (44) studied boiling from the surface of a horizontal 3/8-inch diameter cylinder immersed in a saturated sodium pool. Heat fluxes up to 800,000 Btu/hr ft^2 were measured, and the surface temperature of the cylindrical test section varied from 1200 to 1500°F. Burnout data were taken at pressures between 0.5 and 1.5 psia. In the nucleate boiling regime, the following empirical equation provided a good fit for the data:

$$q/A = 180\ (\Delta T_{sat})^{2.35} \qquad (6)$$

ΔT_{sat} represents the difference in temperature between the heater surface and the boiling temperature of the sodium at the existing pressure.

No variation in ΔT_{sat} at a given heat flux due to pressure variation was noted. Later work by Noyes (45) with 1/4-inch diameter cylinders indicated that equation (6) also holds for 1/4-inch test sections. However, in this experiment audible thumps and bumps were heard and were accompanied by large fluctuations in the temperature of the test section surface.

Subbotin et. al. (46) reported sodium boiling data which were taken with 1.5-inch diameter horizontal stainless steel, nickel, and copper surfaces heated by electron bombardment. These surfaces were used in the bottom of a 6.3-inch diameter stainless steel vessel with a sodium depth of 6 to 7.9 inches. The data of Subbotin, et. al. show considerable scatter which can probably be attributed to the use of three different types of boiling surfaces.

Figure 1 shows the data of Lyon et. al. (41), Noyes (44), and Subbotin, et. al. (46) for pool boiling of sodium. Lyon's data and Noyes' data compare well only in the low heat flux region. Subbotin's data generally fall somewhat lower than the data of Noyes for a given heat flux. Both Noyes' and Subbotin's data indicate that critical heat fluxes for sodium are near 1,000,000 Btu/hr ft^2.

Marto and Rohsenow (47) studied the effects of surface conditions on nucleate pool boiling of sodium. They found that surface roughness and past history can affect the nucleate boiling process significantly. Marto and Rohsenow (48) studied the nucleate boiling instabilities of sodium also.

Wiener (49) and Colver and Balzhiser (50) studied pool boiling of potassium. Wiener's results were in reasonable agreement with the

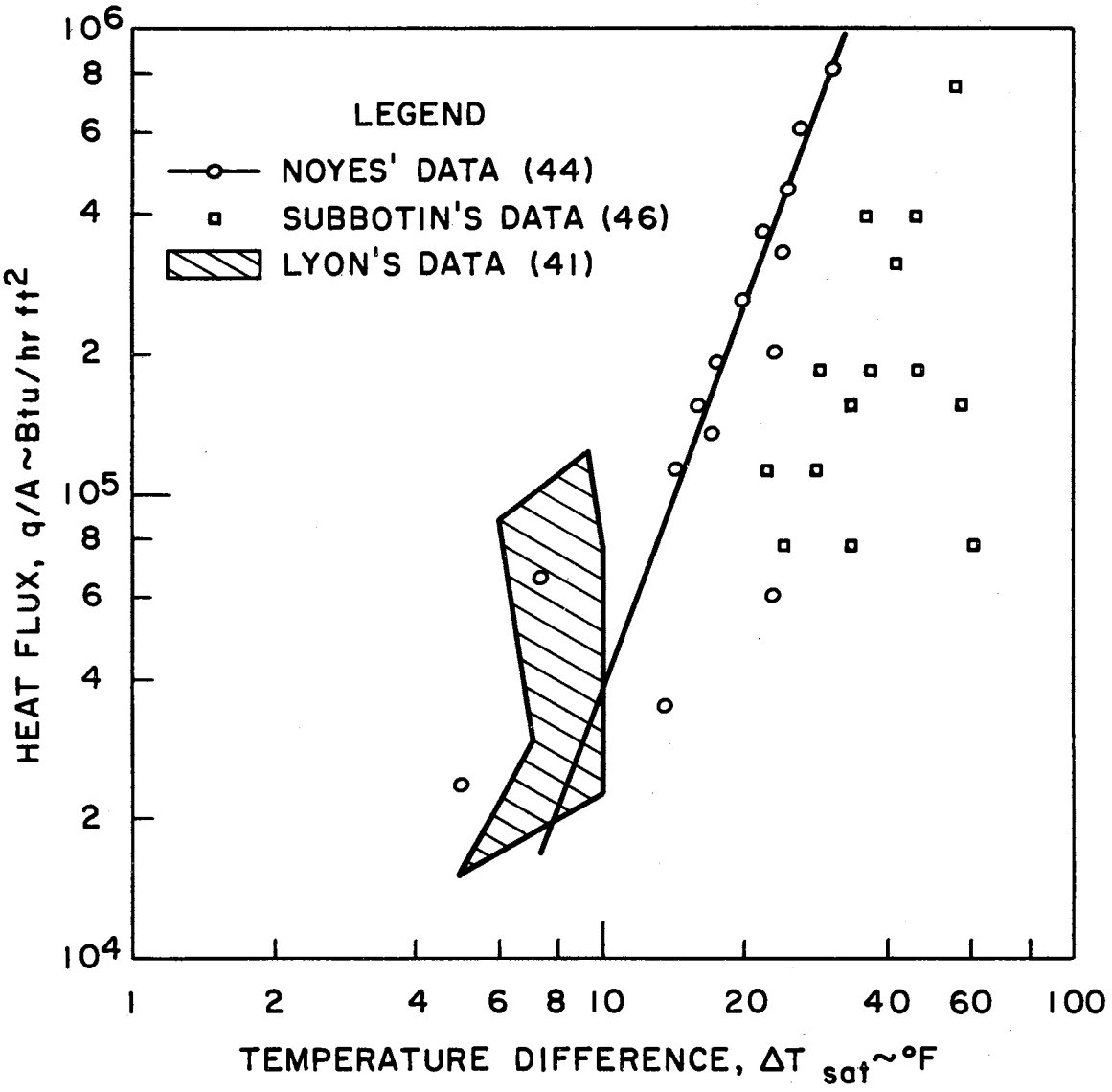

Figure 1. Pool Boiling Data for Sodium.

results of Colver and Balzhiser.

Adams (51) has used a quenching technique to obtain heat transfer data from a 3-inch diameter tungsten sphere to magnesium.

Krakoviak (52) and Holtz (53) have studied the conditions necessary for bubble nucleation from heated surfaces exposed to liquid metals. Krakoviak, by modeling the behavior of the liquid metals upon fluids such as water, was able to estimate the amount of superheat in the liquid necessary for bubble nucleation. For sodium at atmospheric pressure exposed to a surface similar to one on which it takes 30°F of superheat to sustain a bubble in water, Krakoviak calculated that 258°F of superheat would be necessary to initiate a bubble. If compared to distilled, degassed water, then the superheat required for bubble nucleation in sodium becomes 774°F. This, of course, provides an explanation for the bumping observed by several investigators when liquid metals were boiled. Since the liquid can become highly superheated, when a bubble does nucleate, the energy of superheat in the surrounding fluid can be rapidly released and a small "explosion" occurs. Holtz also used a similarity modeling between the liquid metals and water but in a different manner. Holtz' results were in fair agreement with those of Krakoviak.

In addition to the references cited previously, much data exists for boiling heat transfer in pipe and channel flow. Much of this data concerns the problem of two-phase flow in channels caused by the boiling phenomenon. Tang (54) has recently presented a very good review

of this literature, and the reader is referred to his review if more information concerning this problem area is desired.

CHAPTER III

ANALYTICAL STUDIES

Introduction

The problem of film boiling from a sphere to a liquid, such as sodium flowing past the sphere, is quite complicated. At present, there are no satisfactory analytical solutions for this problem. Even the relatively simple problem of the velocity distribution in a fluid moving past a sphere must be solved by using a "Blasius" type solution "(55)". In this solution, the velocity of the potential flow around the sphere is assumed to have the form of a power series in x, where x is measured along the surface of the sphere from the stagnation point. The velocity distribution in the boundary layer is also represented by a power series in x with the coefficients assumed to be functions of y, the direction normal to the sphere surface. By using these power series approximations, a solution for the velocity distribution around a sphere can be found.

Film boiling is normally characterized by the existence of a vapor film completely surrounding the heated surface. At some distance from the solid surface, there exists an interface between the vapor film and the surrounding liquid. Since the liquid is forced past the sphere, relative motion between the sphere, the vapor, and the liquid will occur. The model used for this phenomenon is shown in Figure 2. The problem may be thought of as one of two boundary layer systems

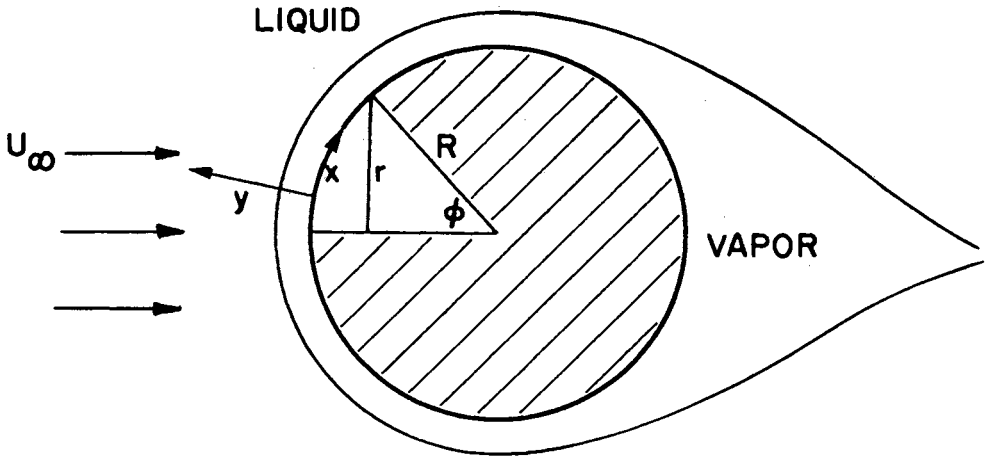

Figure 2. Model for Forced Convection Film Boiling Around a Sphere.

occurring simultaneously. The first, the vapor film, moves past the solid sphere surface and is influenced in its motion by the presence of the sphere surface and also by the presence of the liquid at the liquid-vapor interface. The second, the liquid layer over-riding the vapor film, actually feels the influence of the vapor layer only. It cannot actually "see" the sphere surface. Mass crosses the liquid-vapor interface from one boundary layer system to the other as the liquid flows past the sphere.

The problem is further complicated by the fact that the bulk liquid may be at a temperature lower than the boiling temperature of the liquid at the existing pressure. This condition of the liquid is referred to as subcooled. This condition allows heat to be transferred away from the liquid-vapor interface into the bulk of the liquid. This effect will be most severe for liquids such as sodium which have extremely high thermal conductivity. The thickness of the vapor film is intimately affected by the heat transferred into the bulk of the liquid as will be shown in a subsequent section of this chapter.

The problem has now been formulated and consists of two phases of a fluid flowing past a sphere with simultaneous heat transfer occurring in both phase regions. The bounday layer treatment will be applied to both the vapor boundary layer and the liquid boundary layer to obtain a solution for this problem.

Liquid Boundary Layer

The liquid will be assumed to move around the sphere in laminar flow. As stated previously, it shall be assumed that the liquid feels only the influence of the vapor film. If it is assumed that the

liquid-vapor interface is smooth and is in dynamic equilibrium, then the shearing stress acting upon the liquid-vapor interface in the liquid must be equal in magnitude to the shear stress acting upon the liquid vapor interface in the vapor. The following relation can be written

$$T_l = T_v. \tag{7}$$

The subscripts, l and v, refer to conditions in the liquid and vapor respectively, and the symbol, T, stands for shearing stress. The shearing stress may be written in an alternate form as

$$\mu_\ell \left(\frac{\partial u}{\partial y}\right)_\ell = \mu_v \left(\frac{\partial u}{\partial y}\right)_v. \tag{8}$$

Equation (8) simply relates the product of viscosity, μ, and velocity gradient, $\frac{\partial u}{\partial y}$, in the liquid at the liquid-vapor interface to the corresponding product in the vapor. The velocity gradient in the liquid may be written as:

$$\left(\frac{\partial u}{\partial y}\right)_\ell = \frac{\mu_v}{\mu_\ell} \left(\frac{\partial u}{\partial y}\right)_v . \tag{9}$$

For conditions sufficiently far from the critical point, the ratio of viscosities, $\frac{\mu_v}{\mu_\ell}$, is quite small. For sodium at one atmosphere and at its boiling point, the ratio is equal to 0.071. Further, for purposes of this analysis, the velocity gradient, $\left(\frac{\partial u}{\partial y}\right)_v$, will be assumed to be sufficiently small in magnitude so that $\left(\frac{\partial u}{\partial y}\right)_\ell$ remains small. This assumption permits the use of potential flow theory for the calculation of the velocity field in the liquid sodium. Actually, this greatly simplifies the problem, and a solution can be obtained which, without this assuumption, may have been impossible.

By using spherical coordinates, assuming axial symmetry, and neglecting conduction in the ϕ-direction, as compared to convection in that direction, the differential equation describing the temperature distribution around the spherical vapor film becomes,

$$u_r \frac{\partial T}{\partial r} + u_\phi \frac{1}{r} \frac{\partial T}{\partial \phi} = \alpha \left(\frac{\partial^2 T}{\partial r^2} + \frac{2}{r} \frac{\partial T}{\partial r} \right) , \qquad (10)$$

where T is temperature and α is the thermal diffusivity of the liquid. The velocity components, u_r and u_ϕ, in accordance with the assumption of frictionless flow, can be written as,

$$u_r = -3 U_\infty \frac{r-R}{R} \cos \phi, \quad u_\phi = \frac{3}{2} U_\infty \sin \phi . \qquad (11)$$

These are obtained directly by differentiating the stream and potential functions for frictionless flow around a sphere "(56)".

Sideman (57) has shown that if the assumption is made that the heat transfer takes place in a thin layer near the interface, the term $\frac{2}{r} \frac{\partial T}{\partial r}$ may be neglected in comparison to the term $\frac{\partial^2 T}{\partial r^2}$ in equation (10). This further implies that the product of the Reynolds number and Prandtl number, called the Peclet number, is much larger than unity. The Reynolds number and Prandtl number are defined by the following equations,

$$Re = \frac{\rho U D}{\mu} , \quad Pr = \frac{C_p \mu}{k} , \qquad (12)$$

where ρ is density, U, is velocity, D is the diameter of sphere, μ is viscosity, C_p is specific heat capacity, and k is the thermal conductivity of the liquid. Equation (10) can be simplified to

$$u_r \frac{\partial T}{\partial r} + u_\phi \frac{1}{r} \frac{\partial T}{\partial \phi} = \alpha \frac{\partial^2 T}{\partial r^2} . \qquad (13)$$

The boundary conditions are

$$\begin{aligned} T &= T_B, & r &= \infty & \phi &\geq 0 \quad , \\ T &= T_{sat}, & r &= R & \phi &> 0 \quad , \\ T &= T_B, & \infty &\geq r \geq R & \phi &= 0 \quad . \end{aligned} \tag{14}$$

The assumption has also been made that the penetration of heat into the liquid layer is limited to small distances. Equation (13) and (14) are solved in Appendix A. The resulting expression for the temperature distribution in the liquid around the sphere is

$$\frac{\Delta T}{\Delta T_B} = \text{erfc} \left[\frac{\psi}{2\sqrt{M\eta}} \right] , \tag{15}$$

where $M = \frac{2}{3} \frac{R\alpha}{U_\infty}$

$\eta = \int_0^\phi \sin^3 \phi \, d\phi$

$\psi = y \sin^2 \phi$

$y = r - R$

$\Delta T = T - T_B$

$\Delta T_B = T_{sat} - T_B$

and R is the radius of the sphere, U_∞ is the velocity of the bulk liquid, α is the thermal diffusivity of the liquid, and r is the radial coordinate. Differentiation of equation (15) will give the heat flux as also shown in Appendix A. The resulting expression for heat transfer from the liquid-vapor interface into the bulk liquid is

$$\frac{q}{A} = k \frac{\Delta T_B}{\sqrt{\Pi}} \frac{\sin^2 \phi}{\sqrt{M\eta}} \quad . \tag{16}$$

Vapor Boundary Layer

The solution to the heat transfer problem in the liquid

boundary layer which is subject to the prescribed restrictions allows the case of the vapor boundary layer to be considered. The boundary layer equations for axisymmetric flow of a fluid past a sphere are given in reference (55) and are presented below.

$$\frac{\partial(ur)}{\partial x} + \frac{\partial(vr)}{\partial y} = 0$$

$$u\frac{\partial u}{\partial x} + v\frac{\partial u}{\partial y} = -\frac{1}{\rho}\frac{\partial p}{\partial x} + \frac{\mu}{\rho}\frac{\partial^2 u}{\partial y^2} \qquad (17)$$

$$u\frac{\partial T}{\partial x} + v\frac{\partial T}{\partial y} = \alpha\frac{\partial^2 T}{\partial y^2} \quad .$$

These are the equations of conservation of mass, momentum, and energy, respectively. The coordinate system is given in Figure 2, with x measured along the surface of the sphere and y normal to the surface of the sphere. In addition, u is the velocity of the x-direction, v is the velocity in the y-direction, and p is the pressure. Implicit in equation (17) is the assumption that the vapor film thickness is much smaller in magnitude than the radius of the sphere.

The following additional assumptions concerning the problem were made:

1. The vapor is pure and incompressible.
2. The sphere surface is isothermal.
3. The physical properties of the vapor are constant with respect to temperature.
4. The liquid-vapor interface is smooth.
5. Inertia effects and energy convection effects in the vapor film can be neglected.

6. The vapor is transparent to thermal radiation; i.e., the vapor does not participate in the thermal radiation heat transfer process.
7. The velocity of the liquid-vapor interface can be approximated by the velocity calculated from potential theory.
8. The liquid-vapor interface is at saturation temperature.

Assumption 7 is consistent with the preceding development for the liquid layer.

Reportedly, sodium vapor is highly absorptive to thermal radiation at some wavelengths "(58)". Sparrow (38) has investigated the effect of a participating vapor upon film boiling and reports that for fluids such as water under normal pressure conditions, the effect is negligible. Sparrow also points out that very little is known about the radiative properties of vapors, particularly vapor emissivities. In addition, it will be shown in a subsequent section of this chapter that radiative contribution to the net heat transfer is unimportant. Therefore, assumption 6 can be used for this case.

Verification of assumption 4 has been accomplished in part by Bradfield, et al. (30). He observed that during film boiling from variously shaped hydrodynamic bodies, including a sphere, ripples were seen to form at the liquid-vapor interface if the surrounding liquid were at rest with respect to the body. If, however, the liquid were set in motion, the effect was to damp out these ripples and the liquid-vapor interface became much smoother. As the velocity was increased further, turbulence developed and the liquid-vapor interface became

unstable and broke down. Bradfield described this type of flow as "froth" flow.

Justification of assumption 2 is more difficult, and, in truth, it cannot be totally justified. Bromley et al. (16) observed during film boiling experiments from horizontal cylinders that the heat transfer rates were higher on the forward side of the cylinders than on the backward side and consequently the forward portion was somewhat cooler than the rear portion. This is due to the phenomenon of flow separation which occurs in film boiling just as in single phase flow past a sphere or any bluff body. However, Kutateladze et al. (59) have measured heat transfer rates from a circular cylinder during cross flow of a liquid metal and have observed that variation in heat transfer rates around the periphery of the cylinder are far less severe than corresponding variations in fluids such as air, see Figure 3. This is due in part to the extremely high thermal conductivity of the liquid metals which causes the flow patterns of the liquid around the body to take on a relatively small role in determining the heat transfer rates from the body to the liquid. For the case of subcooling in liquid sodium, the amount of heat transferred from the sphere is proportional to the heat transferred from the liquid-vapor interface into the bulk of the liquid as will be shown in succeeding paragraphs. Potential flow of the liquid sodium above the vapor film has been assumed, but Kutateladze's data was taken with the liquid in contact with the solid surface. Kutateladze has shown, however, that it makes little difference whether potential flow or viscous flow is assumed; the measured heat transfer rates compare

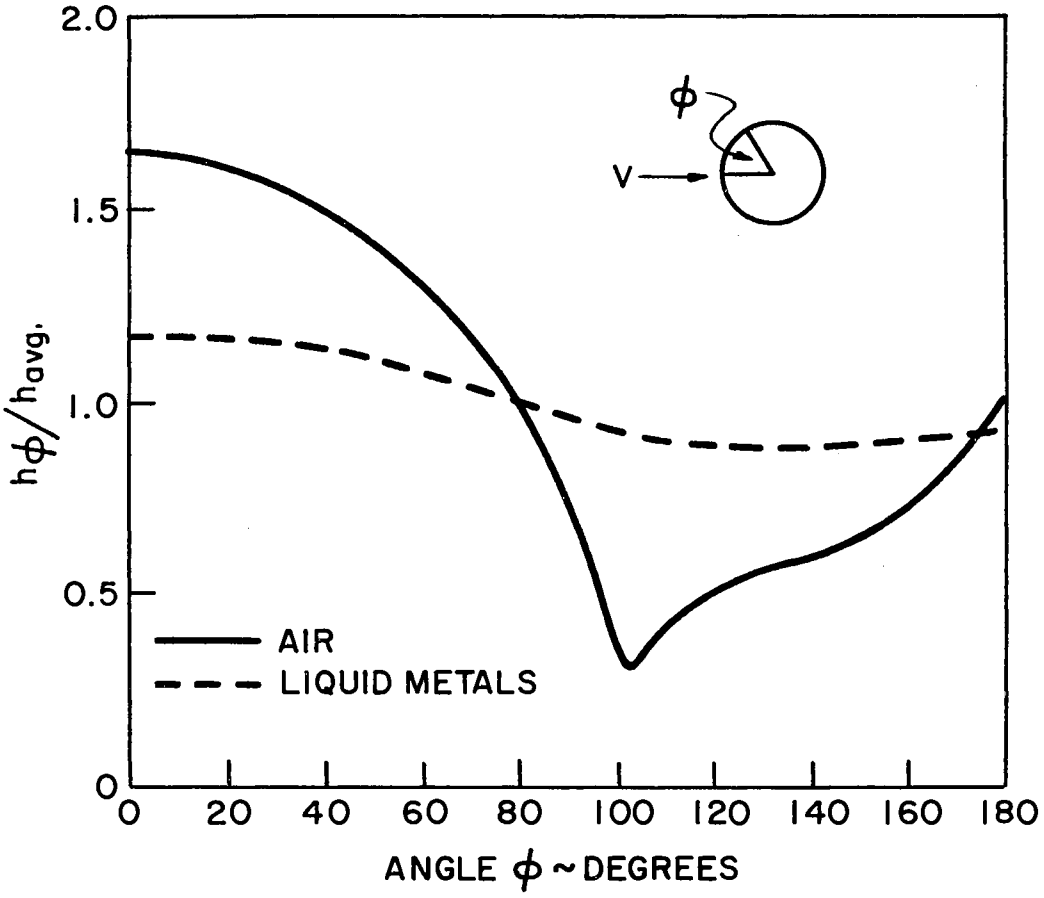

Figure 3. Comparison of Heat Transfer Coefficients for Flow of Air and Liquid Metal Around a Cylinder.

well with either of the theories. Therefore, it would appear that for a liquid such as sodium, and for relatively large degrees of subcooling, assumption 2 will be valid. It must be noted, however, that this assumption will not hold for liquids such as water, and will be increasingly in error as the liquid sodium approaches its saturation temperature.

The solution to the momentum and energy conservation equation (17) may easily be written in accordance with assumption 5. These solutions are shown in Appendix A. The expression for velocity at any point in the vapor film is,

$$U = \frac{3}{2} U_\infty \sin \phi \left[\frac{3}{4} \frac{\rho U_\infty}{\mu R} (\cos \phi)(y\delta - y^2) + \frac{y}{\delta} \right] . \tag{18}$$

The temperature distribution, which turns out to be linear, is

$$\frac{T - T_{sat}}{T_W - T_{sat}} = 1 - y/\delta \tag{19}$$

where T_{sat} is the boiling or saturation temperature of the liquid, T_w is the sphere surface temperature, and δ is the vapor film thickness.

Energy Balance on Differential Film Element

Writing an energy balance on a differential element of the vapor film which is shown in Figure 4, one obtains

$$dq_c + dq_r = dq_{vap} + dq_b \quad . \tag{20}$$

Equation (20) simply states that the energy leaving the sphere surface, composed of conductive and radiative parts, arrives at the liquid-vapor

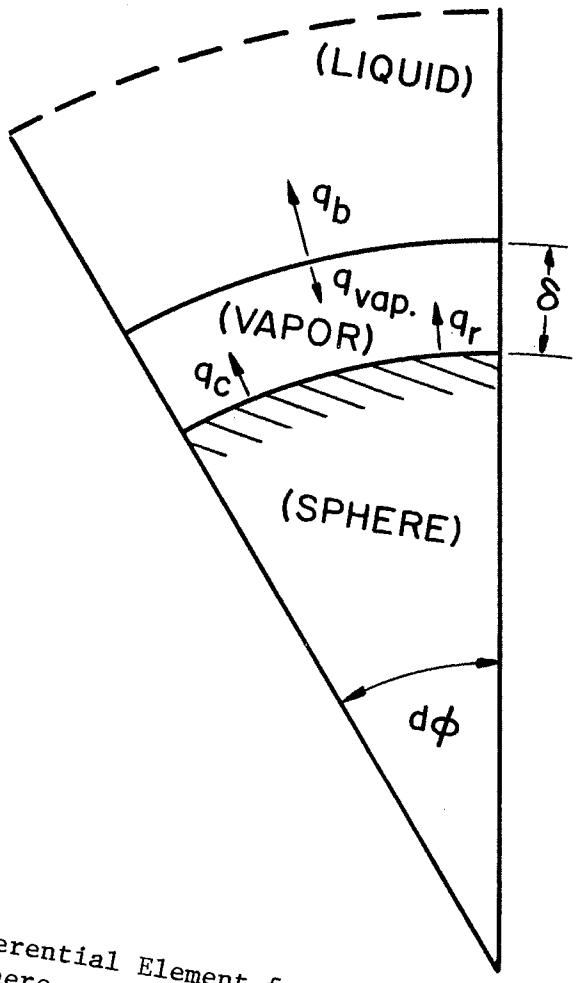

Figure 4. Differential Element for Film Boiling Around a Sphere.

interface, is used partially to form vapor, and is partially transferred to the bulk liquid. If the bulk liquid is at saturation temperature, then all the energy arriving at the liquid-vapor interface goes into forming vapor, and the last term, dq_b, in equation (20) is not necessary. The energy used to vaporize liquid at the liquid vapor interface can be written as the product of the effective heat of vaporization and the increase in the mass flow rate in the differential film element,

$$d\,q_{vap} = \lambda' \, dw. \tag{21}$$

The increase in mass flow rate in the film element must come from vapor which is formed at the liquid-vapor interface. Bromley (22) has shown for laminar film condensation that the assumption of a linear temperature profile is valid as long as an "effective" latent heat of vaporization is used in an energy balance on an element of the film. Bromley has also used this concept in film boiling analyses with good success. The expression for the effective latent heat of vaporization, λ', as derived by Bromley is

$$\lambda' = \lambda \left[1 + \frac{0.4\, C_p\, \Delta T}{\lambda}\right], \tag{22}$$

where $\Delta T = T_w - T_{sat}$. This expression actually accounts for the heat capacity of the vapor.

The increase in mass flow rate, dw, can be written as,

$$dw = d(\rho\, A_c\, \bar{u}), \tag{23}$$

where A_c is the flow cross section of the film and $\bar{u}$ is the average velocity of the vapor flowing through A_c. A_c can be written in terms of the film thickness and angular position as

$$A_c = 2\pi R\delta \sin\phi. \tag{24}$$

The average velocity, $\bar{u}$, can be found from the relation,

$$\bar{u}\delta = \int_0^{\delta} u\, dy\ . \tag{25}$$

Replacing u by its value as given by equation (18), one obtains

$$\bar{u} = \frac{1}{\delta}\int_0^{\delta} \frac{3}{2} U_\infty \sin\phi \left[\frac{3}{4}\frac{\rho U_\infty}{\mu R}(\cos\phi)(y\delta - y^2) + \frac{y}{\delta}\right] dy. \tag{26}$$

Evaluation of this integral gives,

$$\bar{u} = \frac{1}{\delta}\left[\frac{3}{2} U_\infty \sin\phi \left(\frac{3}{4}\frac{\rho U_\infty}{\mu R}(\cos\phi)\frac{\delta^3}{6} + \frac{\delta}{2}\right)\right]\ . \tag{27}$$

Equation (23) may now be written in terms of the film thickness and angular position as,

$$dw = d\left(\rho 2\pi R(\sin\phi)\frac{3}{2} U_\infty \sin\phi\left[\frac{3}{4}\frac{\rho U_\infty}{\mu R}(\cos\phi)\frac{\delta^3}{6} + \frac{\delta}{2}\right]\right). \tag{28}$$

Now, also equation (20) becomes

$$\frac{k\Delta T}{\delta} dA + q_r/A\ dA = \lambda' 2\pi R\rho \frac{d}{d\phi}\left[\frac{3}{2} U_\infty \sin\phi \left\{\frac{3}{4}\frac{\rho U_\infty}{\mu R}(\cos\phi)\frac{\delta^3}{6} + \frac{\delta}{2}\right\}\right] d\phi + \frac{k_\ell}{\sqrt{\pi}}\frac{\sin^2\phi}{\sqrt{M\eta}}\Delta T_B\, dA, \tag{29}$$

where dA refers to the area element on the sphere surface adjacent to the film element. The heat transferred into the bulk of the liquid has been derived in a previous section of this chapter. The radiative heat transfer rate, q_r, is calculated by assuming the surface of the sphere and the liquid-vapor interface are approximated by parallel infinite plates. Liquid sodium is highly absorptive to thermal radiation and, therefore, the absorptivity of the liquid-vapor interface is assumed to be unity. The heat transfer rate due to radiation becomes

$$\frac{q_r}{A} = \sigma\varepsilon\,(T_w^4 - T_{sat}^4) \tag{30}$$

where σ = Stefan-Boltzmann constant,

ε = emittance of the sphere surface.

The differential area element, dA, can be written as

$$dA = 2\pi R^2 \sin\phi d\phi \quad . \tag{31}$$

Substituting this into equation (29), one obtains

$$k\frac{\Delta T}{\delta} 2\pi R^2 \sin\phi d\phi + \sigma\varepsilon(T_w^4 - T_{sat}^4) 2\pi R^2 \sin\phi d\phi =$$

$$\lambda' 2\pi R\rho \frac{d}{d\phi}\left[\frac{3}{2} U_\infty \sin^2\phi \left(\frac{3}{4} \frac{\rho U_\infty}{\mu R}(\cos\phi)\frac{\delta^3}{6} + \frac{\delta}{2}\right)\right] d\phi +$$

$$\frac{k_\ell}{\sqrt{\pi}} \frac{\sin^2\phi}{\sqrt{M\eta}} \Delta T_B \; 2\pi R^2 \sin\phi d\phi \quad . \tag{32}$$

Simplification of equation (32) gives

$$k\frac{\Delta T}{\delta} + \sigma\varepsilon (T_w^4 - T_{sat}^4) = \frac{3}{2} \frac{\rho U_\infty \lambda'}{R \sin\phi} \frac{d}{d\phi}\left[\sin^2\phi \left(\frac{3}{4} \frac{\rho U_\infty}{\mu R}(\cos\phi) \frac{\delta^3}{6} + \frac{\delta}{2}\right)\right]$$

$$+ \frac{k_\ell}{\sqrt{\pi}} \frac{\sin^2\phi}{\sqrt{M\eta}} \Delta T_B \quad . \tag{33}$$

Equation (33) gives a description of the film thickness variation around the periphery of the sphere. Both the effect of subcooling in the bulk liquid and thermal radiation on the film thickness are included. Solution of equation (33) for film thickness would allow the calculation of the heat transfer from the sphere surface during film boiling to a surrounding fluid. The total heat transfer rate would become the direct sum of the heat transferred due to conduction and that due to thermal radiation.

For highly subcooled liquids, such as sodium at less than 950°F and at atmospheric pressure, the contribution of the vapor film to the net energy exchange between the sphere and the surrounding liquid can be

neglected. For a tantalum sphere which has relatively low emittance, the effect of radiation heat transfer on the vapor film thickness can also be neglected. In fact, even if the emittance of the sphere surface were equal to unity, the contribution of radiative heat transfer compared to the heat transferred into the bulk of the subcooled liquid sodium amounts to less than 10 percent of the total heat transfer rate. Consequently, the second term on the left and the first term on the right of the equation (33) can be neglected. Equation (33) can then be written as,

$$\frac{k\ \Delta T}{\delta} = \frac{k_\ell}{\sqrt{\pi}}\ \frac{\sin^2\phi}{\sqrt{M\eta}}\ \Delta T_B \quad . \tag{34}$$

The solution of equation (34) for the film thickness gives,

$$\delta = \frac{k\Delta T\ \sqrt{\pi M\ \eta}}{k_\ell\ \sin^2\phi\ \ \Delta T_B} \tag{35}$$

A simpler result of the neglect of these two terms in equation (33) is due to the realization that the vapor film thickness must adjust its thickness to accommodate the heat transferred through it and subsequently into the subcooled liquid. The heat transfer rate from the sphere can now be found by calculating the amount of heat which is transferred from the liquid-vapor interface into the bulk of the liquid. The following expression which was derived in Appendix A is obtained,

$$q/A = \frac{k_\ell}{\sqrt{\pi M}}\ \frac{\sin^2\phi}{\sqrt{\eta}}\ \Delta T_B \quad . \tag{36}$$

The basic theory developed for this study is presented in this chapter and Appendix A.

CHAPTER IV

EXPERIMENTAL APPARATUS

The experimental apparatus used in this investigation is shown in Figure 5. The basic parts of the apparatus were a tank to contain liquid sodium, a tantalum sphere with a thermocouple imbedded in it supported by a tantalum support tube, and a motor to propel the heated sphere through the liquid sodium pool. The basic apparatus in its initial stage of construction is shown in Figure 6. The tank and support structure was constructed of type 304 stainless steel. The tank was semi-circular with a radius of 10 inches and 4 inches wide. The tank was designed in the semi-circular shape to keep the amount of sodium required for the experiment to a minimum.

The motor used in this experiment to move the sphere through the sodium pool was a Photocircuits Corp. Model 488 printed circuit D.C. motor. One of the requirements for this experiment was a constant linear sphere velocity as the sphere moved through the sodium pool. This printed circuit motor has its armature windings "printed" upon a thin ceramic disc. Consequently the motor has very low internal inertia and relatively high angular acceleration. For the range of velocities in this experiment, the motor reached a constant angular velocity in 90-degrees of rotation or less. At extremely low velocities, the velocity of the sphere varied slightly in its motion through the sodium pool. However, this variation never exceeded 10 percent, and an average value for velocity was used whenever this

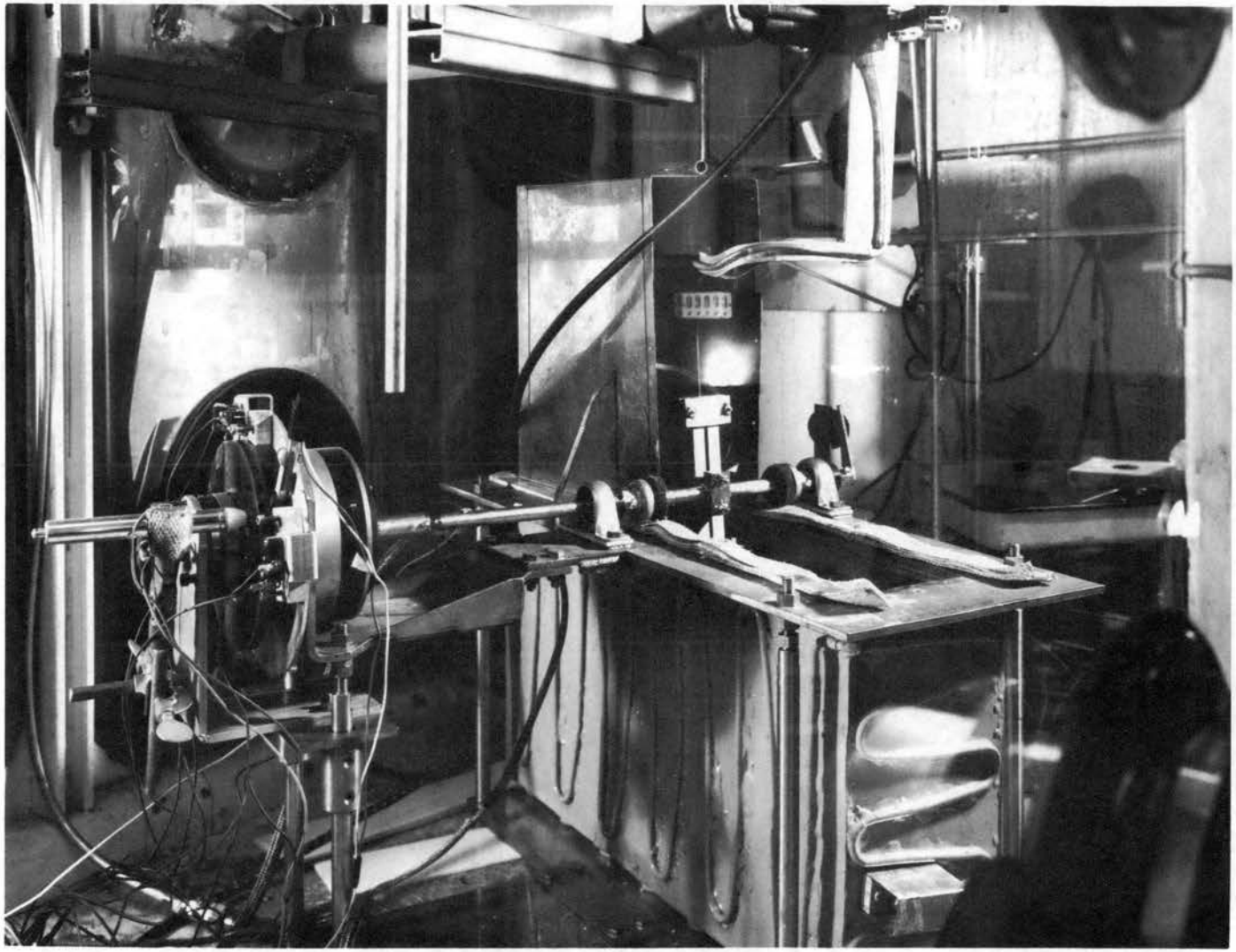

Figure 5. Sodium Heat Transfer Apparatus - Ready for Operation.

Figure 6. Sodium Heat Transfer Apparatus - Early Stage of Construction.

occurred.

The motor was connected to a stainless steel shaft which extended over the sodium tank and was supported by bearings contained in pillow blocks. These pillow blocks were mounted on Teflon shims to protect the bearings as much as possible from overheating. During data runs, the motor was connected to the shaft by a simple sleeve connector. This provided a rigid connection and insured that the motion of the sphere did not lag behind the motion of the motor.

The motor was driven by an EICO Model 1064 D.C. power supply. The velocity of the motor is a function of the applied voltage and torque. The torque was applied by a friction brake which is discussed in a subsequent section of this chapter. It was found that for a particular voltage setting and applied torque, the velocity of the motor was reproducible to within 10 percent.

The sodium was heated from below by two Hevi-Duty 50 KTS flat type electrical resistance heating units limited to heater temperatures up to 2190°F. These heaters were contained in an insulating box which fit closely over the sodium tank, as shown in Figure 7. These heaters were connected in parallel to a General Radio Type W20V D.C. (Variac) power supply.

Sphere Thermocouple Assembly

A 1/2-inch diameter tantalum sphere was used as the test body in this experiment. Tantalum was chosen because of its high melting

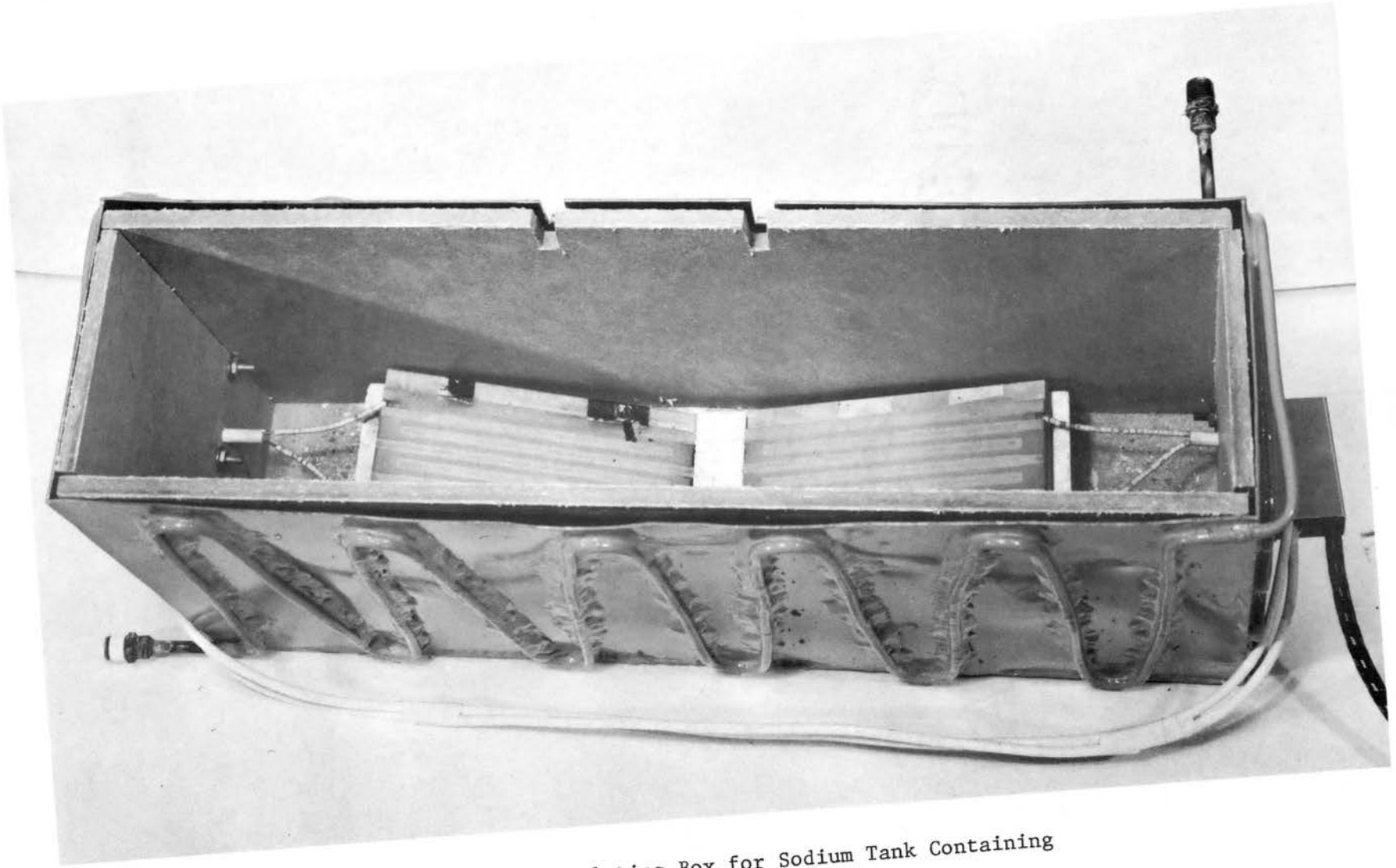

Figure 7. Insulating Box for Sodium Tank Containing Electrical Heaters.

temperature (5425°F) and its relative ease in machining. The thermal properties of tantalum are also practically constant from room temperature to near its melting point. These properties were taken from Hampel (60).

Installed in this sphere was a tungsten-5% rhenium/tungsten-26% rhenium thermocouple. The wires of this thermocouple were 30 gage and were contained in a 0.062-inch O.D. tantalum sheath. Surrounding the wires was vitrified beryllium oxide powder which served as an insulator. The thermocouple bead was welded to the bottom of the sheath.

The method of fabrication was as follows. A tantalum sphere was machined on a special Hardinge lathe and a billet of excess tantalum was left on the forward portion of the sphere. A hole 0.066 inch in diameter was drilled to within 0.031 inch of the tangent line of the forward portion of the sphere. A 1/8-inch O.D. tantalum tube was fitted into a countersunk hole in the rear of the sphere and electron beam welded. The thermocouple was then inserted into the hole and was Heli-arc welded to the bottom of the hole by applying the arc to the outside of the sphere. The assembly, before welding, is shown in Figure 8. After the welding of the thermocouple was completed, the sphere was again put into the lathe and the excess material was removed from the front portion of the sphere. The sphere-thermocouple assembly directly after welding is shown in Figure 9. The finished product was practically mirror smooth and is shown in Figure 10 after bending into the desired shape. A cross-section of the sphere drawn

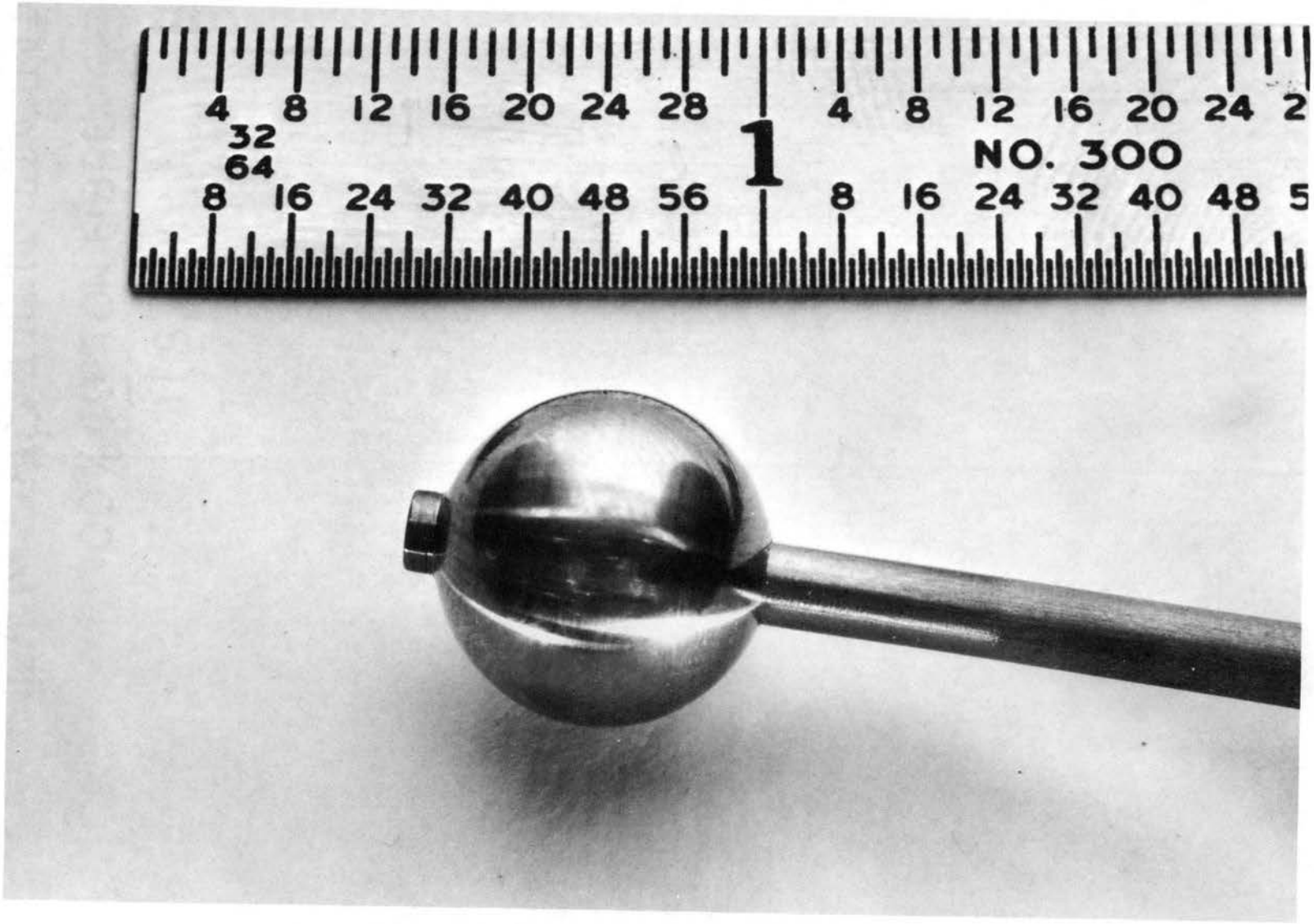

Figure 8. Tantalum Sphere and Support Tube - Before Welding.

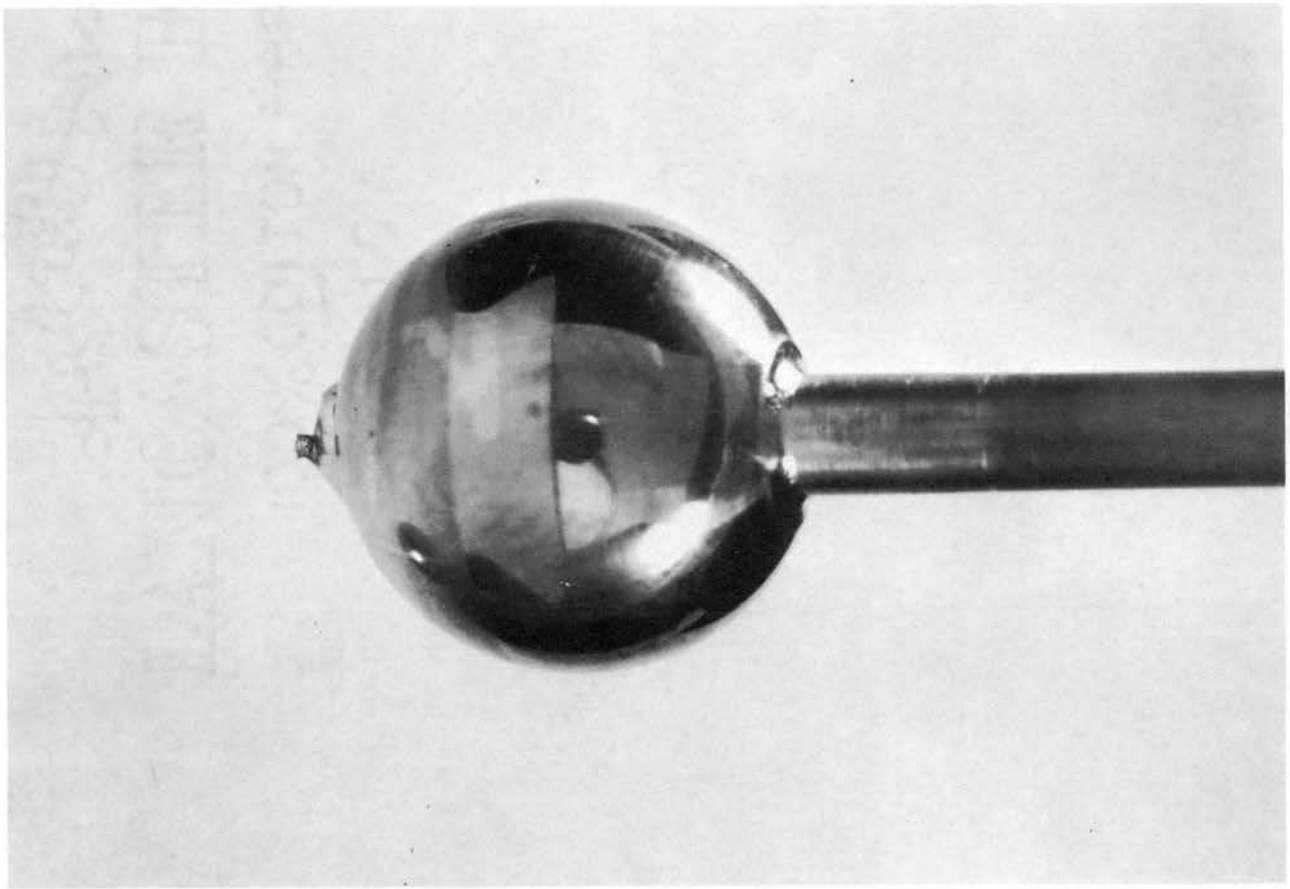

Figure 9. Sphere-Thermocouple Assembly - After Welding.

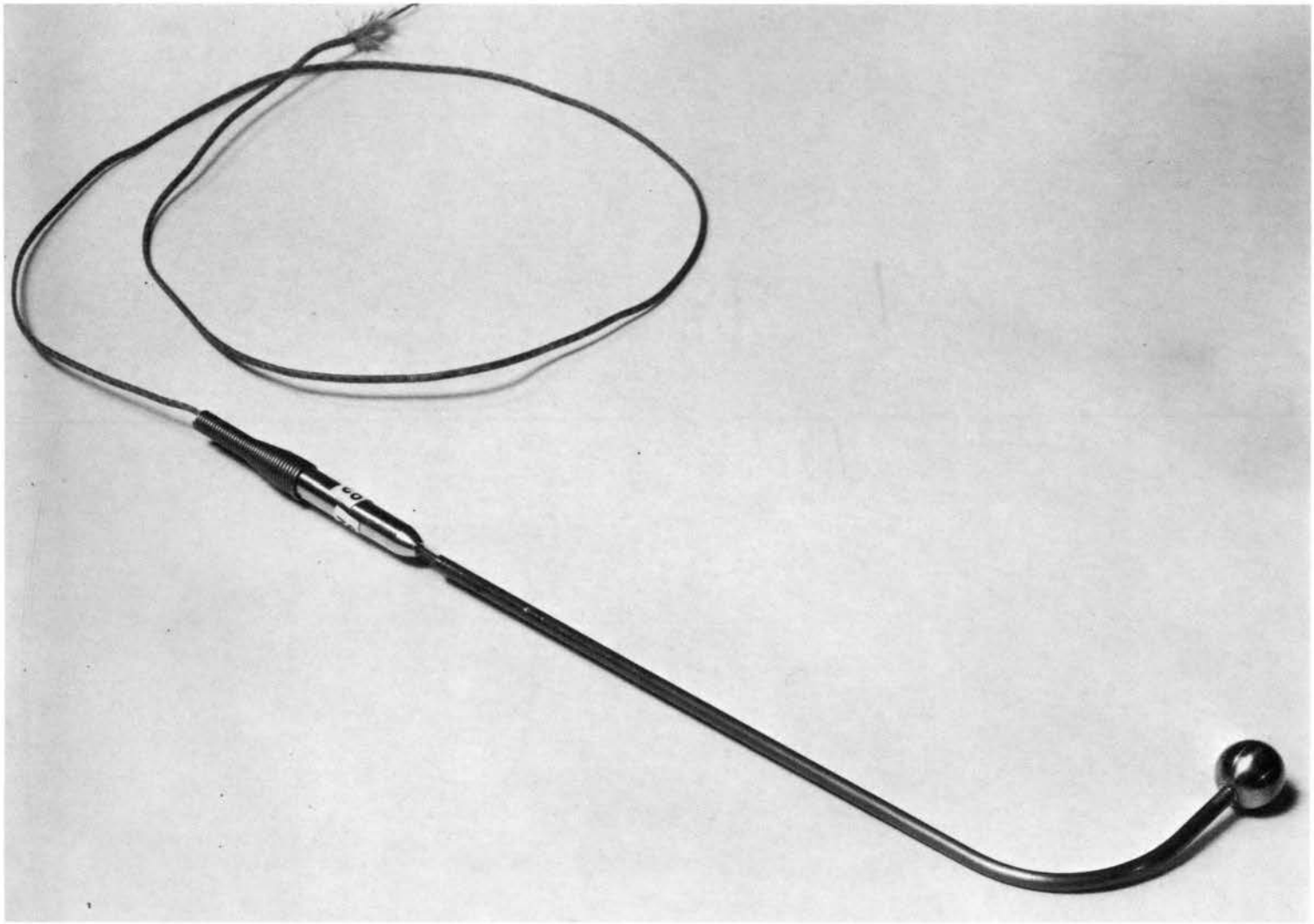

Figure 10. Sphere-Thermocouple Assembly - Ready for Use.

to scale is shown schematically in Figure 11. By attaching the thermocouple in this manner, the best possible thermal contact between the sphere and the thermocouple was maintained.

The sphere-thermocouple assembly was attached to the shaft by a simple clamping device. The sphere support tube was clamped to a holder which was, in turn, clamped to the motor shaft. This arrangement is shown in Figure 5 which shows the completed apparatus ready for operation. The distance from the shaft axis to the sphere could be varied with this attaching device.

X-ray photographs were taken of the sphere in an effort to locate the thermocouple bead very precisely. However, because of the scattering effect of the tantalum at the curved forward portion of the sphere, the X-ray photographs were of poor resolution. Therefore, the location of the thermocouple had to be estimated from mechanical measurements.

Temperature Recording System

The output of the tungsten-rhenium alloy thermocouple inside the sphere was recorded with a high frequency oscillograph. The oscillograph used was a Honeywell-Heiland Model 906A Visicorder. This instrument uses galvanometers to achieve accurate response to rapidly changing input signals. A mirror is suspended upon the galvanometer wires and rotates as the input signal varies. The galvanometer is a current sensitive device as compared to potentiometric recorders which are voltage sensitive. The galvanometer used to record the sphere temperature was an M-1000 Heiland galvanometer with a natural frequency of

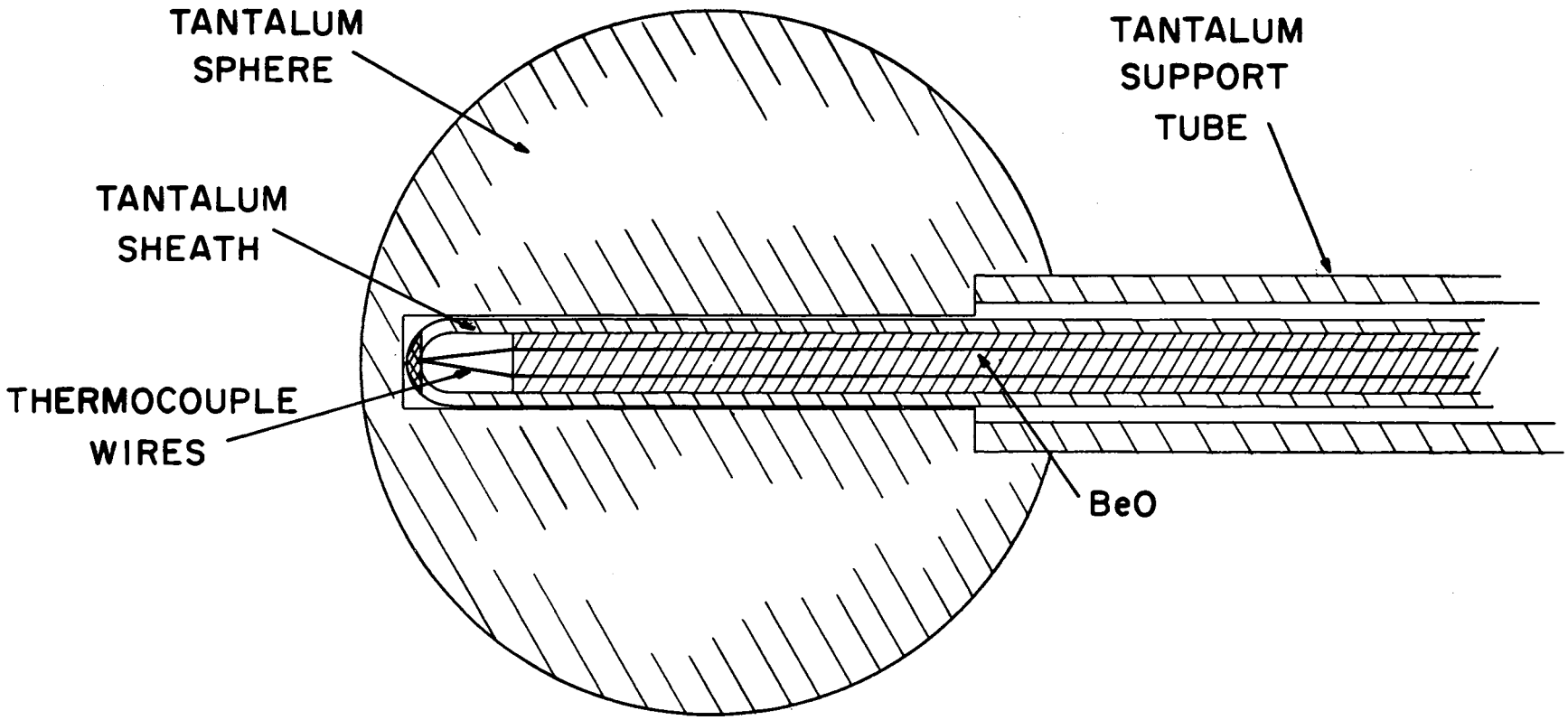

Figure 11. Cross-Section of Sphere-Thermocouple Assembly.

1000 cycles/sec. However, in order to damp this galvanometer adequately, it was placed in a resistance circuit which reduced the frequency response to approximately 640 cycles/sec.

Because of the relatively low output of the tungsten-rhenium thermocouple, and the low sensitivity of the M-1000 galvanometer, the input thermocouple signal had to be amplified. An EICO Model A12 D.C. amplifier was used to drive the galvanometer. The use of the amplifier also eliminated a problem which would have been present if the amplifier were not used. Since galvanometers are basically current sensitive devices, the change of resistance with temperature of the thermocouple leads must normally be considered. However, the input impedance of the EICO amplifier is 10,000 ohms so that small changes in source resistance are negligible in comparison to this large impedance.

A bias circuit was integrated into the temperature recording system as shown schematically in Figure 12. This bias circuit allowed the galvanometer trace to be deflected so that when the sphere was heated, a 1000°F temperature range was displayed on the 6-inch recording paper used in the Visicorder. This was done in order to minimize the effect of light beam trace width on the magnitude of the recorded temperature. The light beam could be positioned anywhere on the paper with this circuit. The bias circuit was calibrated periodically during data runs to give an output of 50 millivolts at 0.5 milliamperes and proved to be stable.

Although the operating specifications for the various electrical

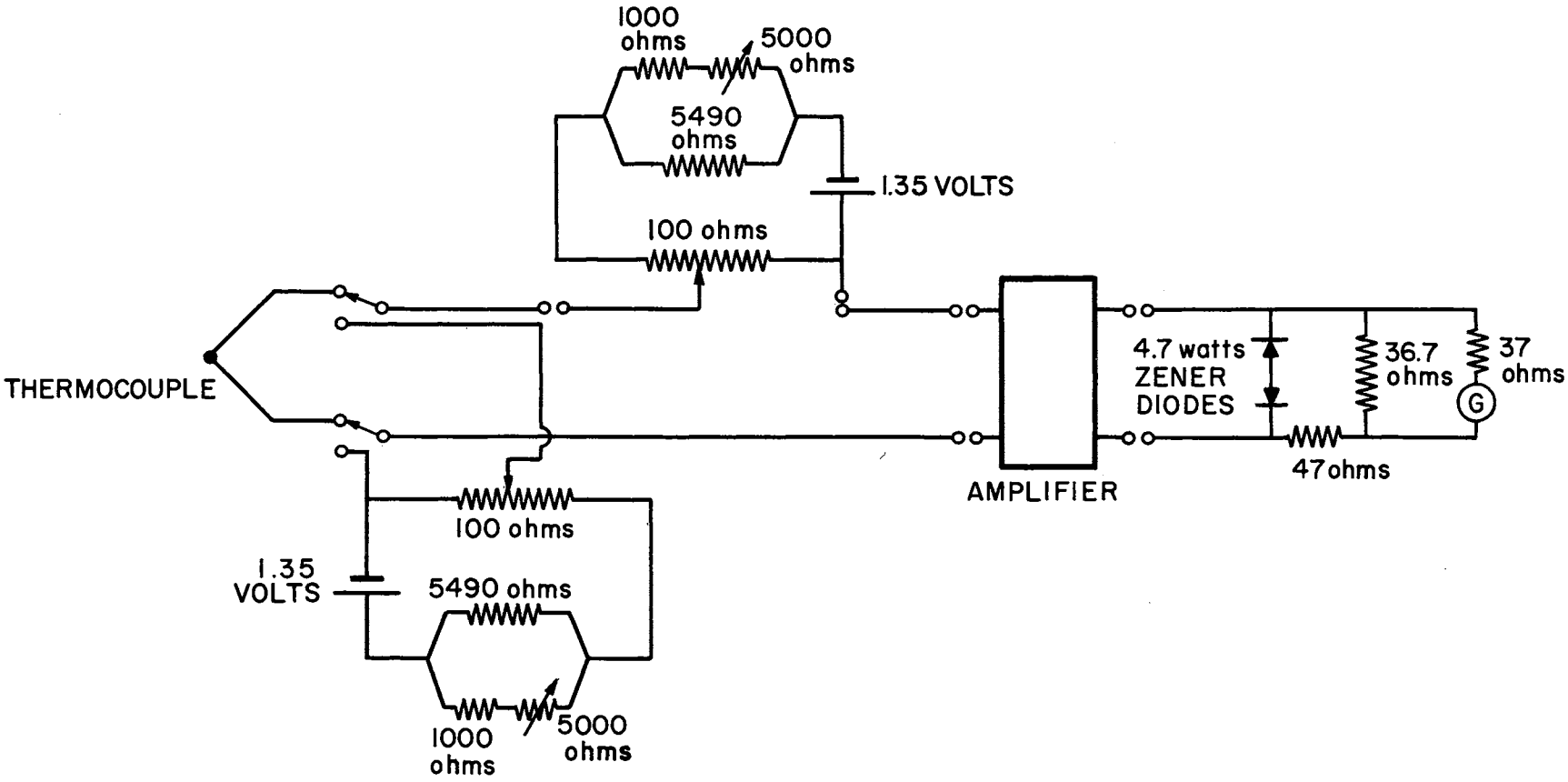

Figure 12. Schematic Diagram of Temperature Recording Circuit.

components indicated that the frequency response of the system would be adequate, a simple test for the response of the system was performed. An electrical input of sufficient magnitude to give a galvanometer deflection of 5 inches was applied to the system in the form of a step function input. The signal was applied with a simple push type switch. The signal actually overshot the correct value of the step input slightly and then assumed the correct value. The total time required by the amplifier-galvanometer system for the response to the complete step input was less than 5 milliseconds. This was adjudged to be more than adequate for accurately recording the signals anticipated in this experiment.

A calibration circuit identical to the bias circuit was also included in the system so that spot checks of the system calibration could be made. Later it was found that the bias circuit output was stable and the calibration circuit was actually used very little. To protect the M-1000 galvanometer from high current, two Zener diodes were placed back to back in parallel with the galvanometer. A complete circuit diagram for the temperature recording system is shown in Figure 12.

Measurement and Control Instrumentation

The angular velocity of the motor was measured by a timing device located at the rear of the D.C. motor. All the measurement and control instrumentation for the motor was located at the rear of the motor to protect it from the high temperatures of the sodium pool. This instrumentation is shown in Figure 13. The timing device consisted of a light

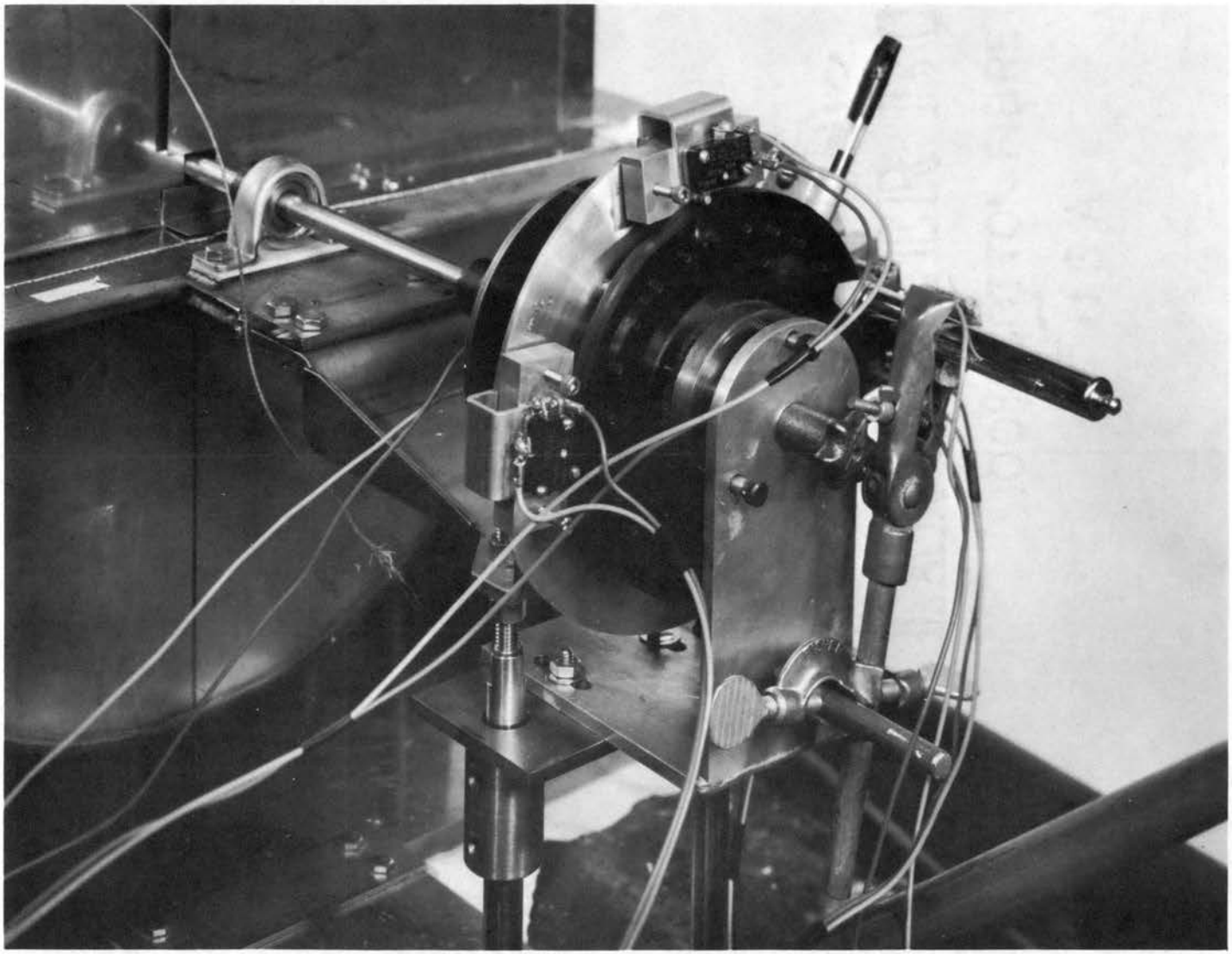

Figure 13. Measurement and Control Instrumentation.

source and a photoconductive cell separated by a plexiglass wheel. The plexiglass wheel was perforated with drill holes at 15-degree intervals on a base circle 2.5 inches in radius. As the motor shaft turned, the timing wheel also turned. The face of the wheel was darkened, and as holes alternately moved between the light source and the photo-cell, the resistance of the cell decreased sharply. The cell was contained in a circuit which also contained the recording device. This circuit is shown in Figure 14. The decrease in cell resistance caused a recording galvanometer to deflect. This galvanometer was contained in the Honeywell-Heiland Model 906A Visicorder described previously. Timing lines are placed on the record by special galvanometers. With this device, a record of the deflections which occurred as the motor moved the sphere through the sodium was made. The angular velocity was calculated by measuring the time between several galvanometer deflections as the sphere moved through the sodium and dividing it into the total angle traversed in this time increment. The linear velocity of the sphere was then calculated by multiplying this calculated angular velocity by the measured distance from the motor shaft axis to the center of the sphere.

Figure 13 also shows three micro-switches mounted around the periphery of the motor. These micro-switches were part of a relay circuit which provided for remote control of the motor. This relay circuit provided for the following modes of operation:

1. Forward motion from the sphere heating device, through the sodium pool, and to rest above the

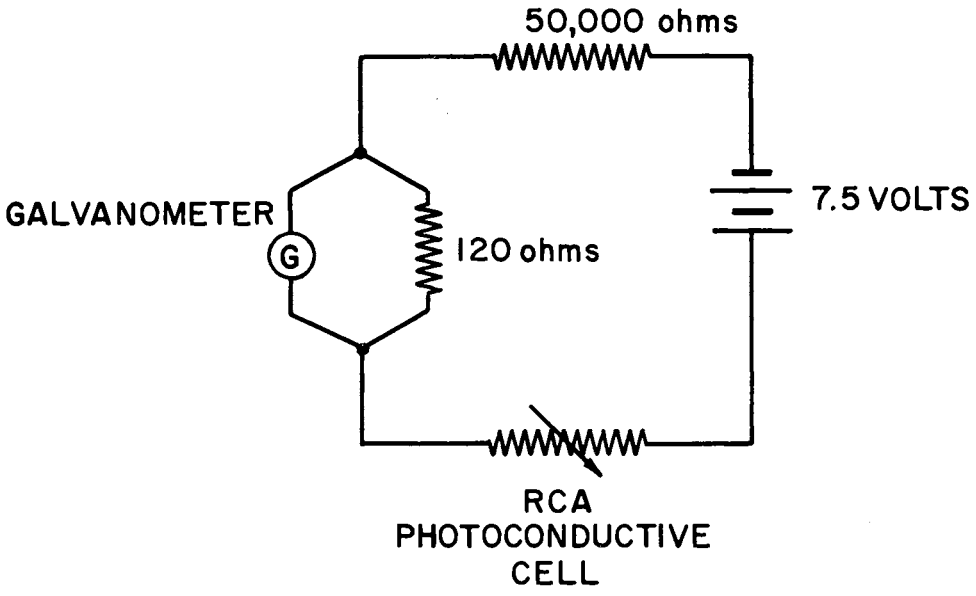

Figure 14. Velocity Recording Circuit.

sodium pool. (This was the data gathering mode of operation.)

2. Backward motion through the sodium pool to the sphere heater.
3. Backward motion through the sodium pool to a position above the sodium pool but outside the sphere heater.
4. Backward motion from the position described in (3) to the sphere heater.

The control panel for this circuit is shown in Figure 15. This photograph also shows the power supply for the D. C. motor, the Honeywell-Heiland Visicorder and timing unit, and the amplifier used in the temperature measuring circuit.

The torque for the D. C. motor was provided by a friction brake shown in Figure 13. This brake consisted of a spring-loaded felt-faced disc pressed against the plexiglass timing wheel. The pressure exerted by the disc upon the wheel could be varied by turning a single nut mounted on the center-line of the brake. As stated previously, by varying the torque with this friction brake, and varying the voltage to the motor, the motion of the sphere could be closely controlled.

Sphere Heating Apparatus

The tantalum spheres used in this experiment were heated inductively in a copper coil connected to a Thermonic Model 1500 induction generator. Induction heating operates on the principle that a conductor placed in the electrical field of another current carrying

Figure 15. Control Panel, Power Supply, Amplifier, Timing Unit, and Visicorder for Sodium Heat Transfer Apparatus.

body has an electrical current induced in it. The Thermonic generator which was used in this experiment operated at 250 kilocycles. At this frequency, the induced current penetrates only a small portion of the outer skin of the sphere. The interior of the sphere must then be heated by conduction.

Three coil designs were used in the course of this investigation. In general, these coils were ellipitcal in shape and built so that the sphere could freely move in and out. The number of turns in these various heating coils were one and three. The first coil which was used can be seen on the right in Figure 16. It consisted of a single turn of copper plate. Copper tubing carrying cooling fluid was soldered to the outside of the coil. The sphere was very tightly coupled to this coil; i.e., the distance between the sphere and the sides of the coil was very small. It was impossible to achieve high sphere temperatures with this coil. Arcing between the coil and the sphere surface occurred at relatively low generator power settings. A three-turn coil was designed which was not so tightly coupled. This coil is also shown in Figure 16. The third coil design can be seen in Figure 17. It consisted of three turns of copper tubing and was more tightly coupled than the other three-turn coil. Both three-turn coils were capable of heating 1/2-inch tantalum spheres to well over 3600°F. Both of these coils were used in the course of this experimental program. The loosely coupled three-turn coil greatly diminished the arcing problem.

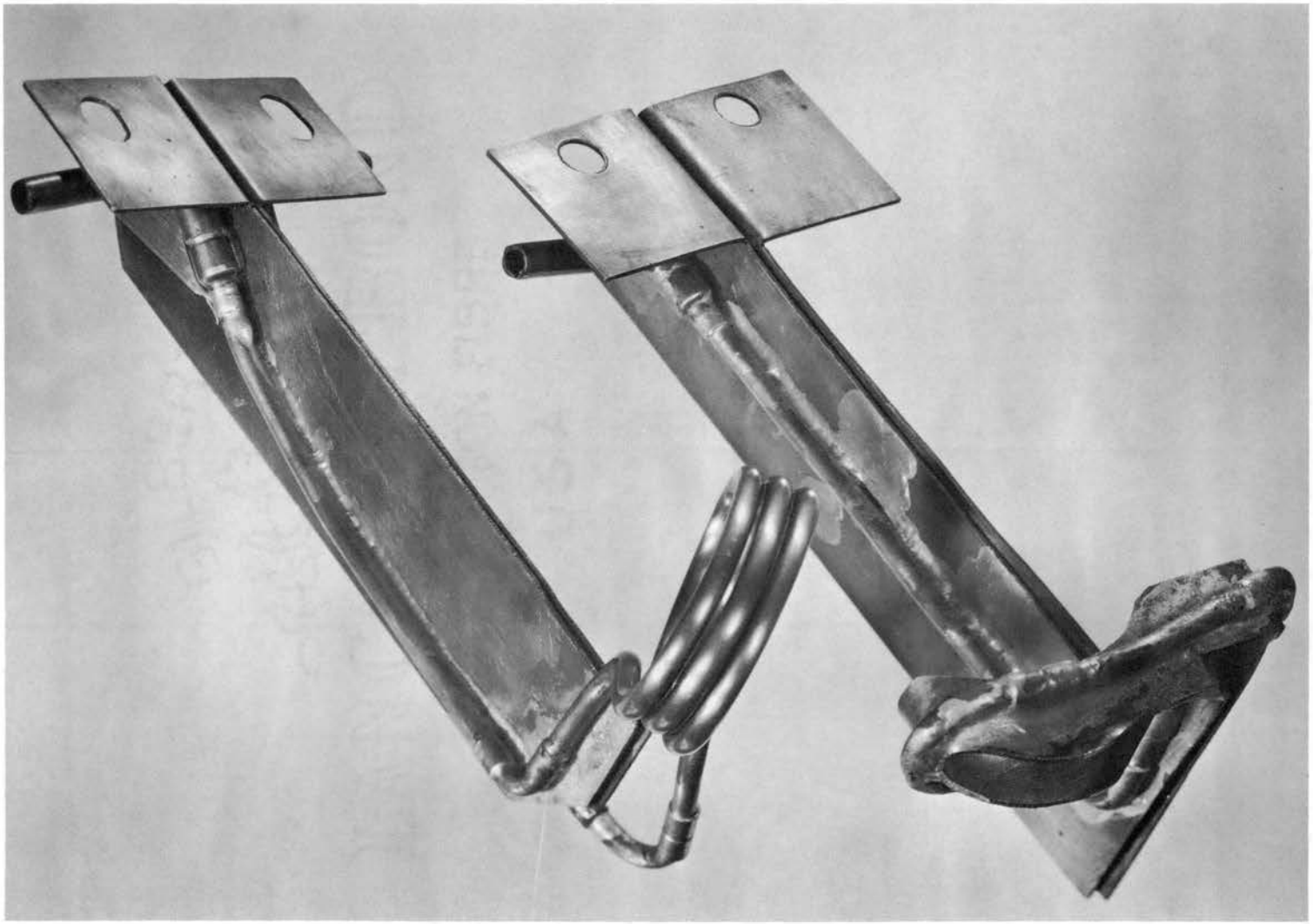

Figure 16. Induction Heating Coils Used to Heat Tantalum Sphere.

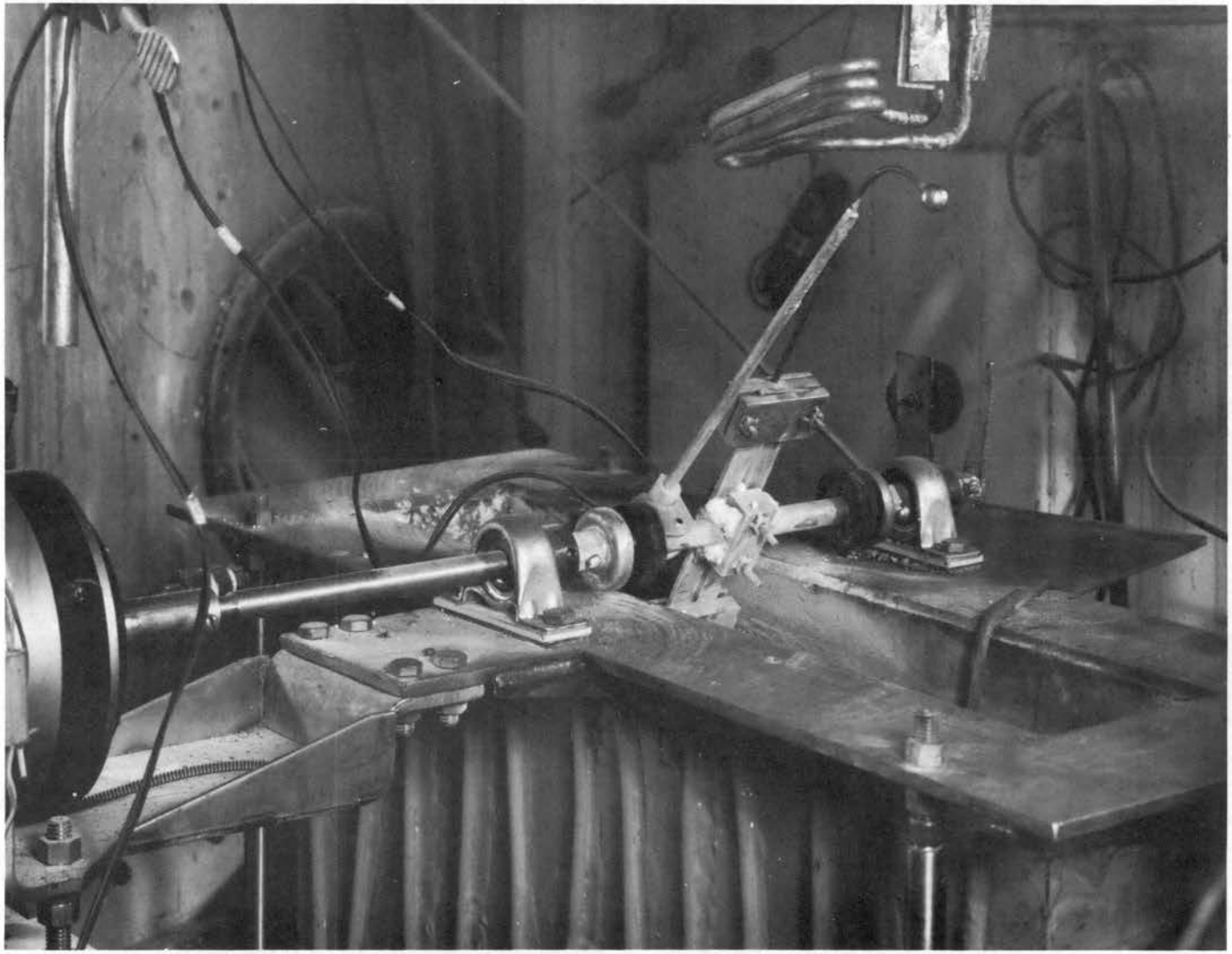

Figure 17. Heat Transfer Apparatus Showing 3-Turn Induction Heating Coil.

Glovebox and Auxiliary Equipment

This experiment had to be performed in a dry, inert atmosphere since sodium is highly reactive with both oxygen and water vapor. The apparatus described in the preceding sections of this chapter was contained in a two-module argon atmosphere glovebox shown in Figure 18. Argon gas is continually circulated from the glovebox through a purification system. The gas in the system was continually sampled, and the oxygen and water vapor content was determined. The purification system was capable of maintaining both the oxygen and water vapor content of the argon gas below 5 ppm.

The purification system consists of a palladium catalyst bed and a molecular sieve. The molecular sieve removes water vapor from the circulating argon gas. If the atmosphere becomes high in oxygen content, hydrogen gas is added to the flowing gas prior to passing through the palladium bed. The palladium bed serves as a catalyst to react hydrogen with oxygen to form water vapor. The gas then flows through the molecular sieve which removes the water vapor. The purified gas then returns to the glovebox.

A coaxial cable from the Thermonic induction generator into the glovebox was provided. Other auxiliary equipment included a silicone oil recirculating system for cooling the induction heating coil, an air lock for introducing materials into the box without contaminating the atmosphere, grounded electrical outlets inside the box, and a bubbler to provide a safety release for any sudden pressure increases inside the box.

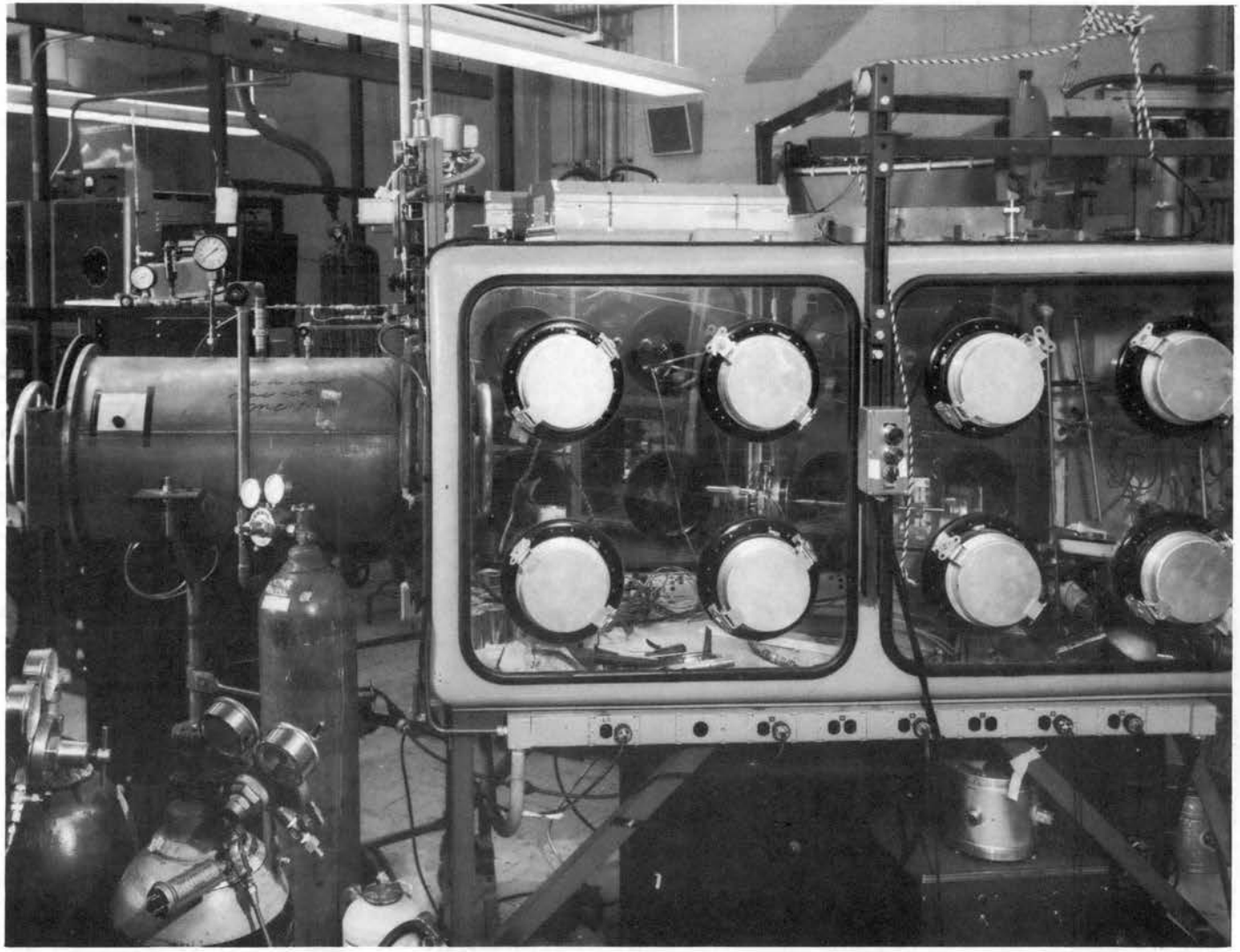

Figure 18. Argon Atmosphere Glovebox.

Modifications to the system, made specifically for this experiment, include the installation of a set of electrical lead-throughs for the motor control circuits, lead-throughs for an additional silicone oil recirculating system which was used to cool the outside of the copper box which contained the electrical heaters for the sodium tank, and the introduction of a set of W-26% Re/W-5% Re thermocouple wire lead-throughs. The manner in which these auxiliary systems were introduced into the system is shown in Figure 19.

The sodium temperature was measured with a chromel-alumel thermocouple contained in a stainless steel thermocouple well inserted into the sodium pool. Another chromel-alumel thermocouple was attached to the outside of the sodium tank copper heat exchanger box. Both these thermocouples were connected to chromel-alumel thermocouple lead-throughs provided in the glovebox. These thermocouples were connected to a Brown Electronik 17 recorder.

The operating procedure for conducting the experimental studies with this equipment is given in the following chapter.

Figure 19. Argon Atmosphere Glovebox Modifications.

CHAPTER V

EXPERIMENTAL PROCEDURES

The experimental data collected in this investigation consisted of temperature-time traces of a thermocouple at a known location in a tantalum sphere as the sphere passed through a pool of molten sodium. The apparatus for obtaining these data was discussed in Chapter IV. Briefly, the data were obtained in the following manner. The sphere was heated to the desired initial temperature in the induction heater. The motor was then actuated and the heated sphere moved in a circular arc from the induction heating coil, through the sodium pool, and to rest above the sodium pool. The output of the thermocouple was continuously recorded during this entire sequence of events. The velocity of the sphere in its motion from the heating coil through the sodium pool was recorded simultaneously with the temperature of the sphere.

In addition to the experimental procedures associated with the acquisition and accuracy of the experimental data, there were procedures associated with safety requirements which were followed.

Safety Procedures

Rigid safety standards were required for this experiment because of the potential danger of molten sodium coming in contact with oxygen or water. As stated in Chapter IV, all cooling systems used silicone oil as the primary coolant. Secondary heat exchangers were located

outside the box, and water was used as the secondary coolant. Periodic checks of the oil in these systems were made to insure that water had not leaked into the oil. Standard safety glass panels were used for the glovebox windows.

In addition to the bubbler provided on the glovebox, a solenoid valve was set to release gas into an exhaust system if the pressure difference between the box and the surroundings exceeded 0.90 inches of water. The sodium tank and heaters were enclosed in a copper heat exchanger which was described in Chapter IV. This was done in order to prevent heating of the argon atmosphere by natural convection from the sodium tank and electrical heaters. Overheating of the argon gas could result in a pressure increase in the glovebox.

Another potential hazard in this experiment was the use of beryllium oxide as the insulating material in the W-26% Re/W-5% Re thermocouple. BeO is very toxic and very low concentrations in air are extremely dangerous. However, the BeO in the thermocouples was vitrified and was contained in a tantalum sheath. Whenever there was any danger of exposing BeO to the air, all work was done with rubber gloves inside a hood.

Thermocouple Calibration

The accuracy of the sphere temperature measurements was assured by calibration of the output of the tungsten-rhenium alloy thermocouples which were used in the tantalum spheres. This was done after all phases of their installation into the spheres were completed. Because these

thermocouples were to be used to measure relatively high temperatures, an optical pyrometer was used as the calibrating device.

A Leeds and Northrup Model 8622-C optical pyrometer was calibrated against a tungsten filament lamp certified by the National Physical Laboratory of England. Actually, three pyrometers were compared to the tungsten filament lamp, and the one which compared best was used as the secondary calibration device. Figure 20 shows the results of this comparison. All pyrometers compared very favorably up to approximately 2200°C, where one of the pyrometers began to show erroneous readings. However, the other two pyrometers agreed very well with the certified lamp over the entire range of temperatures, and did not vary from the filament temperature by more than 10°C at any temperature.

A blackbody enclosure system for calibrating the thermocouples was designed and tested. This method was designed in an attempt to eliminate the problem of having to use tantalum emittance properties to compute the true sphere temperature. The apparatus used in the "blackbody" calibration is shown schematically in Figure 21. The sphere was heated inside a cylindrical blackbody enclosure. The 0.75-inch diameter tantalum cylinder which served as the blackbody enclosure was heated by a circular induction heating coil, and, in turn, heated the sphere by radiation. The electrical output of the thermocouple and the reading of an optical pyrometer were simultaneously recorded whenever equilibrium was reached. The cylinder was enclosed at the bottom, and the sphere was inserted into it from the top. A tight fitting cover cut to conform to

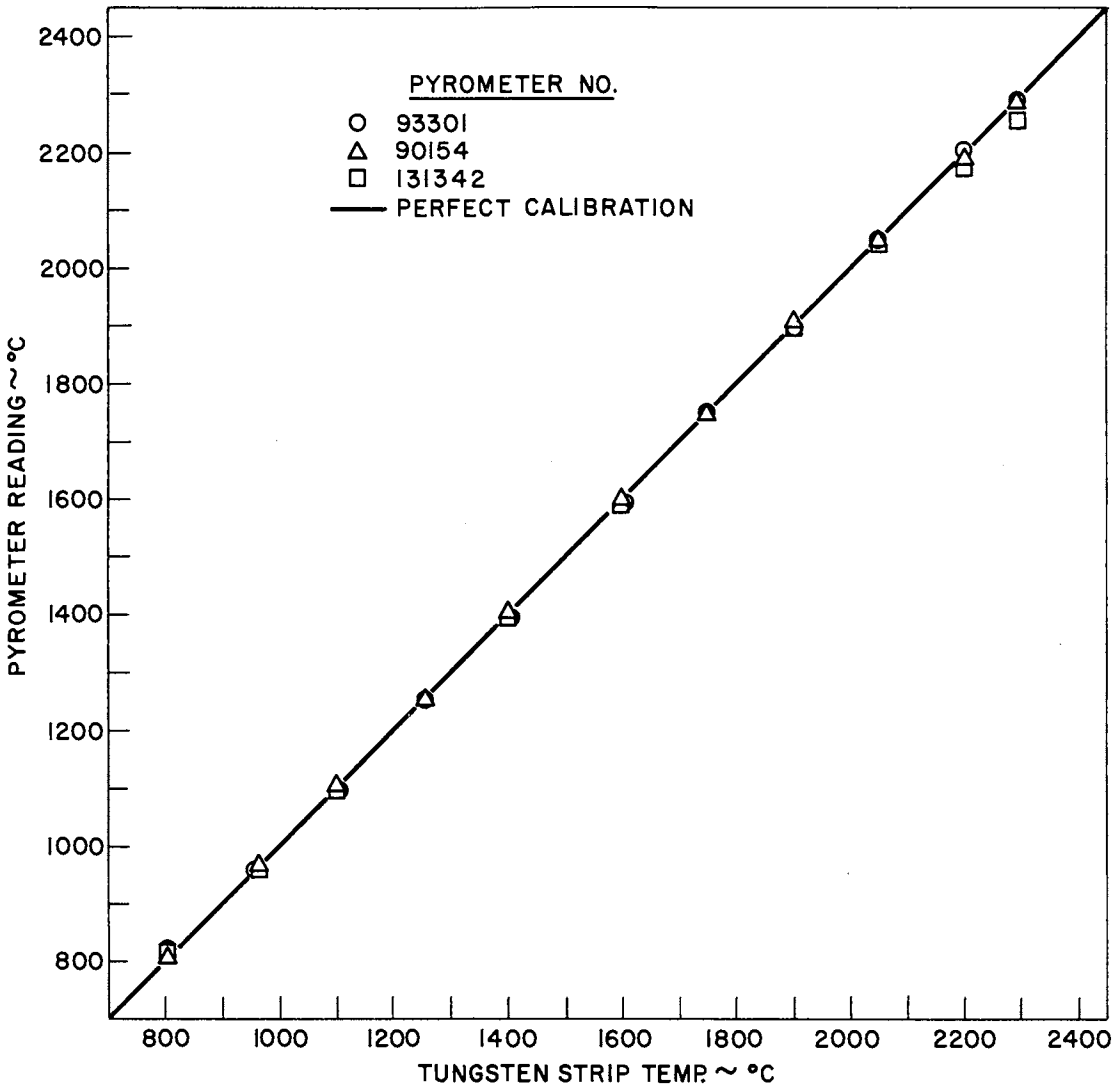

Figure 20. Leeds and Northrup Pyrometer Calibration Curve.

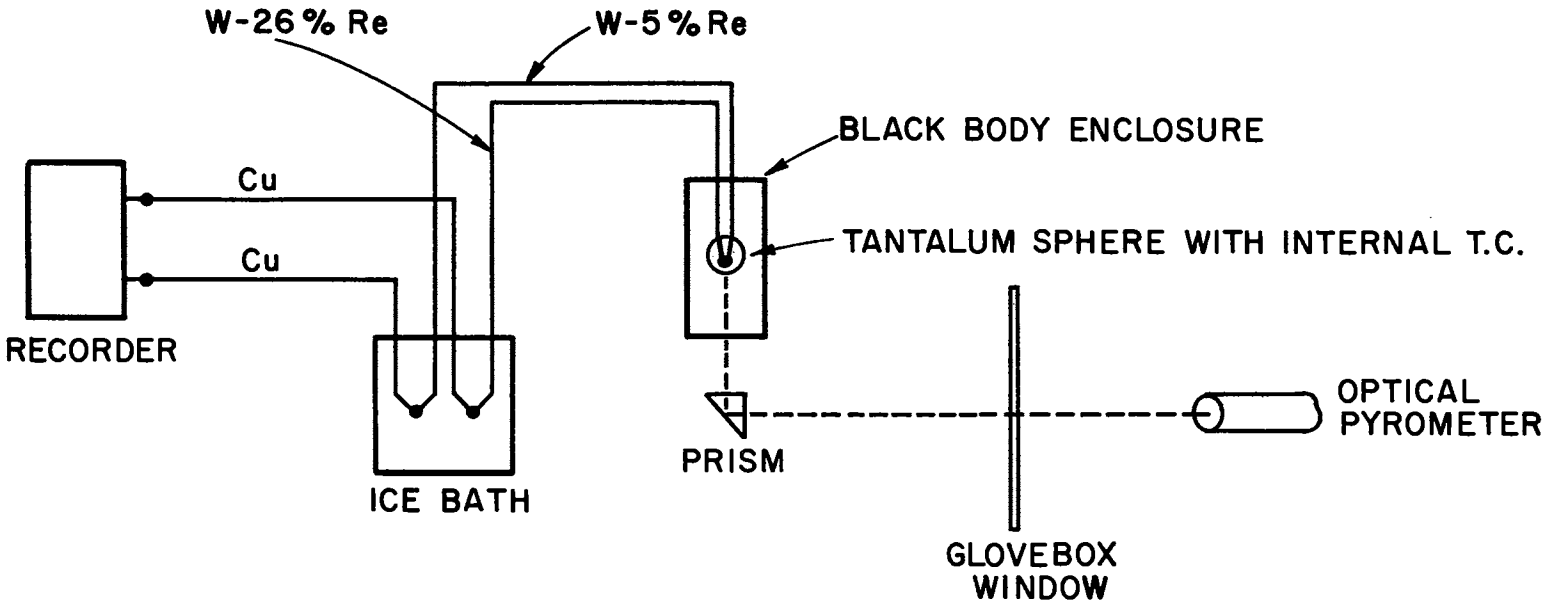

Figure 21. Schematic Diagram of Blackbody Calibration Apparatus.

the shape of the sphere support tube formed the top of the blackbody enclosure. A 0.060-inch diameter hole was drilled in the bottom of the enclosure, and a right angle prism was used to sight the optical pyrometer upon the hole. An additional hole was drilled in the side of the enclosure so that the opposing wall of the enclosure could be compared to the sphere surface. This was to insure that the enclosure was at equilibrium before any calibration points were recorded. The calibration had to be done in an inert atmosphere because tantalum oxidizes readily when heated in air. The calibration apparatus was contained in the argon atmosphere glovebox described in Chapter IV.

The glovebox window and the prism absorbed a small amount of the radiant energy as it passed through them. These effects were taken into account by actually measuring the difference in temperature by observing a tungsten filament lamp directly, and then observing the lamp through the window glass and the prism. At high temperatures, these corrections become appreciable, as can be seen in Figures 22 and 23.

The blackbody calibration data which are shown in Figure 24 indicated sufficient discrepancy to warrant refinement in the calibration technique. Calibration points for one of the thermocouples measured by the blackbody method are shown in Figure 24. Also shown in Figure 24 are points taken by looking directly at the sphere surface and correcting the observed temperature for emittance effects. If a true blackbody existed, these two sets of points should agree rather closely. However, as it can be seen, quite a bit of discrepancy exists between

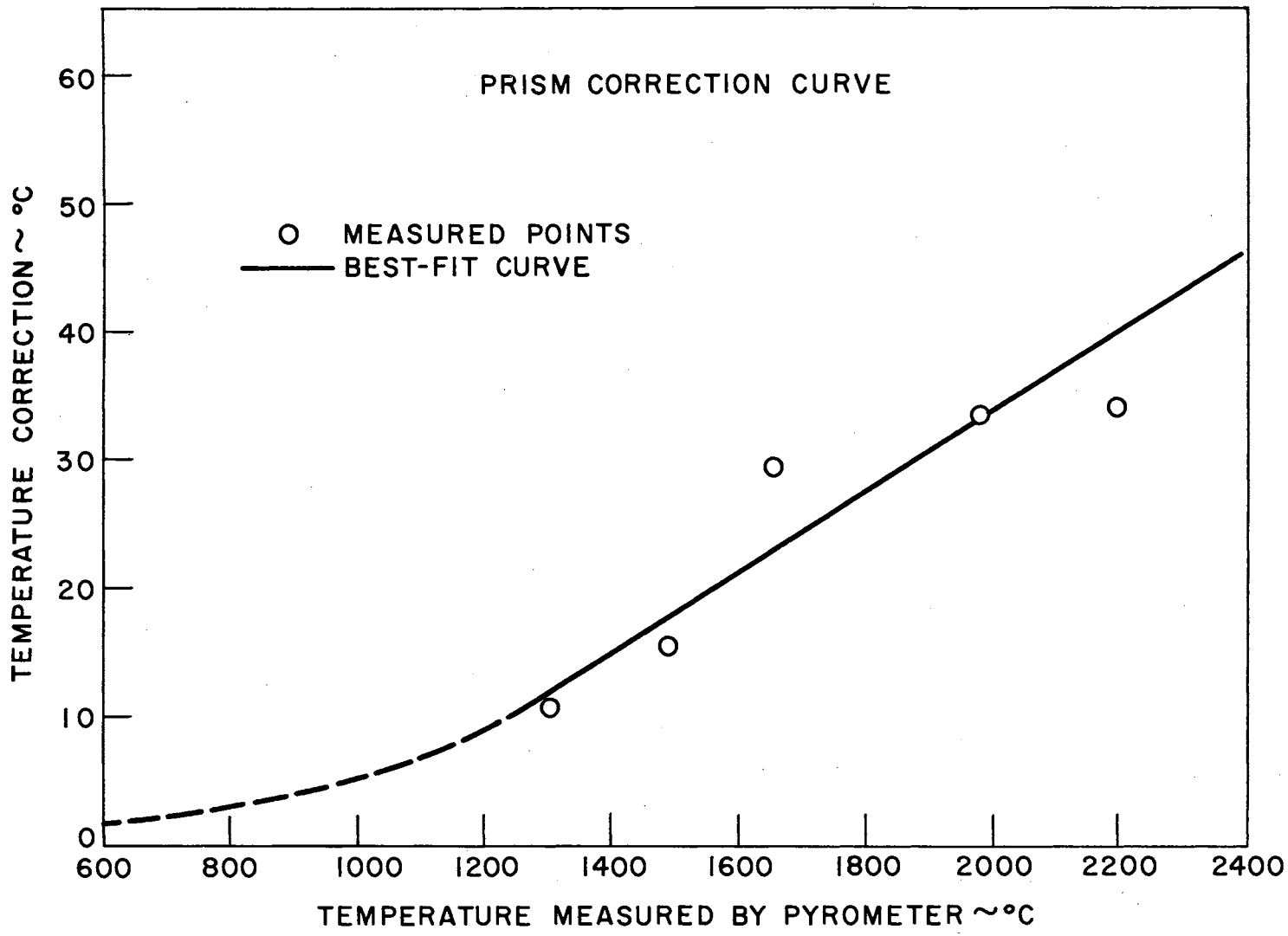

Figure 22. Prism Temperature-Correction Curve.

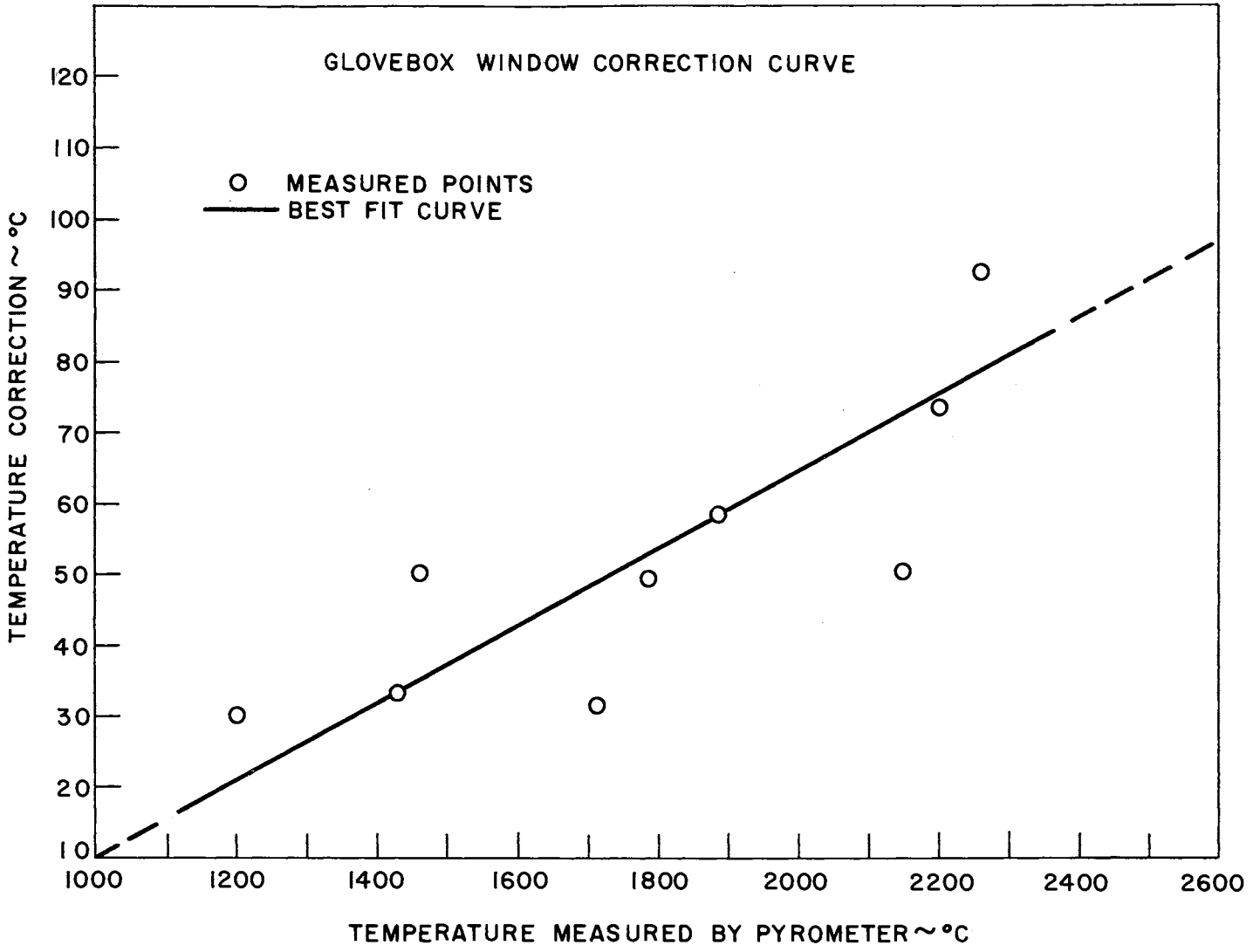

Figure 23. Glovebox Window Temperature-Correction Curve.

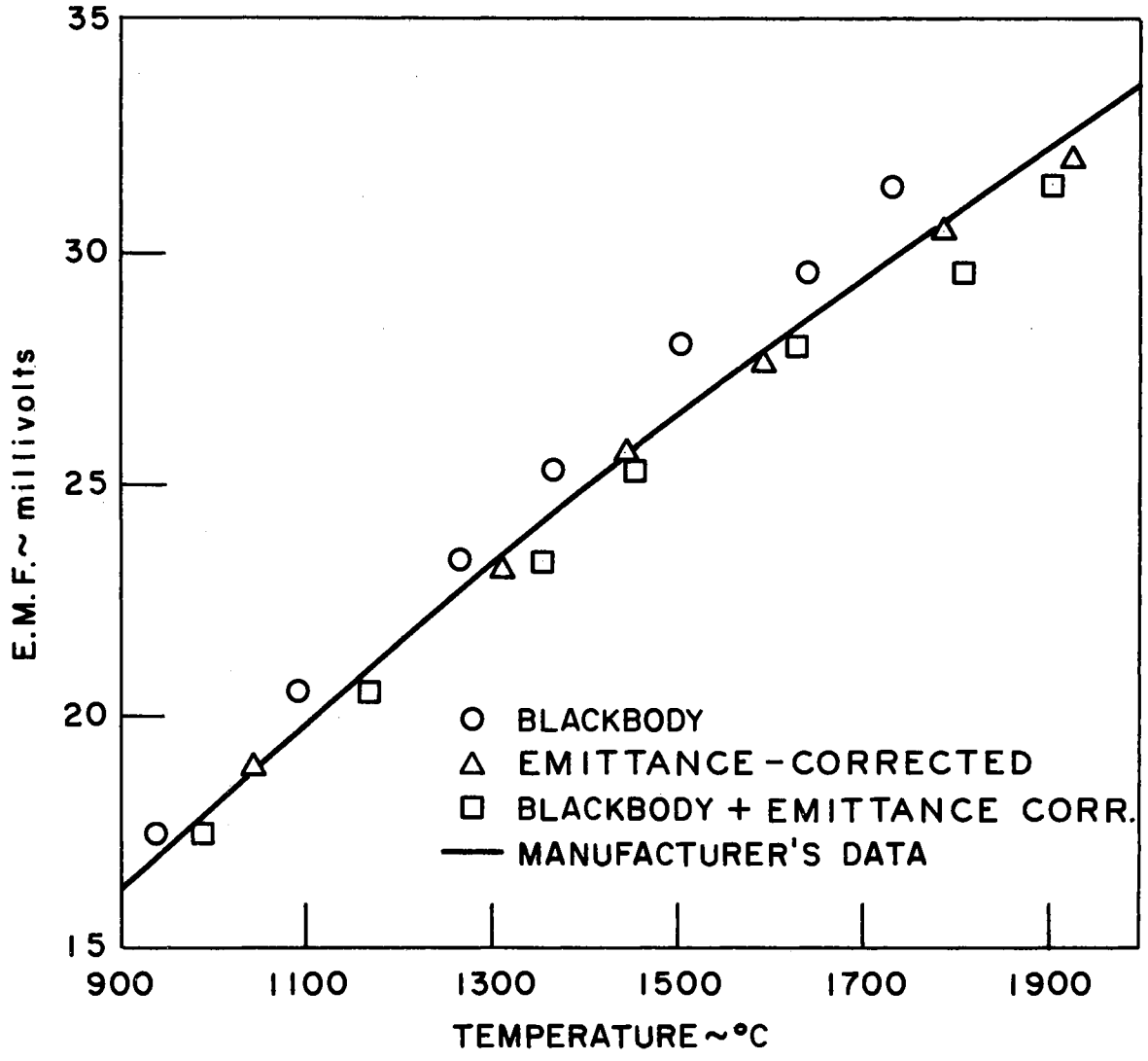

Figure 24. Comparison of Calibration Techniques.

the data sets. The emittance correction was also applied to the points which were presumably taken under blackbody conditions, and these points are also plotted in Figure 24. Actually, these points agree fairly well with the emittance-corrected points. The circular induction coil provided a very uniform temperature distribution on the portion of the tantalum enclosure inside the coil. However, near the ends where the cylinder extended outside the coil for support purposes, considerable temperature variation occurred. The enclosure apparently did not approximate blackbody conditions closely enough for this method to be used. Consequently, the emittance-corrected temperature technique was used in the calibration of sphere thermocouples.

The thermocouples which were used in this experiment were furnished by the Pyro Electric Co. and the Thermo-Couple Products Co. In general, the measured output of the thermocouples did not vary greatly from the manufacturer's data. A typical calibration curve for one of the thermocouples is shown in Figure 25. This curve shows the calibration only up to approximately 1700°C. This particular thermocouple-sphere assembly was used for relatively low temperature data, and consequently the calibration was not carried to higher temperatures. Other thermocouples, however, were calibrated up to approximately 2000°C.

Sphere Heating Difficulties

The major difficulty encountered in the acquisition of the experimental data was in heating the tantalum sphere to relatively high temperatures. In the first set of data runs in which a single turn induction coil was used to heat the tantalum sphere, it was found that

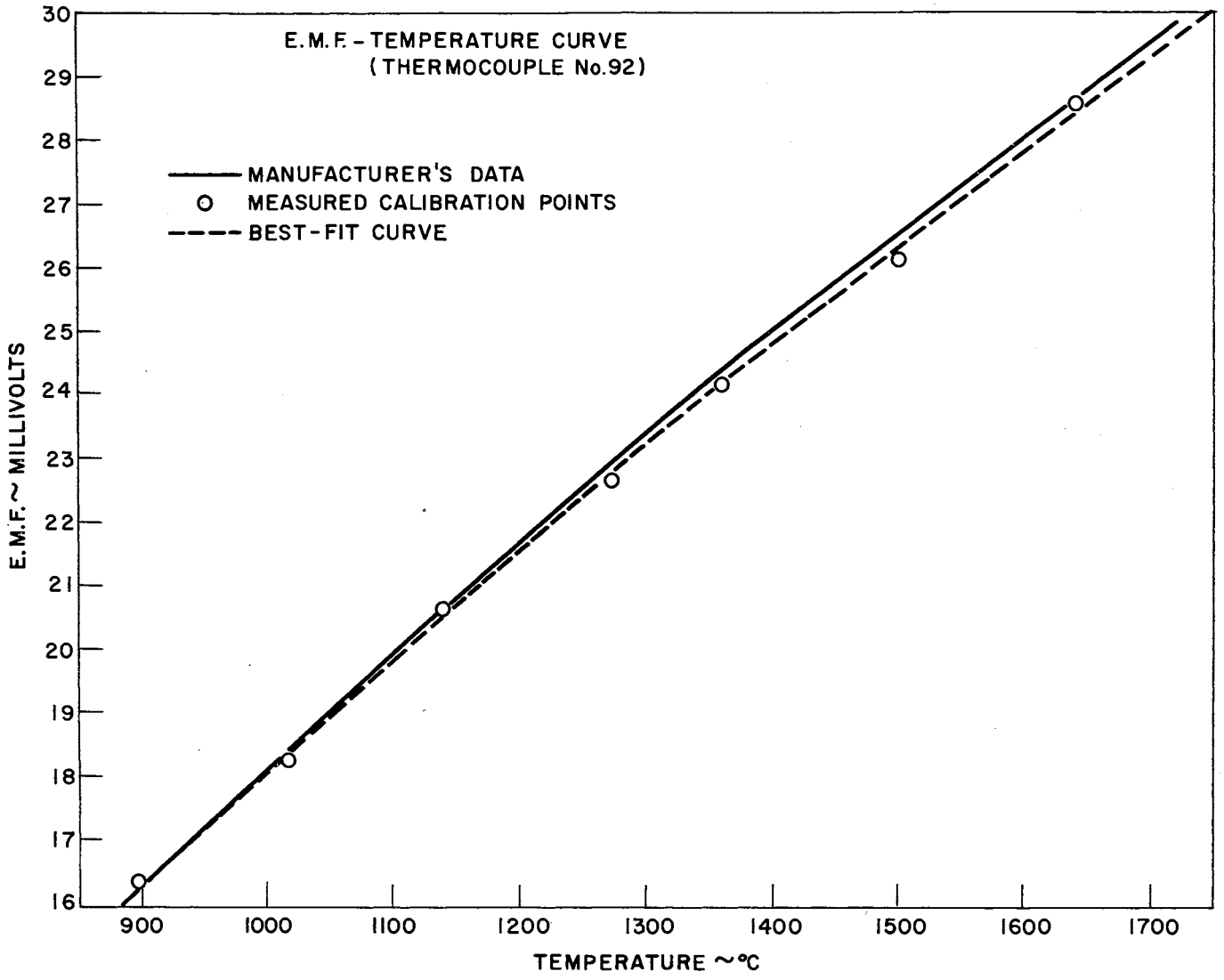

Figure 25. Typical Thermocouple Calibration Curve.

$\sim$ 2750°F was the upper limit for attainable sphere temperature. Usually, prior to attaining 2750°F, arcing between the induction coil and the sphere occurred. Some of these arcs were quite violent in nature, and the surface of the sphere was slightly pitted by them. When the arcing occurred, the induction generator had to be shut down. The reason for the arcing appeared to be ionization of argon gas between the coil and the sphere. Later it was found to be caused by the ionization of sodium vapor rising from the sodium pool surface upward between the coil and the sphere assembly. The problem of arcing was never completely solved, but was minimized greatly by building a more loosely coupled induction coil.

In an effort to achieve more efficient sphere heating, a three turn coil was designed. It was elliptical in shape, and the sphere assembly was free to move in and out of the coil. This coil was somewhat more efficient than the single turn coil and a sphere could be heated to 3700°F with ease if sodium vapor were not present. However, when the sodium was molten and forming vapor, arcing was again prevalent.

A third coil was designed and tested. It was also elliptical in shape but much larger than the previous two coils. A tantalum susceptor was placed inside this coil with the sphere inside the susceptor. It was hoped that the coil would heat the susceptor and the susceptor would, in turn, heat the sphere by radiation. This was done because, apparently, the sphere was absorbing sodium from the pool, and as it was reheated, it outgassed this sodium as great quantities of

vapor, thereby enhancing the arcing problem. Sphere temperatures of approximately 2900°F were achieved by using this technique. Higher sphere temperatures which were necessary for this experiment would have required higher susceptor temperatures than were attainable. The low view factor between the susceptor and the sphere and the low emittance of the tantalum susceptor surface prevented efficient heating of the sphere.

After the failure of the susceptor heating method, the operation of the induction generator was checked. The generator was found to be operating at only 2/3 of its capacity because of two faulty fuses. Upon replacing these fuses, it was found that the third coil design was efficient enough to heat the sphere to well over 3700°F without the use of the susceptor. Since the coil was so loosely coupled to the sphere, the problem of arcing was held to a minimum.

The problem of sphere contamination from exposure to liquid sodium which was mentioned previously was eventually solved by applying rigid cleanliness requirements to the sphere. It was found that if a sphere was used for no more than four data runs and then removed from the apparatus and cleaned with alcohol and abrasive cloth, it could be kept relatively clean. After removing the superficial deposition from the sphere with abrasive cloth, the sphere was returned to the apparatus and reheated to approximately 3450°F. This had the effect of removing any discoloration remaining on the sphere surface, and the sphere returned to a bright, shiny condition identical to its

original as-fabricated condition.

One of the spheres which had been exposed to liquid sodium for several runs was sectioned, polished, and photomicrographed. For comparison, a sphere which had not been exposed was also photomicrographed. The results can be seen in Figure 26. The surface of the exposed sphere is relatively rough with apparent corrosion pitting of the surface, and with cracks extending down into the sphere to a depth of approximately 0.020 inches. These cracks were probably caused by thermal stresses experienced by the sphere as it passed through the liquid sodium.

Tantalum is very susceptible to hydrogen absorption. Since opportunities were present for the tantalum sphere to absorb hydrogen during the experiments, it was felt that perhaps this had occurred and was contributing to the heating problem. The addition of hydrogen in the purification system provided the opportunity for hydrogen to be present in the system. Consequently, one of the spheres which had been used in experimental runs was subjected to a vacuum diffusion test for hydrogen. The hydrogen content proved to be rather high, approximately 100 ppm. As a check, a piece of tantalum from the rod stock which was used to make the sphere was also subjected to the same test. This sample actually showed higher hydrogen content, 200 ppm., than the sphere. Therefore, the idea that hydrogen contamination of the tantalum sphere was contributing to the heating problems was discarded.

While heating the sphere in the induction heating device, the

(a)

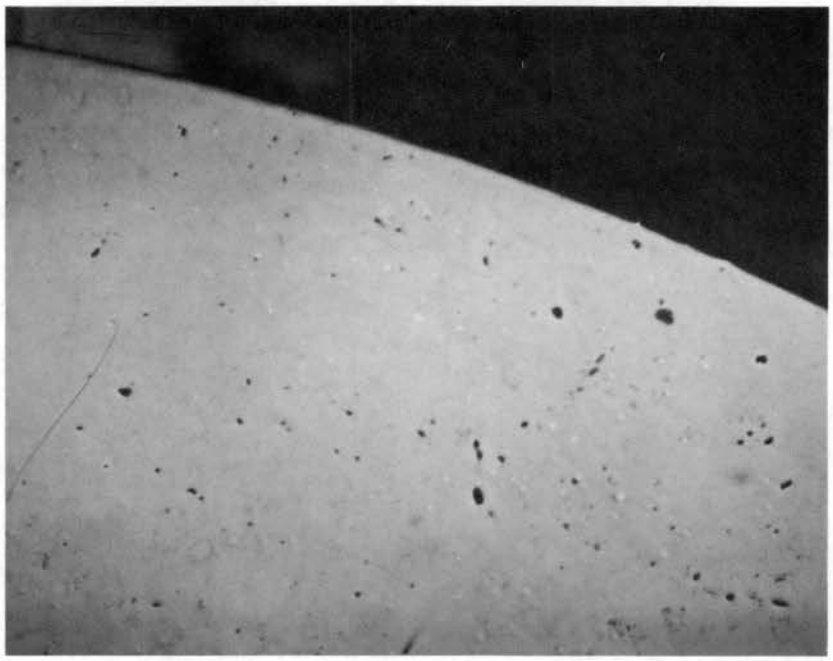

(b)

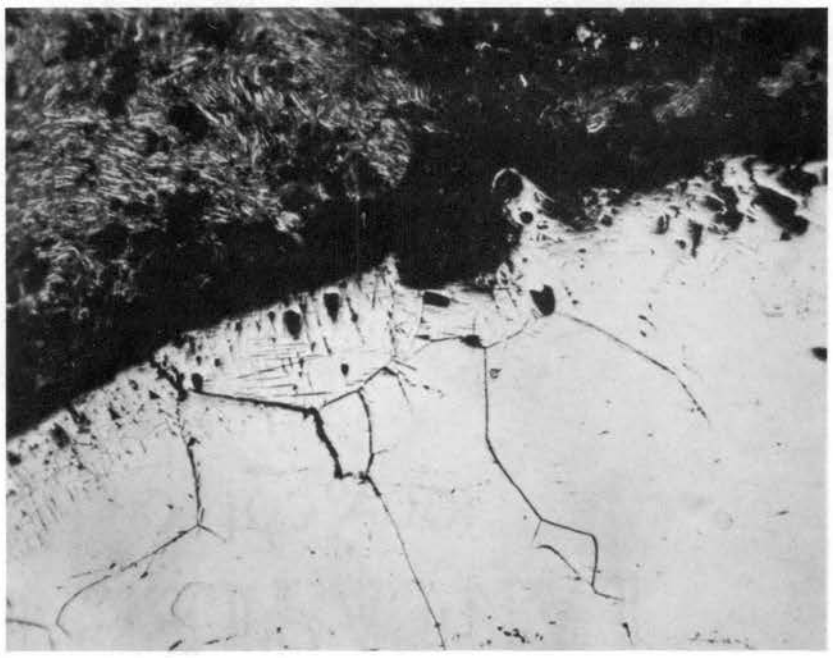

Figure 26. Photomicrograph of Tantalum Sphere: (a) As-Fabricated, (b) After Several Data Runs (90X).

high frequency of the induced current seriously affected the sphere temperature recordings. The galvanometer deflected very randomly and rapidly. The light beam appeared to be approximately 1/2-inch wide to an observer's eye, and also was altered somewhat from the actual value of the thermocouple signal. As soon as the induction generator was shut down, the signal assumed its proper value in a matter of only 20 to 30 milliseconds. This, therefore, did not seriously affect the operation of the equipment since the sphere moved from the induction coil prior to striking the sodium pool. The generator was also shut down prior to the sphere leaving the coil. However, this phenomenon did prevent duplicate runs from being made, since the initial temperature of the sphere could never be predicted with any degree of accuracy.

Sodium Cleanliness

On one occasion upon heating the sodium with relatively high oxygen content in the argon gas, a strange formation appeared upon the surface of the sodium pool. This formation appeared quite porous in nature, and in no way resembled the oxide film which normally formed on the sodium pool surface. The experiment was immediately terminated and a sample of the formation was submitted for chemical analysis. It proved to be very high in silicon content. Apparently, silicone oil from the induction heating coil cooling system had been spilled inadvertently into the sodium tank while an induction coil was being changed. Precautions were taken in subsequent experiments to prevent spillage of silicone oil into the sodium, and no further

problems of this kind were experienced.

The sodium which was used for the first 25 data runs was found to be quite dirty upon removing it from the tank. There was a "sludge" near the bottom of the tank which was quite coarse in its composition. A sample of this "sludge" was submitted for chemical analysis. It proved to be highly pyrophoric and extremely difficult to handle. Nothing extraordinary was reported from the analysis. Bearing this in mind, the sodium in the tank was changed frequently, and a very clean sodium pool was maintained.

The sodium used in the experiment was furnished by the Baker and Adamson Co., and was reagent grade. Table I gives the limits of impurities which could have been present in the sodium as specified by the manufacturer.

Table I

LIMITS OF SODIUM IMPURITIES

Substance	Cl	PO_4	Fe	Heavy Metals
Limit of Impurity %	0.0015	0.0005	0.001	0.0005

The percentage of other impurities such as SO_4 and nitrogen were less than those specified by the ACS Code 2188.

Experimental Technique

The operating procedure given in Appendix B was followed for the series of experimental runs with the sodium heat transfer apparatus.

This sequence of events usually took 5 to 8 hours to complete. The actual data-taking took only a small portion of this time. The most time-consuming part of the sequence was heating and cooling the sodium and achieving steady state sodium conditions. Steady state conditions were achieved by simply adjusting the power input to the sodium tank electrical heaters until the heat losses and heat input were balanced at the desired sodium temperature. The temperature of the sodium tended to drift somewhat, and constant vigilance was required to maintain a steady sodium temperature. This did not present a serious problem.

The recorded data obtained in these experiments consisted of thermocouple emf-time traces. The emf-time data were converted into temperature-time data in the following way. During data runs, the bias circuit described in Chapter IV was used to position the galvanometer mirror trace at the desired spot on the recorder paper. Upon the completion of the data run, a plot of emf versus scale deflection for the bias circuit setting which was used in the run was made. The values for this plot were obtained by replacing the thermocouple with a potentiometer and recording the emf values required to deflect the galvanometer mirror trace over the range of the recorder paper. One of these plots is shown in Figure 27. By using a plot of this kind, data were converted into emf-time data. The thermocouple calibration curves such as the one shown in Figure 25 were then used to convert the emf-time data into temperature-time data. A complete description of the data reduction methods is given in Chapter VI.

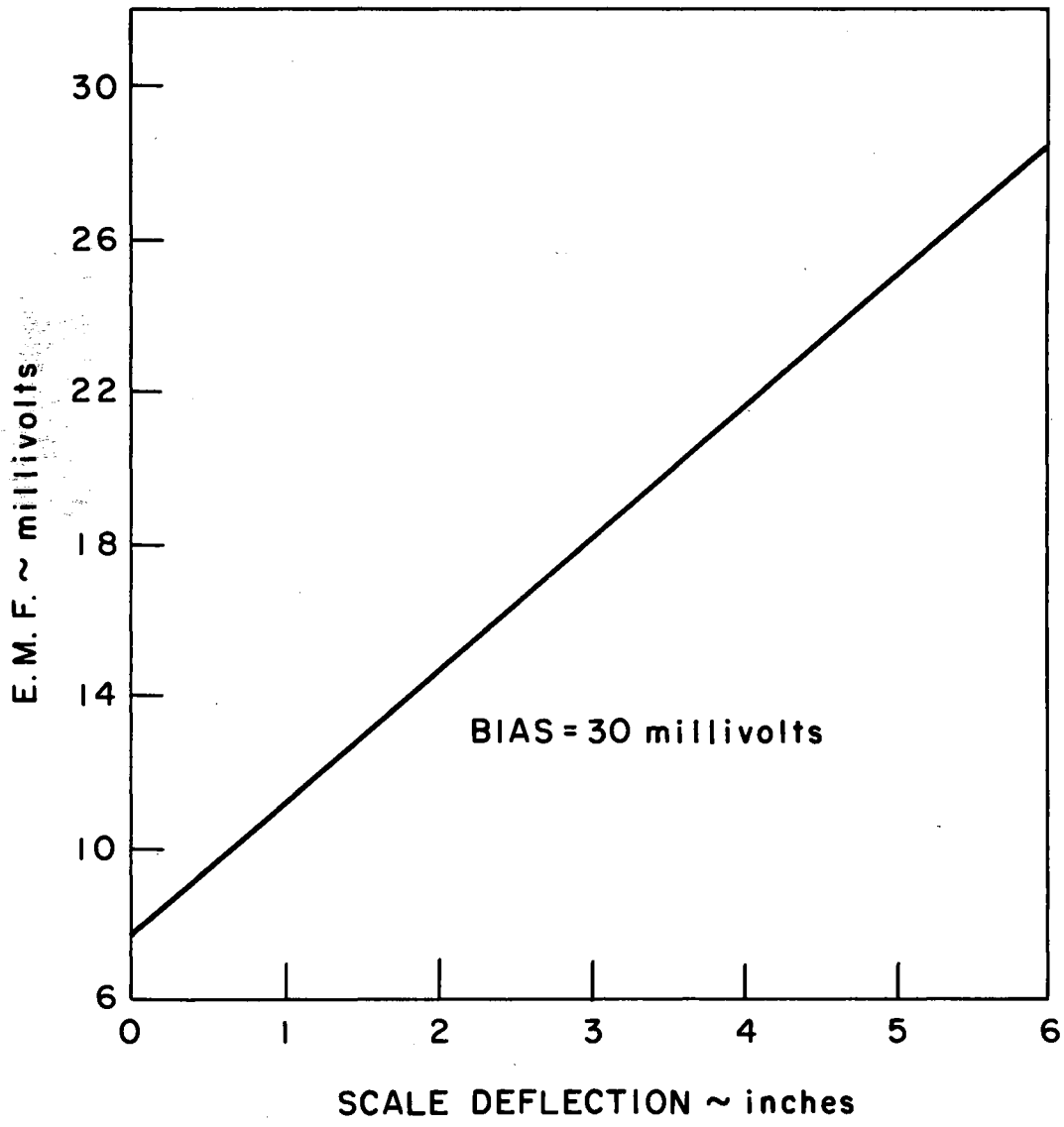

Figure 27. Typical EMF-Deflection Conversion Chart.

CHAPTER VI

EXPERIMENTAL RESULTS

A total of 87 experimental data runs were performed in the course of this investigation. Measurements were made in 572°F (300°C) and 842°F (450°C) sodium. Runs 1 through 27 should be termed exploratory in nature since uncertainty was present concerning the cleanliness of the sodium and the surface conditions of the tantalum sphere. Runs 28 through 31 were not useful since the thermocouple which was used in these runs exhibited poor response characteristics. Runs 32 through 57 were also made with thermocouples with poor response. However enough information was extracted from these runs to enable their use to show reproducibility of data. Run 58 was also exploratory. Runs 59 through 87 were used to compute the heat flux versus surface temperature data which are presented in this chapter.

The experimental data are presented in Appendix C. The experimental runs were numbered consecutively as they were taken. Since Runs 1 through 27 were exploratory and not used in the calculation of heat fluxes, they are not presented. Runs 28 through 57 are presented in tabular form giving the initial temperature, the exit equilibrium temperature, and the time that the sphere was exposed to sodium. Runs 59 through 87 are presented as temperature-time data

as reduced from the data records. The time of entry into the sodium pool is denoted as time = 0.

Methods of Data Reduction

The data were reduced by a technique developed by Stolz (61). This technique enables the calculation of the surface heat flux and surface temperature versus time for a sphere for which a temperature history at a known radial point is known. Initially the sphere must be considered isothermal.

The accuracy of this data reduction method was determined by calculating surface heat flux and temperature for a case where the heat flux and temperature histories were accurately known. The case considered was a 1/2-inch diameter sphere undergoing convective cooling described by the relation,

$$(q/A) = h(T_w - T_B)$$

where T_w refers to the surface temperature of the sphere and T_B to the bulk temperature of the surrounding medium. The heat transfer coefficient, h, was considered constant for purposes of convenience. The analytical solution to this problem is,

$$\frac{T - T_B}{T_i - T_B} = 2\frac{R}{r}\sum_{n=1}^{\infty} \frac{\sin M_n - M_n \cos M_n}{M_n(M_n - \sin M_n \cos M_n)} e^{-M_n^2\theta} \sin\left(M_n\frac{r}{R}\right), \quad (37)$$

where $\theta = \frac{\alpha t}{R^2}$, t is time, and M_n is defined by the relation,

$$1 - M_n \cot M_n = Nu$$

The Nusselt number, Nu, is defined by,

$$Nu = \frac{hR}{k}$$

Figure 28 shows the surface temperature and the temperature at a radial point of 0.85 R for the heat flux which is also shown. The temperature history for the radial point r = .85 R was used as input for the data reduction technique of Stolz. The results of the calculation are shown in Figure 28 as discrete points. Both the heat flux and surface temperature computed by the Stolz method compare very well with the analytical solution. The first calculated heat flux point in time is somewhat low but the method quickly converges to the correct values.

It was found that for some of the data runs in which relatively high initial temperatures were encountered the data reduction method of Stolz had to be augmented by an alternative data reduction scheme. The measured temperatures dropped so rapidly in the initial part of the data run that the Stolz method of data reduction exhibited convergence difficulties unless rather long incremental time steps were used. However, much detail in the heat flux versus surface temperature data was lost if longer time increments were used. Therefore it was felt inappropriate to use these longer increments.

The data reduction difficulty was resolved by utilizing two methods of data reductions and "piecing" the two methods together. The "constant h" analytical solution given in equation (37) was used

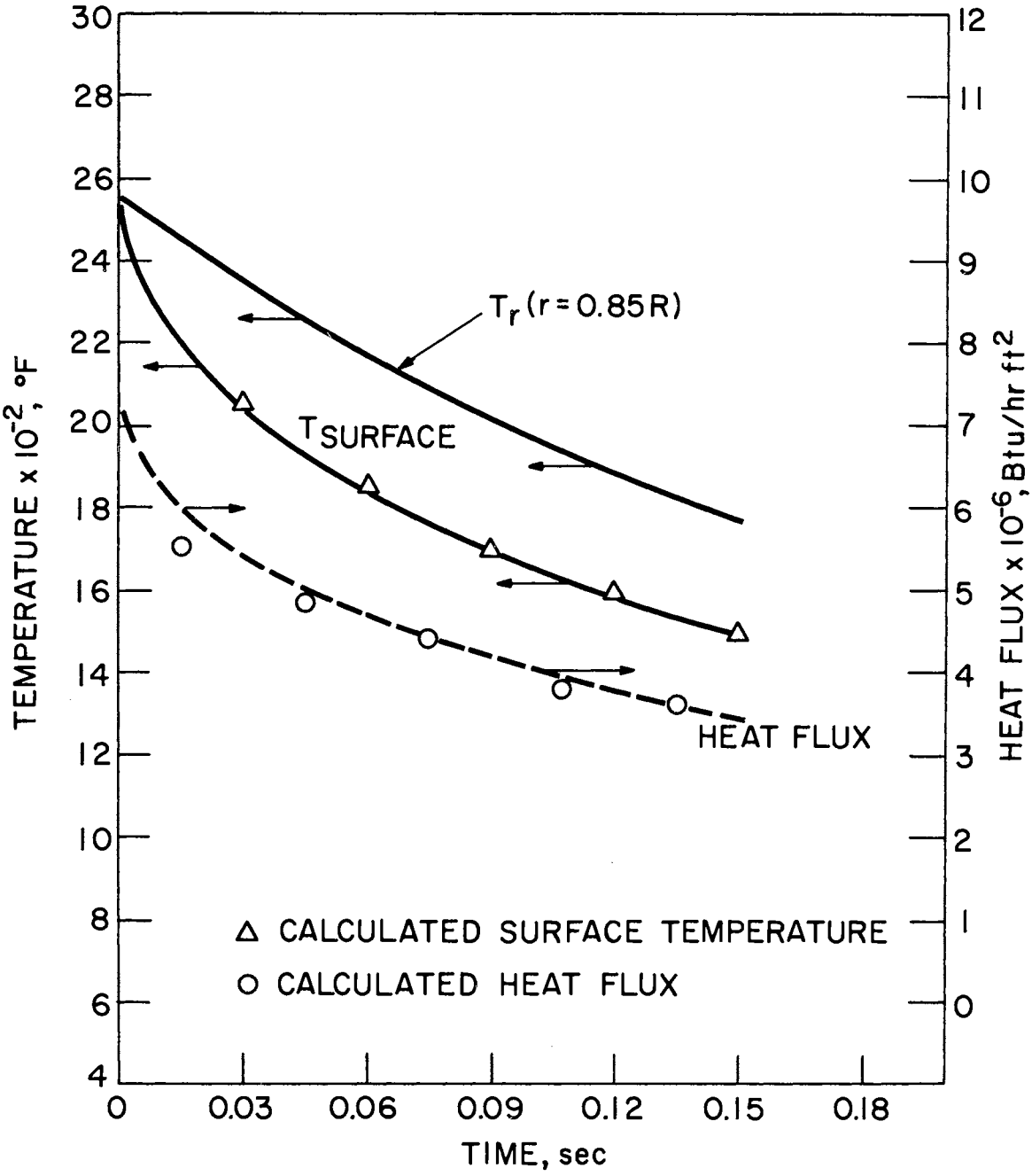

Figure 28. Comparison of Heat Flux and Surface Temperature Calculated by Stolz' Method to Analytical Solution.

as follows. The measured temperature history at the known radial location for a data run was plotted in dimensionless form as shown in Figure 29. Run 71 has been used as an example. An h value was selected in an effort to "match" the measured temperature with the analytical solution. The measured temperature history was matched only over a very short time interval at the beginning of the data run, usually approximately 0.01 sec. Once the correct value for h was found, the heat flux and surface temperatures were calculated. The data reduction method of Stolz was also applied to the data run. A time interval was selected for which the solution would show convergence. Figure 30 shows these calculated points for Run 71. The points which were calculated near the initial part of the data run are omitted. Figure 30 also shows the results of the "h matching" for Run 71. The solutions are "pieced" together by fairing curves through the heat flux and surface temperature points. The points which are calculated further in time by the Stolz method are generally considered more accurate than those which are calculated near the initial portion of the run. Consequently these points and the high temperature points which are calculated by the analytical solution are used primarily to define the heat flux and surface temperature histories for any particular data run for which the "piecemeal" solution was necessary. This piecemeal type of data reduction allowed the data to be reduced without great loss of detail. Both high and low temperature points could be obtained with this method. Computer programs which use these methods were written

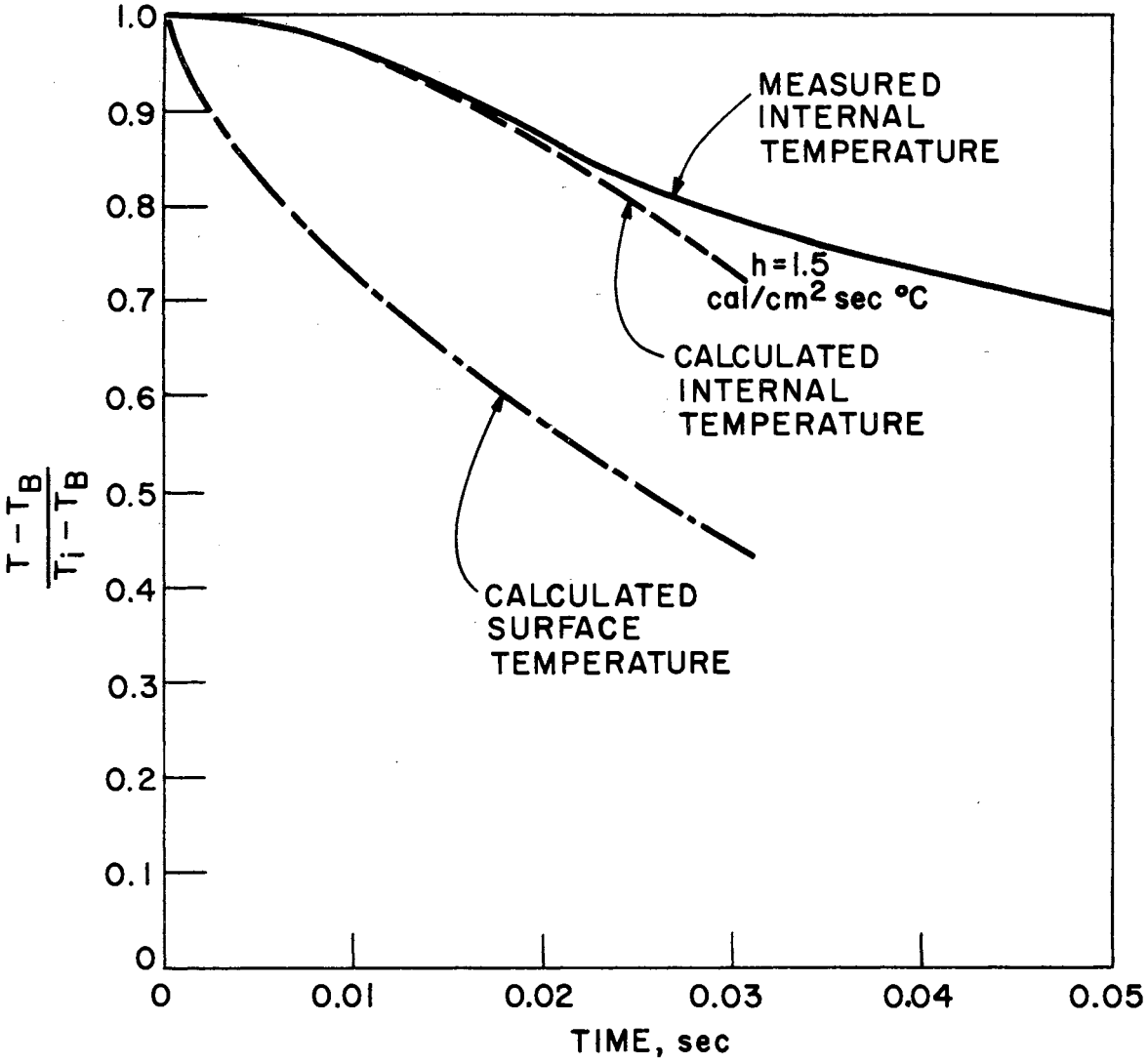

Figure 29. Matching Technique for Data Reduction in Initial Portion of Data Run.

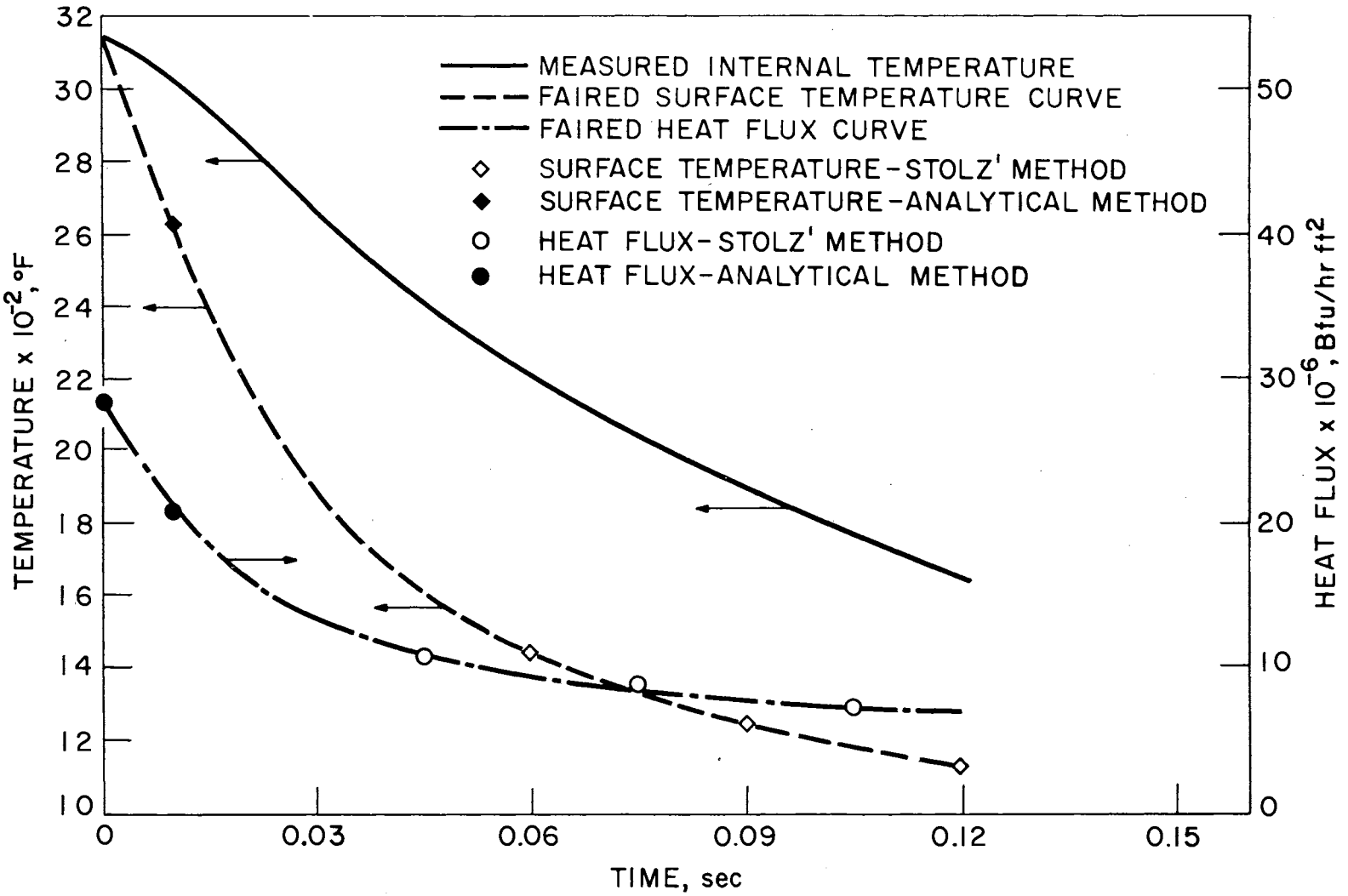

Figure 30. Data Reduction Method Utilizing both Analytical Method and Stolz' Method.

and are shown in Appendix D.

A third method of data reduction was based upon equilibrium consideration of the sphere temperature before and after encountering the sodium pool. This method was used primarily for reduction of data which were taken with thermocouples which exhibited poor response characteristics. Average heat flux at some average sphere temperature could be obtained for each data run by using this technique. The average heat flux from the sphere to the liquid sodium pool due to the sphere's encounter with the pool can be written as,

$$(q/A)_{avg.} = \frac{m\ \Delta H}{A\ \Delta t} \quad ,$$

where m is the mass of the sphere, ΔH is the change in enthalpy, A is the surface area of the sphere, and Δt is the time that the sphere was exposed to sodium. If the change in temperature of the sphere due to its encounter with the sodium pool is known, an accurate estimate of the change in enthalpy can be made.

A technique for obtaining the equilibrium temperature of the sphere after its exit from the sodium pool was developed. The equilibrium temperature of the sphere prior to its striking the sodium pool was simply that temperature recorded by the imbedded thermocouple. This is a very close estimate since cooling of the sphere in argon gas is very slow and the sphere can be assumed to be at one temperature. The technique for obtaining the exit equilibrium sphere temperature is shown in Figure 31. It consists of plotting the measured temperature-time history for

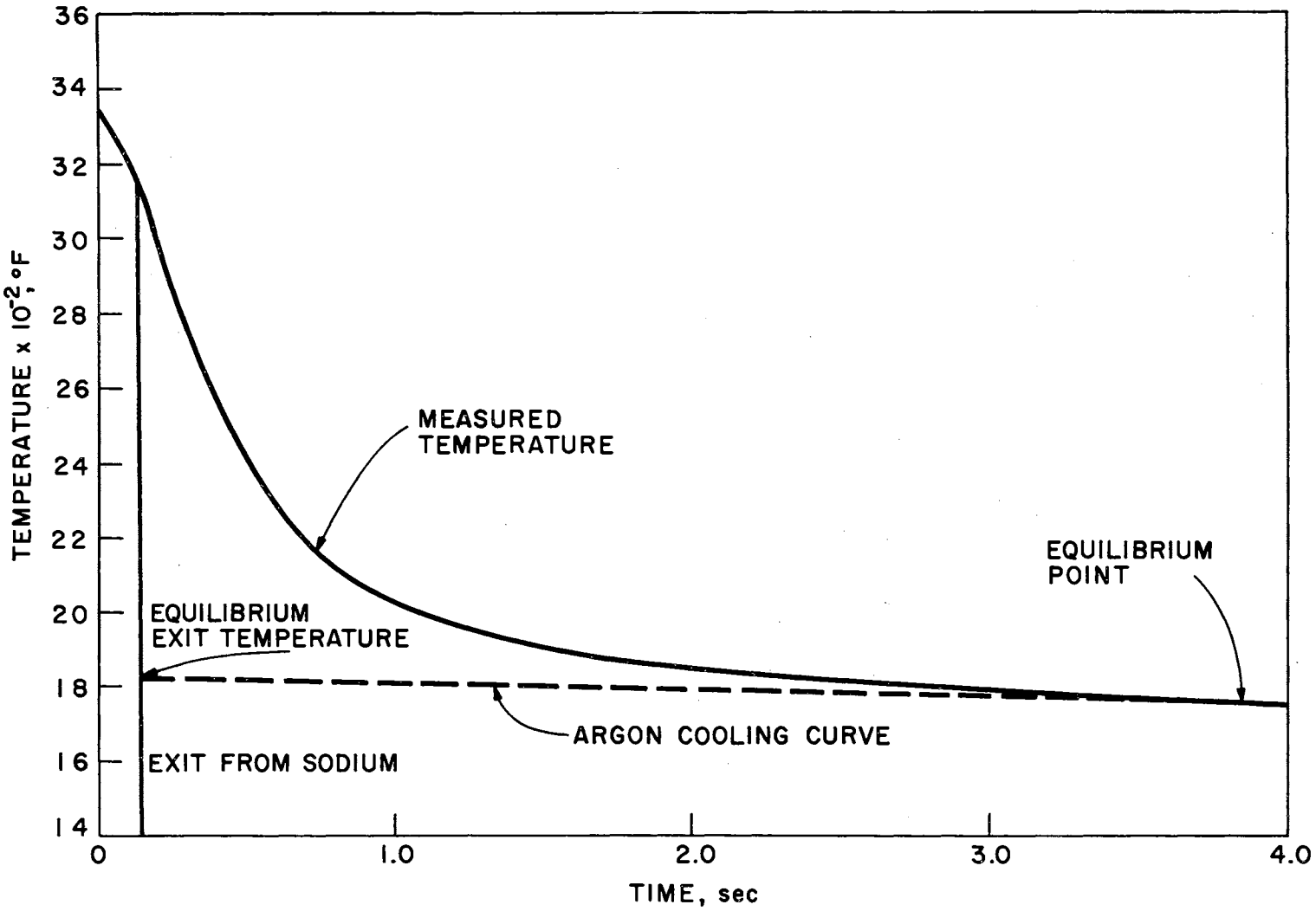

Figure 31. Technique for Obtaining Sphere Exit Equilibrium Temperature.

the data run to the point in time where the sphere has once again reached its equilibrium cooling rate. This was done by superimposing a cooling curve for the sphere in argon gas upon the measured temperature trace. The equilibrium point was taken as the point where the slopes of the curves first coincided. To correct for the amount of heat transferred from the sphere to the argon during the time between exit and the attainment of equilibrium, the argon cooling curve was plotted back to the time of exit. This temperature point was used as the sphere exit equilibrium temperature.

The average heat flux which was obtained in this manner was referenced to an average temperature which was found by arithmetically averaging the entrance and exit equilibrium temperatures.

Reproducibility of Results

Runs 32 through 57 were performed to show reproducibility of heat fluxes obtained from different sphere-thermocouple assemblies. Two different batches of sodium were also used. The thermocouples which were used in these runs exhibited poor response. An example of one of these data records is shown in Figure 32. These data were reduced according to the equilibrium technique described in a previous section of this chapter. These data are presented in Figure 33. Although some experimental scatter is present, very good agreement between data taken with different sphere-thermocouple assemblies exists. No effect of changing sodium was evident. All these data were taken in 572°F (300°C) sodium at a sphere velocity of approximately 10 ft/sec.

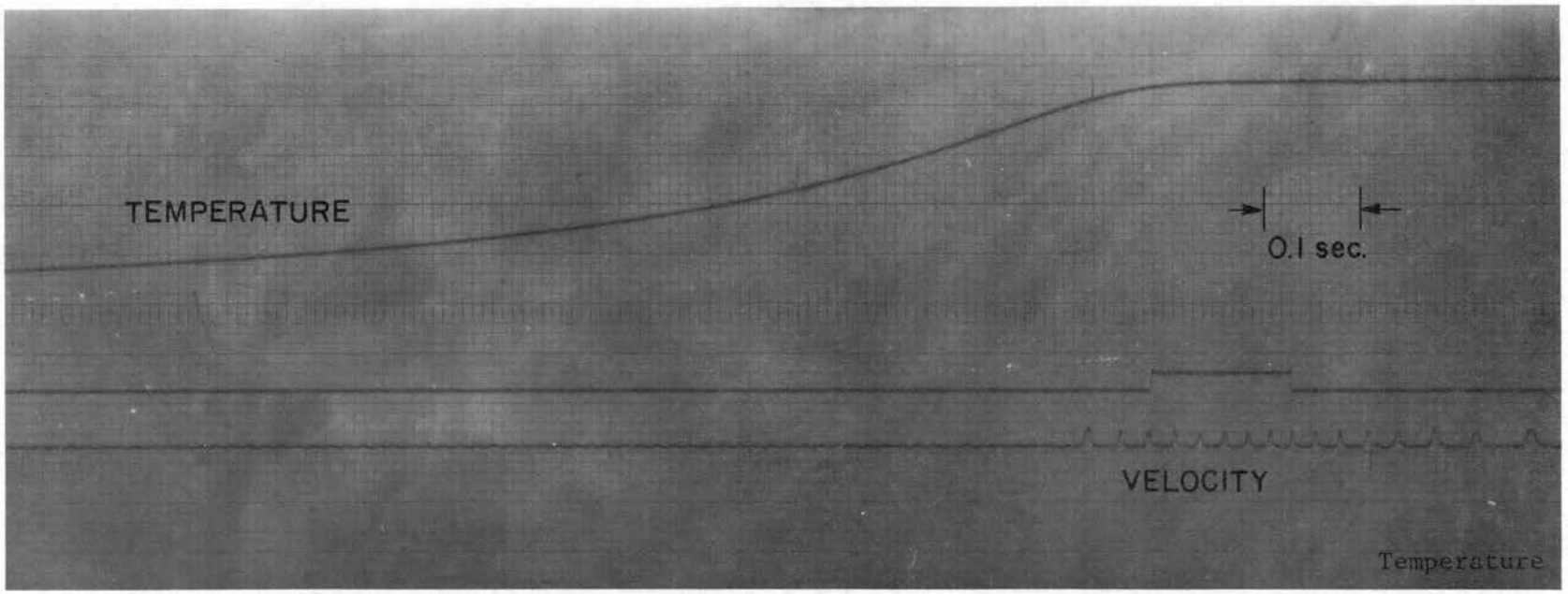

Figure 32. Oscillograph Record - Poor Thermocouple Response.

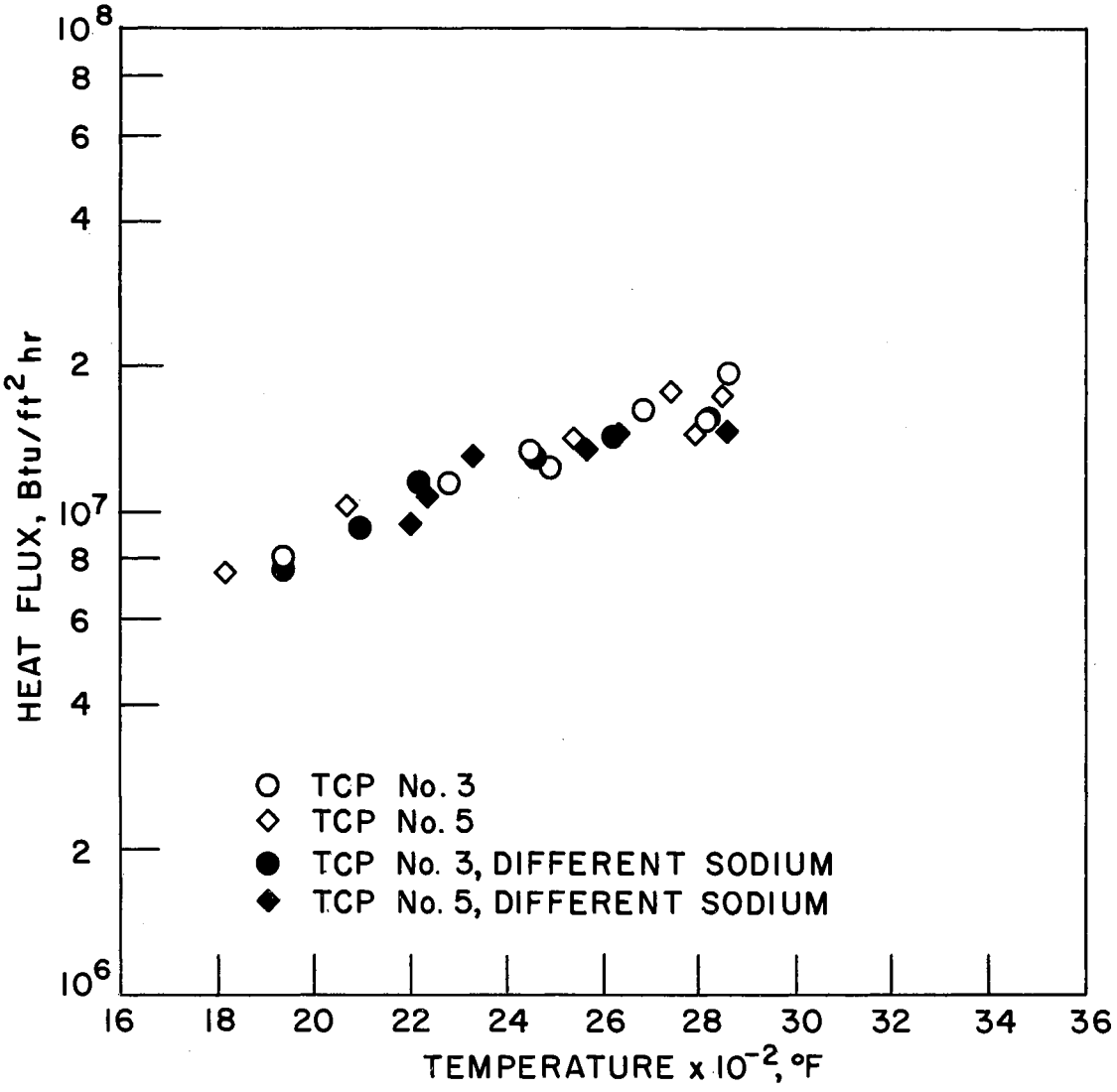

Figure 33. Average Heat Flux versus Average Sphere Temperature: U_∞ = 10.0 ft/sec, T_{Na} = 572°F.

Presentation of Data

Data obtained in Runs 59 through 87 were used to calculate the heat flux versus sphere surface temperature data which are presented in this section. These data were taken with thermocouples which exhibited excellent response characteristics. An example of one of these data runs, Run 59, is shown in Figure 34. Some of the data runs were duplications of previous runs. Consequently only one run of a duplicated run was reduced.

Figures 35 through 38 present the data which were taken in 572° (300°C) sodium. Figure 35 shows data which were obtained at a sphere velocity of approximately 10.0 ft/sec. The data in Figure 35 were obtained with the thermocouple located near the stagnation point of the sphere. This was accomplished by bending the sphere support tube through a 90-degree angle. Consequently the sphere was pushed through sodium with the support tube in the wake region. Figure 36 shows data which were also taken at approximately 10.0 ft/sec but with the support tube straight. Consequently the thermocouple location was near the 90-degree point in the sodium flow field. The data which were taken with the bent support tube are considered more representative of the actual heat transfer process than those taken with a straight support tube. The straight support tube, located at the 90-degree position, could have affected the heat transfer process occurring on the sphere surface. The bent support tube is located at the 180-degree position in the wake

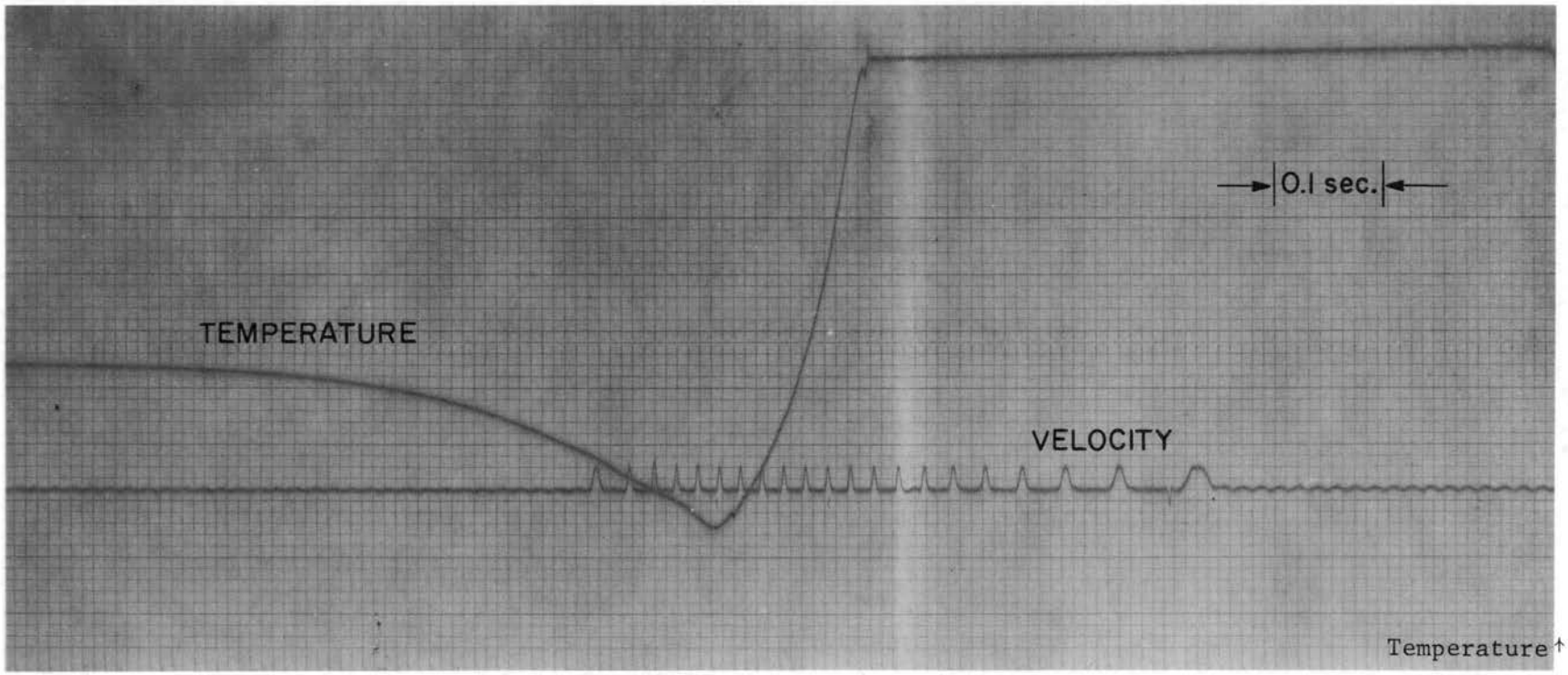

Figure 34. Oscillograph Record - Good Thermocouple Response.

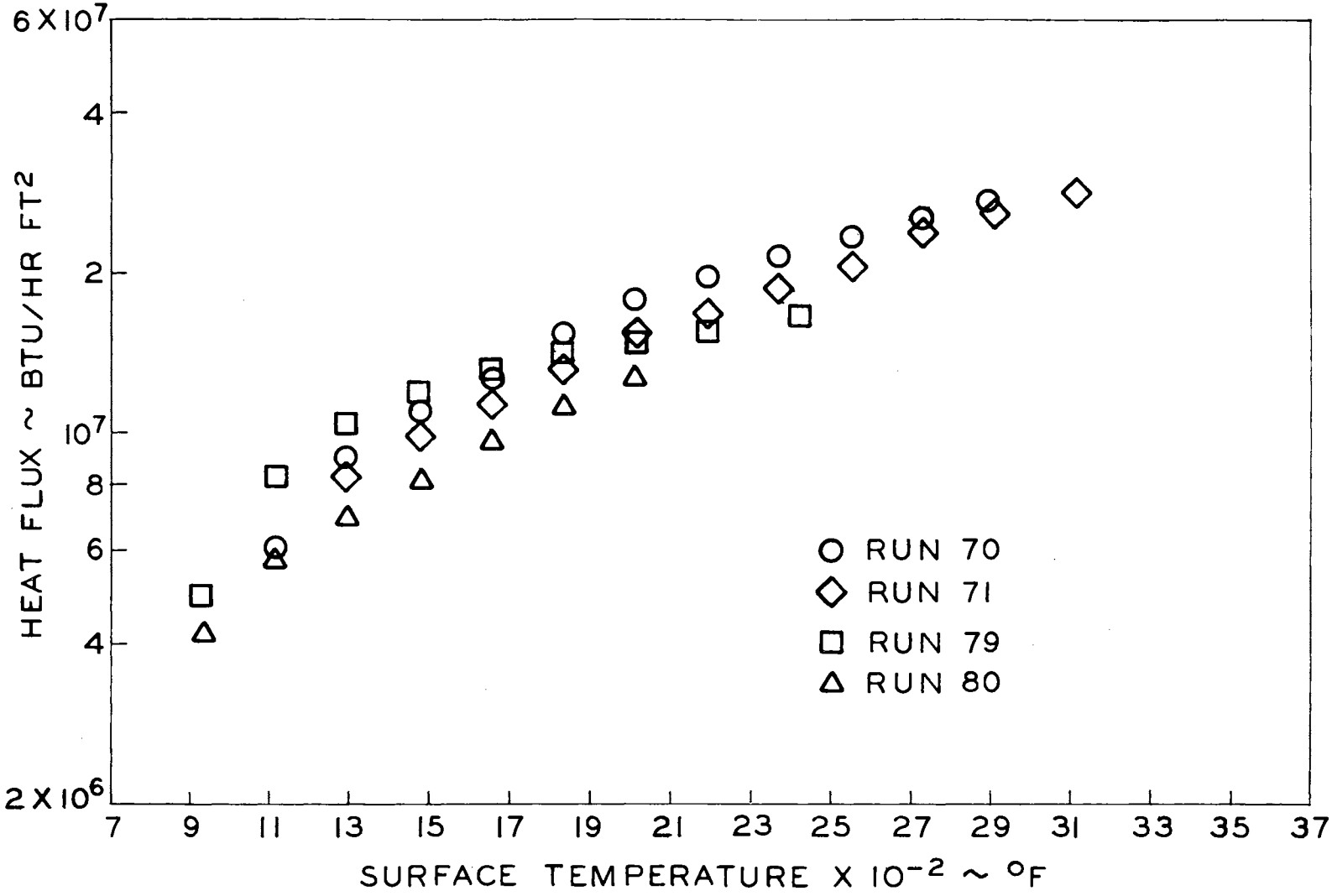

Figure 35. Heat Flux Versus Surface Temperature = U_∞ = 10.0 ft/sec, T_{Na} = 572°F; Bent Support Tube

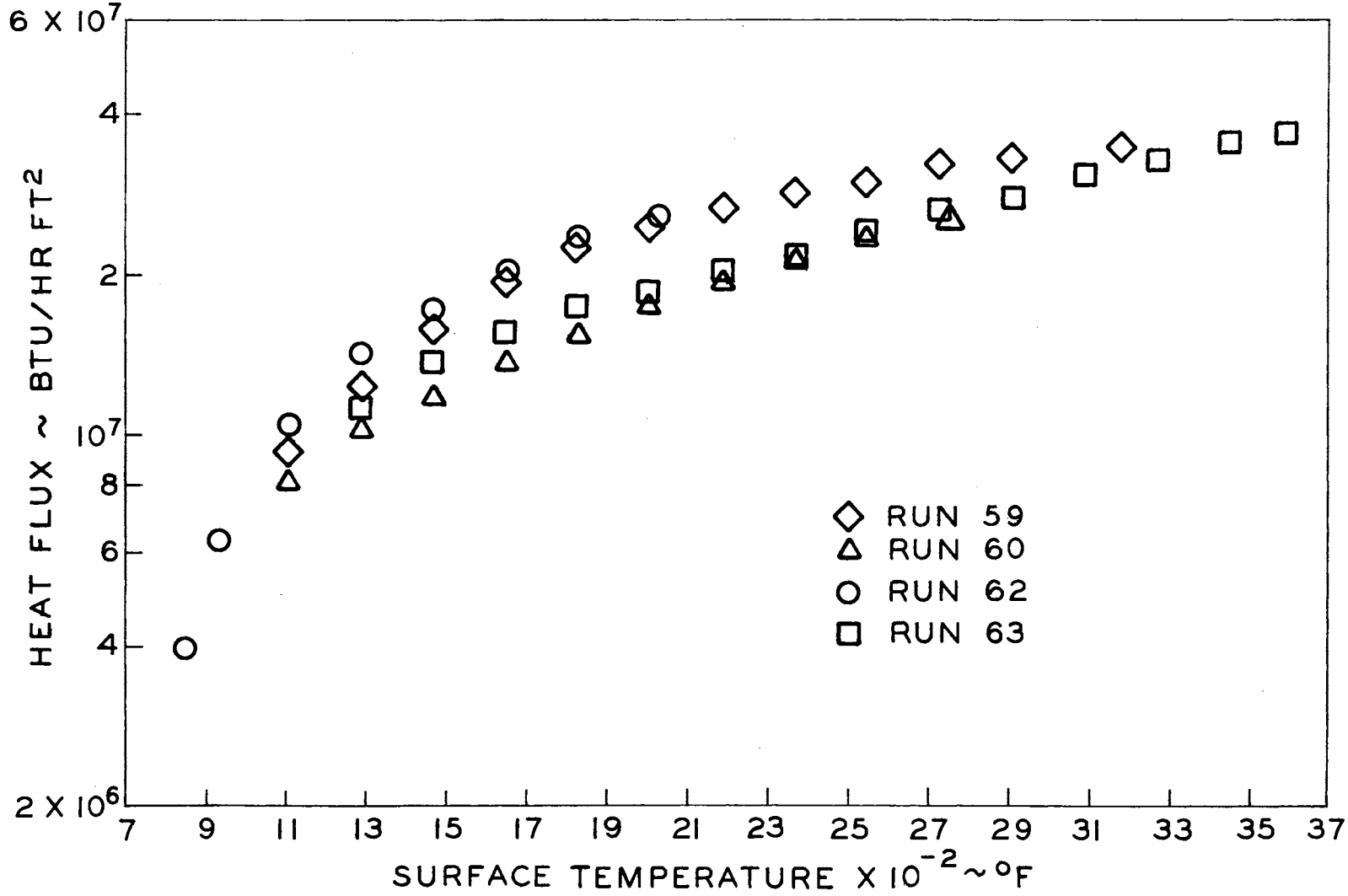

Figure 36. Heat Flux Versus Surface Temperature: U_∞ = 10.0 ft/sec, T_{Na} = 572°F; Straight Support Tube.

where its disturbance of the heat transfer process is not as appreciable as the straight support tube.

Figure 37 shows data which were taken at approximately 6.0 ft/sec. Runs 81, 82, and 83 were taken with a bent support tube. Runs 64, 66, 67, and 68 were taken with a straight support tube. Higher initial sphere temperatures could be achieved by using the sphere-thermocouple assemblies with straight support tubes. This was because a much more efficient induction coil could be used to heat a sphere with a straight support tube. Essentially, this is the reason for taking data with spheres with straight support tubes.

Figure 38 shows data which were taken in 572°F (300°C) sodium at various sphere velocities. These data were taken in an effort to obtain the effect of sphere velocity on the heat transfer rate from the sphere to the liquid sodium.

Figure 39 shows data which were obtained in 842°F (450°C) sodium. These data are rather limited. The reason for this is that these data were extremely difficult to obtain. At 842°F large quantities of sodium vapor were evolved from the surface of the sodium pool. The glovebox system was incapable of removing these quantities of sodium vapor. Condensation of the sodium vapor in the argon atmosphere released energy to the gas which was manifested as a temperature rise with accompanying expansion effects. Consequently the sodium pool had to be tightly covered until a data run was made. Even with this precaution large quantities of vapor were accumulated. The scope of this portion of the experimen-

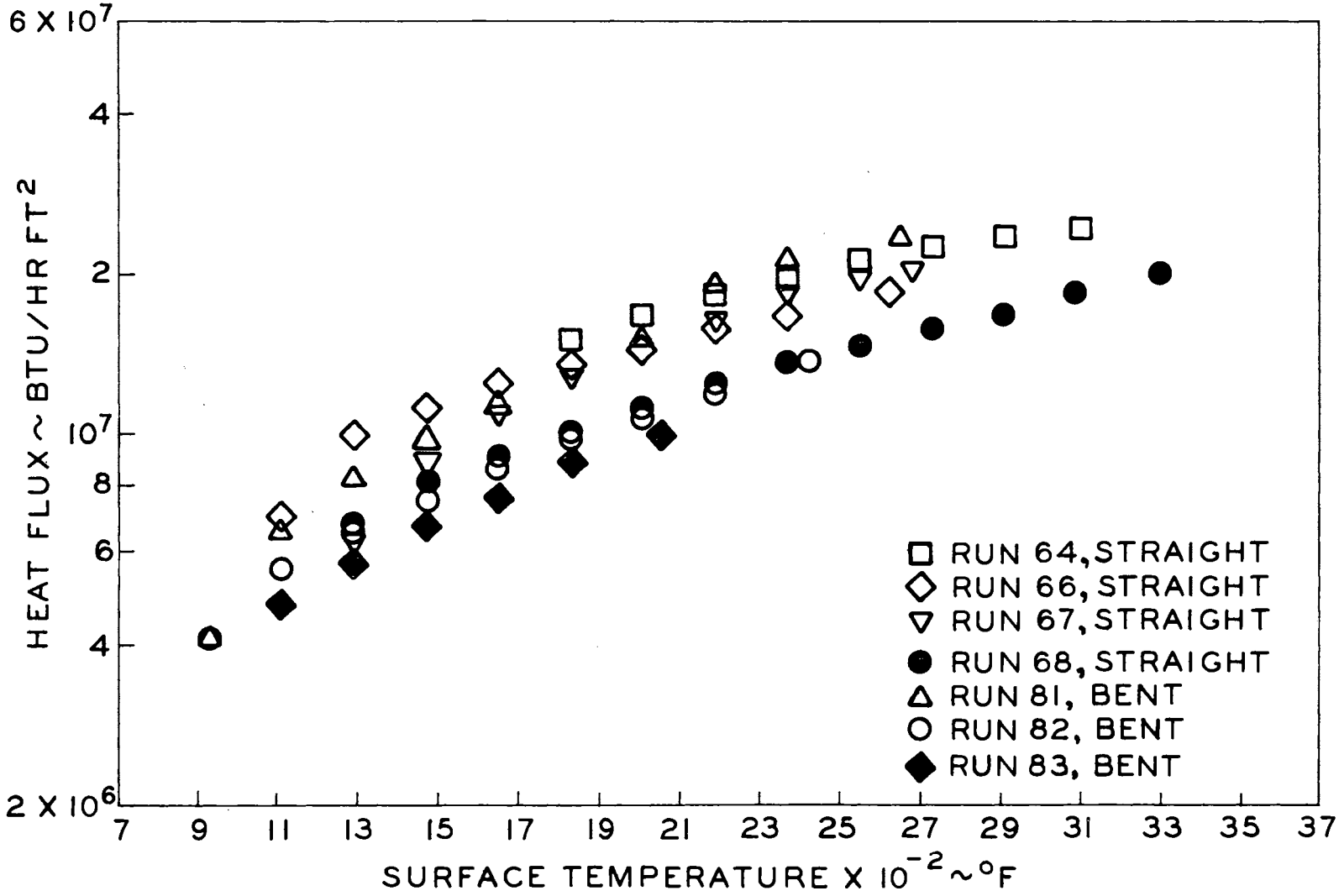

Figure 37. Heat Flux Versus Surface Temperature: U_∞ = 6.0 ft/sec, T_{Na} = 572°F.

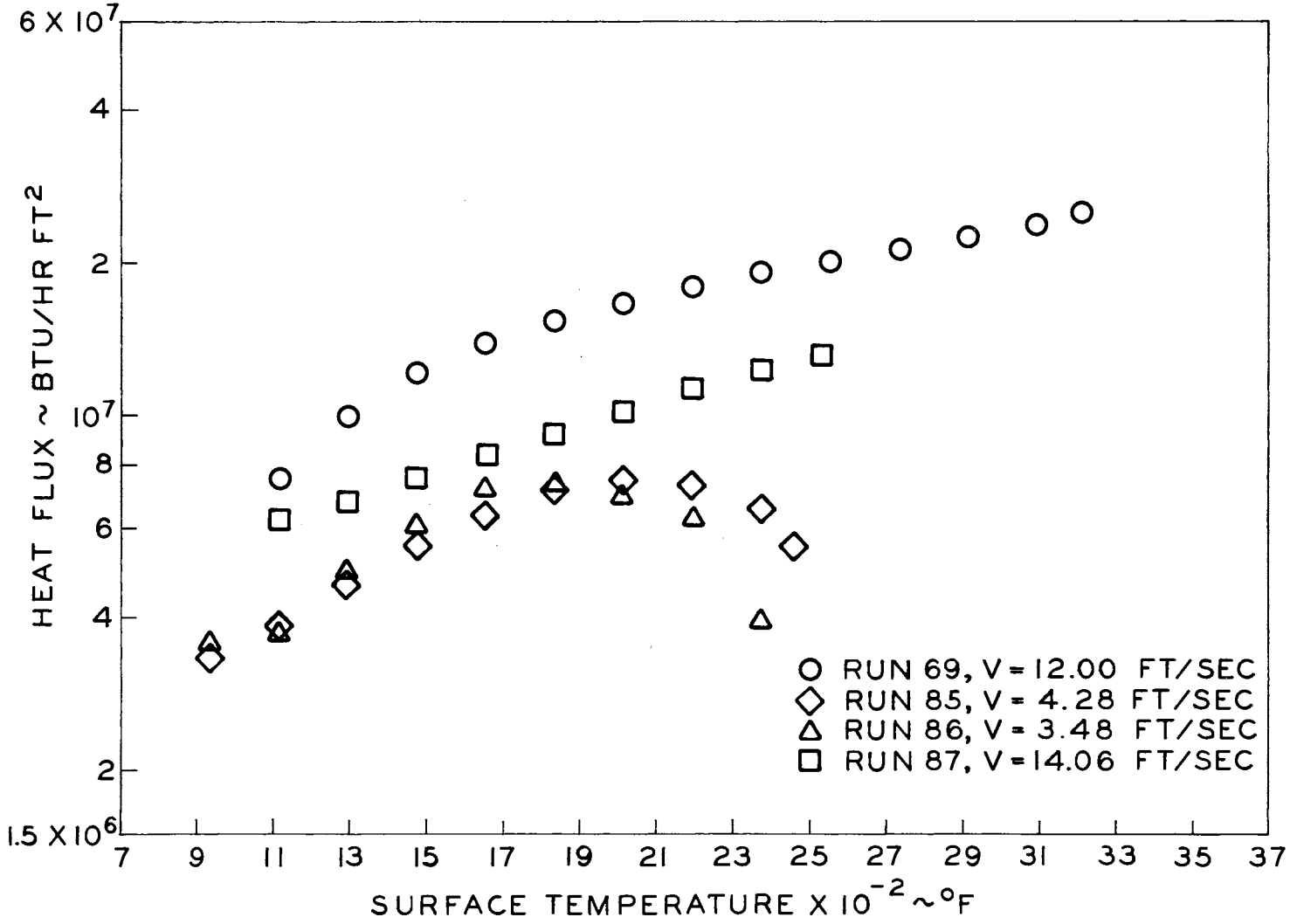

Figure 38. Heat Flux Versus Surface Temperature: Various Velocities, T_{Na} = 572°F.

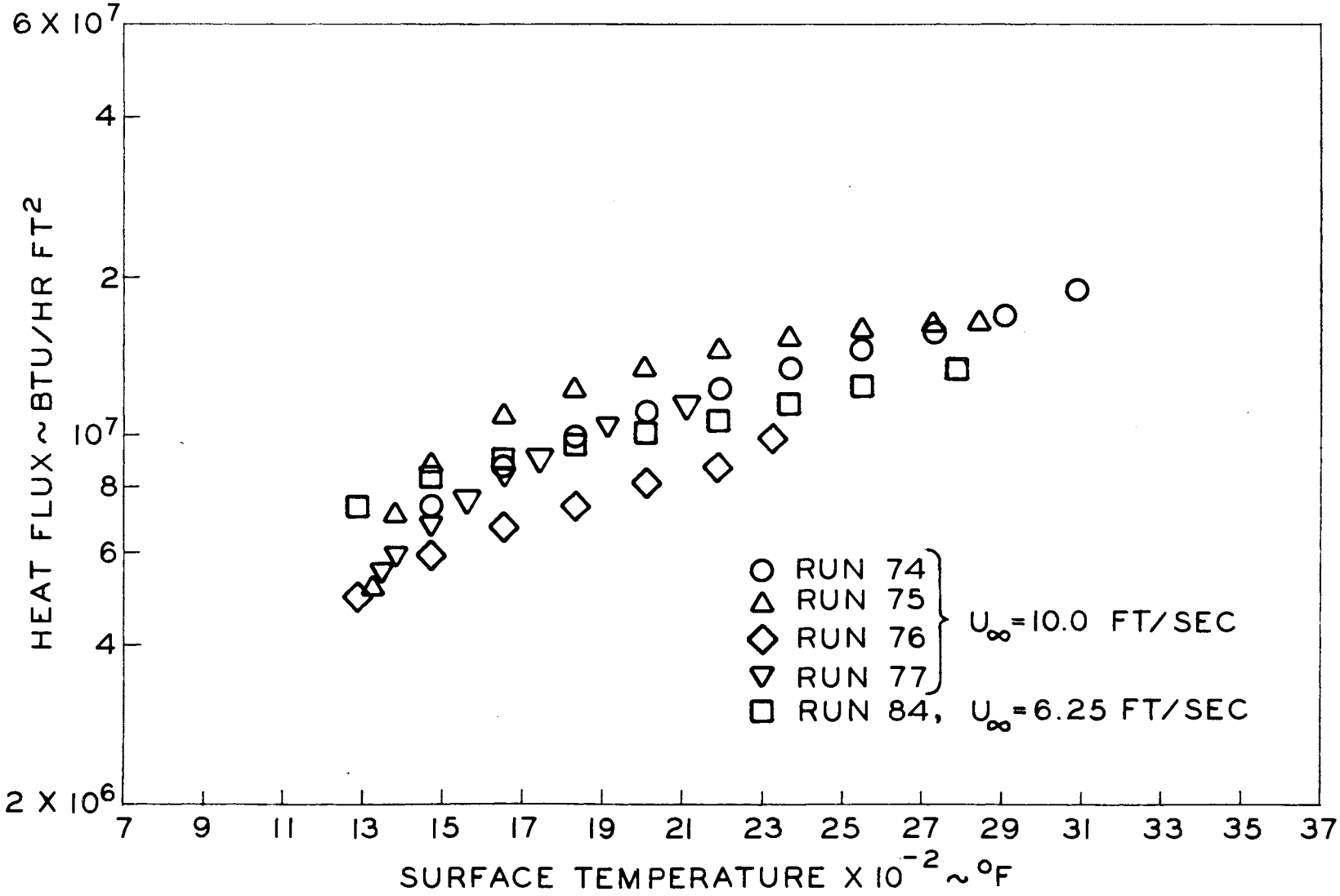

Figure 39. Heat Flux Versus Surface Temperature: T_{Na} = 842°F.

tal program was somewhat limited because of this difficulty.

These data points in Figures 35 through 39 were obtained from the faired heat flux and surface temperature curves for each data run. Heat flux values at various surface temperatures for these data runs were selected and plotted on the heat flux versus surface temperature graphs.

The Effect of Wetting

No noticable effect of non-wetting was observed in the experiments which were performed in this study. A newly fabricated sphere was not wetted by the liquid sodium. As the sphere was heated and quenched in the sodium, wetting was observed. However, no noticable differences in heat fluxes occurred between experiments which were performed under wetting and non-wetting conditions.

Accuracy of Experimental Data

Several factors were involved in the overall accuracy of the heat flux data acquired in this investigation. Since the data were calculated from temperature measurements, the accuracy of the data is directly dependent upon the accuracy of the measured temperatures. Associated with the temperature measurements were thermocouple calibration errors, electronic recording system errors, and reading errors. The accuracy of the data is also affected by the accuracy of the data reduction method.

Each thermocouple which was used in these experiments was calibrated after installation into the tantalum sphere. It is estimated this calibration is accurate to ± 1.5 percent. Possible errors arising from the electronic circuitry in the recording system were quite low and are estimated at not more than ± 1.0 percent. Reading errors could have contributed not more than ± 1.0 percent error to the measured temperatures.

The accuracy of the analytical solution, equation (37), used in most of the data runs at the initial part of the run could be controlled by the number of terms used in the infinite series. Five terms were used. This number of terms at the higher fluxes could have resulted in an error in the calculated heat fluxes of approximately ± 10 percent.

The accuracy of the Stolz data reduction method differs from the accuracy of the analytical solution. The Stolz method involves a numerical error associated with an approximating equation. The analytical technique contains a series truncation error. The Stolz data reduction method was generally used for low heat flux values. This method has been shown to be highly accurate at lower flux levels. The error associated with these flux levels should not exceed ± 3 percent.

The accumulation of these errors could result in overall maximum errors of approximately 20 percent at the highest heat flux levels and 10 percent at the lower heat flux levels. The accuracy of the data is dependent upon the value of the heat flux. These maximum error estimates are made by assuming that all the factors which

contribute toward the overall error are combined in an adverse way. In all probability this would not occur and the most probable error would fall between these maximum estimated errors and zero error. For example by taking the most probable errors as one-half of the maximum error the experimental data can be considered to be from 95 to 90% accurate, depending upon the flux level.

The limits of experimental scatter for the data which is presented in Figures 35, 36, 37, and 39 does not exceed $\pm$ 27% at any value of heat flux. The scatter limits actually tend to stay approximately constant over the entire heat flux range. It must be noted that more data has been collected at the lower heat fluxes than at higher heat fluxes. Therefore the limits of scatter at the higher heat fluxes are based on a much smaller sample. In all likelihood the limits would increase if based on the same amount of data as the limits of scatter at the lower heat flux.

Experimental scatter can be dependent upon variations in the physical process which is being investigated as well as experimental errors. Thus, experimental scatter and experimental errors should not be confused. Experimental scatter can give an indication of the magnitude of the experimental error, however. The comparison of $\pm$ 27 percent maximum experimental scatter to $\pm$ 20 percent maximum estimated experimental error tends to validate the estimated accuracy of the experimental data.

It is concluded that the experimental data which have been obtained in this study are most probably 85 to 90 percent accurate.

CHAPTER VII

DISCUSSION, CONCLUSIONS, AND RECOMMENDATIONS

The experimental results of this investigation, presented in Chapter VI, were compared to the results of the theory developed for film boiling heat transfer from a sphere to a flowing liquid. This theory was developed in Chapter III. A theory in which it is assummed that vapor is prevented from being formed at the sphere surface is developed in this chapter. The conclusions drawn from the comparison of these two theories to the experimental data are presented. Recommendations for further research are presented, also.

Comparison of Experimental Data to Film Boiling Theory

The theory which was developed in Chapter III utilized the assumption that film boiling would occur when an extremely hot spherical body moved through a pool of liquid sodium. An expression for the heat transfer rate from the sphere surface into the bulk of the liquid was derived by using boundary layer theory and by writing an energy balance on an element of the vapor film adjacent to the sphere surface. The resulting equation, equation (33), was simplified by neglecting the radiative contribution and the vapor generation contribution to the net heat transfer process.

The calculated radiative portion of the heat transfer from the sphere surface is two orders of magnitude less than the measured heat fluxes even at sphere surface temperatures near 3600°F. The contribution of the generation of vapor at the liquid-vapor interface to the overall heat transfer rate is also small. A comparison of this term in equation (33) to the term representing the heat flux from the liquid-vapor interface into the bulk of the liquid sodium shows that it is only about 1 percent of the latter term and can be neglected. The preceding statement applies to a sphere at 3472°F moving at 10 ft/sec through 572°F sodium. Thus, equation (33) is greatly simplified and becomes,

$$q/A = \frac{k_\ell \sin^2 \phi}{\sqrt{\Pi M \eta}} \Delta T_B \quad , \qquad (38)$$

where η is a function of geometry and M is defined by

$$M = \frac{2}{3} \frac{R\alpha}{U_\infty}$$

Examination of equation (38) shows that for one particular set of sodium conditions and one sphere velocity, the equation predicts a heat flux independent of sphere surface temperature. The experimental heat fluxes do not exhibit this trend. Figure 40 shows experimental points which were taken from Figures 35 and 36 in Chapter VI compared to a plot of equation (38). The sphere velocity is 10.0 ft/sec and the temperature of the sodium is 572°F. Two cases equation (38) are shown in Figure 40. The line representing at flux was computed assuming that the vapor film was main-

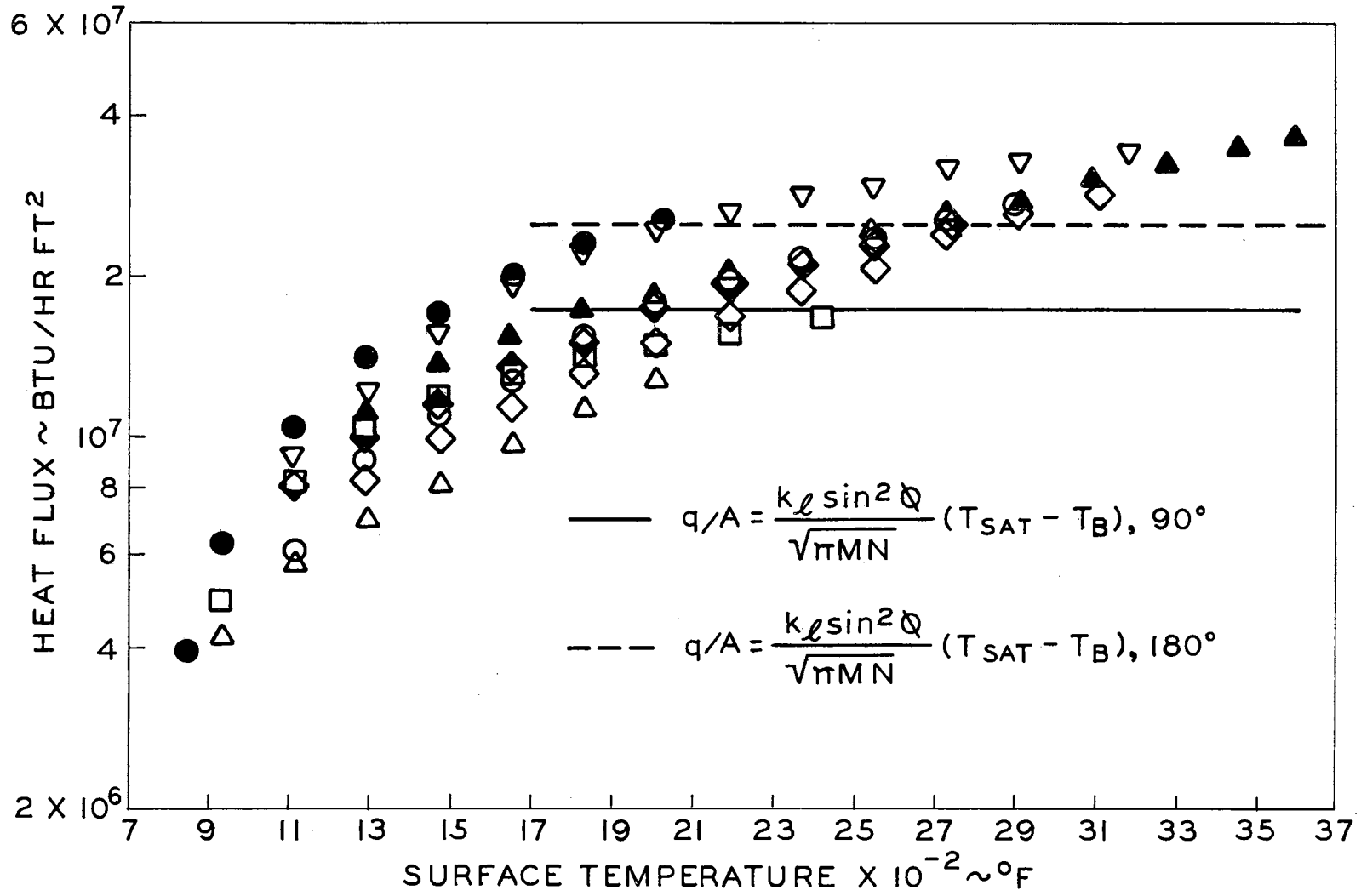

Figure 40. Comparison of Experimental Data and Film Boiling Theory: U_∞ = 10.0 ft/sec, T_{Na} = 572°F.

tained to the 180-degree position of the sphere. It is also possible that the vapor film could "separate" from the sphere surface in a manner similar to that noted by Vliet and Leppert (14) in forced convection boiling of water around a circular cylinder. Hence the line representing the lower heat flux in Figure 40 was computed assuming that "separation" of the vapor film occurred at the 90-degree position on the sphere. In reality, this assumption implies that the heat flux over the back side of the sphere is negligible since the thermal conductivity of the sodium vapor as compared to that of liquid sodium is very low.

The total heat flux from the sphere which was calculated by using equation (38) was found by a numerical summation. The surface of the sphere was split into 10-degree increments and equation (38) was applied in each increment. The following expression was used for the total heat flux;

$$(q/A)_T = \frac{k_\ell \Delta T_B}{(\pi M)^{1/2} A} \sum_{j=1}^{n} \frac{\sin^2 \phi_j}{\eta_J} \Delta A_j$$

where ΔA_j is the incremental sphere surface area associated with each 10-degree increment and A is the total area of the sphere. For the case of the vapor film which is maintained to the 180-degree position, n=18 and for 90-degree separation, n=9.

The properties of liquid sodium were evaluated at the arithmetic average of the liquid-vapor interface temperature and the

sodium bulk temperature. For this case, the liquid-vapor interface temperature was assumed to be the saturation temperature. The properties were taken from Dunning (62).

The film theory results in Figure 40 begin at a surface temperature of 1700°F, which is approximately 80°F above the boiling temperature of the sodium. Examination of Figure 40 shows that the theory predicts the correct order of magnitude for the heat fluxes. However, the experimental results indicate that heat fluxes are not independent of surface temperature as predicted by the theory. The plot of equation (38), assuming no separation which is represented by the upper line in Figure 40, appears to agree more closely with the experimental data than the lower line representing the solution of equation (38) up to the 90-degree point particularly for sphere temperatures sufficiently high that film boiling should occur.

Figure 41 presents a comparison of equation (38) and experimental data points which were taken from Figure 37. The sphere velocity was 6.0 ft/sec and the sodium temperature was 572°F. Figure 42 presents a comparison of data which was obtained at a velocity of 10.0 ft/sec in 842°F sodium to equation (38) which was solved for similar conditions. These experimental data were taken from Figure 38. These plots show the same trend as did Figure 40.

A comparison of average heat flux and an integrated mean heat flux for most of the data runs was made, in order to resolve the

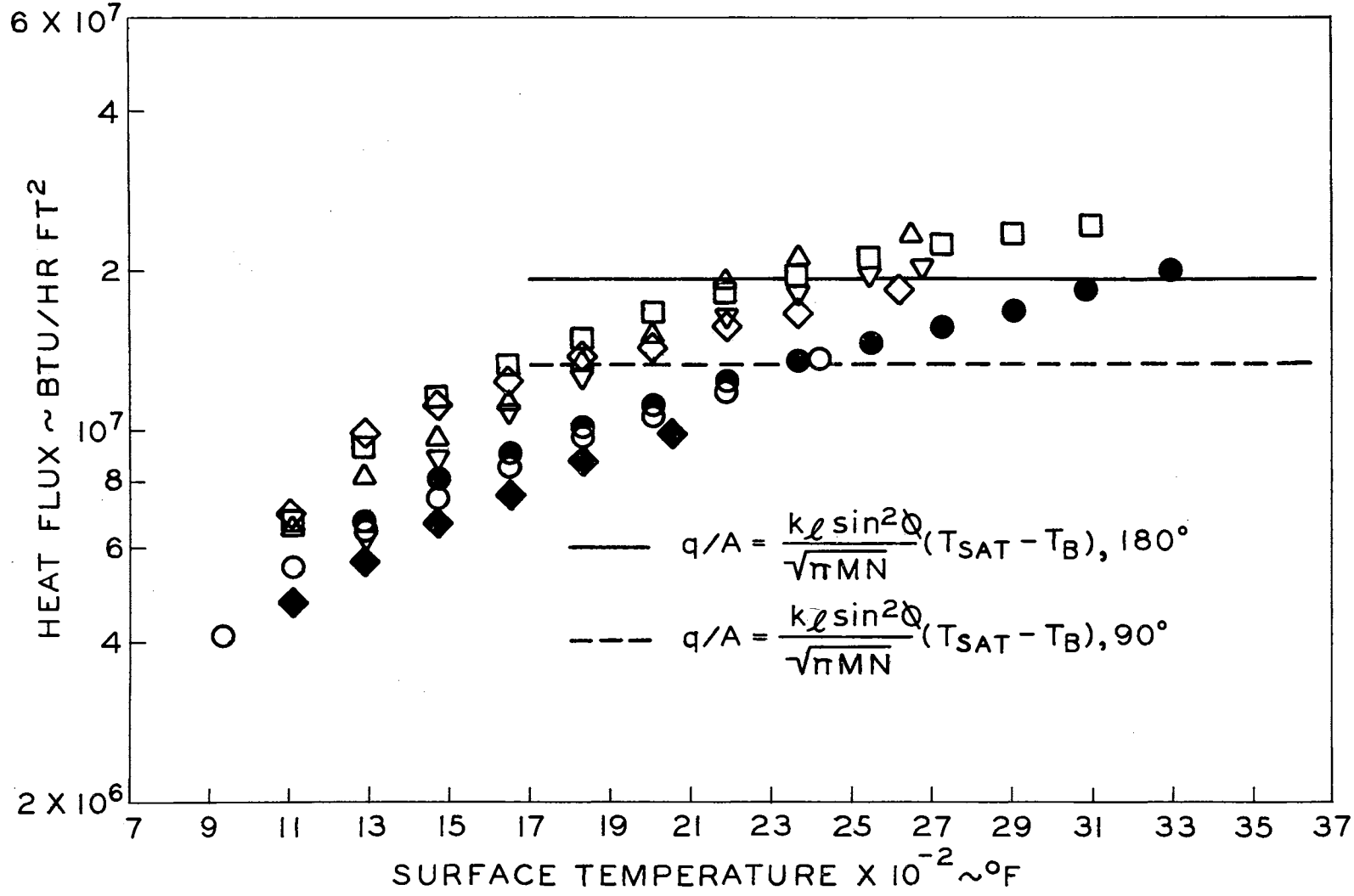

Figure 41. Comparison of Experimental Data and Film Boiling Theory: U_∞ = 6.0 ft/sec, T_{Na} = 572°F.

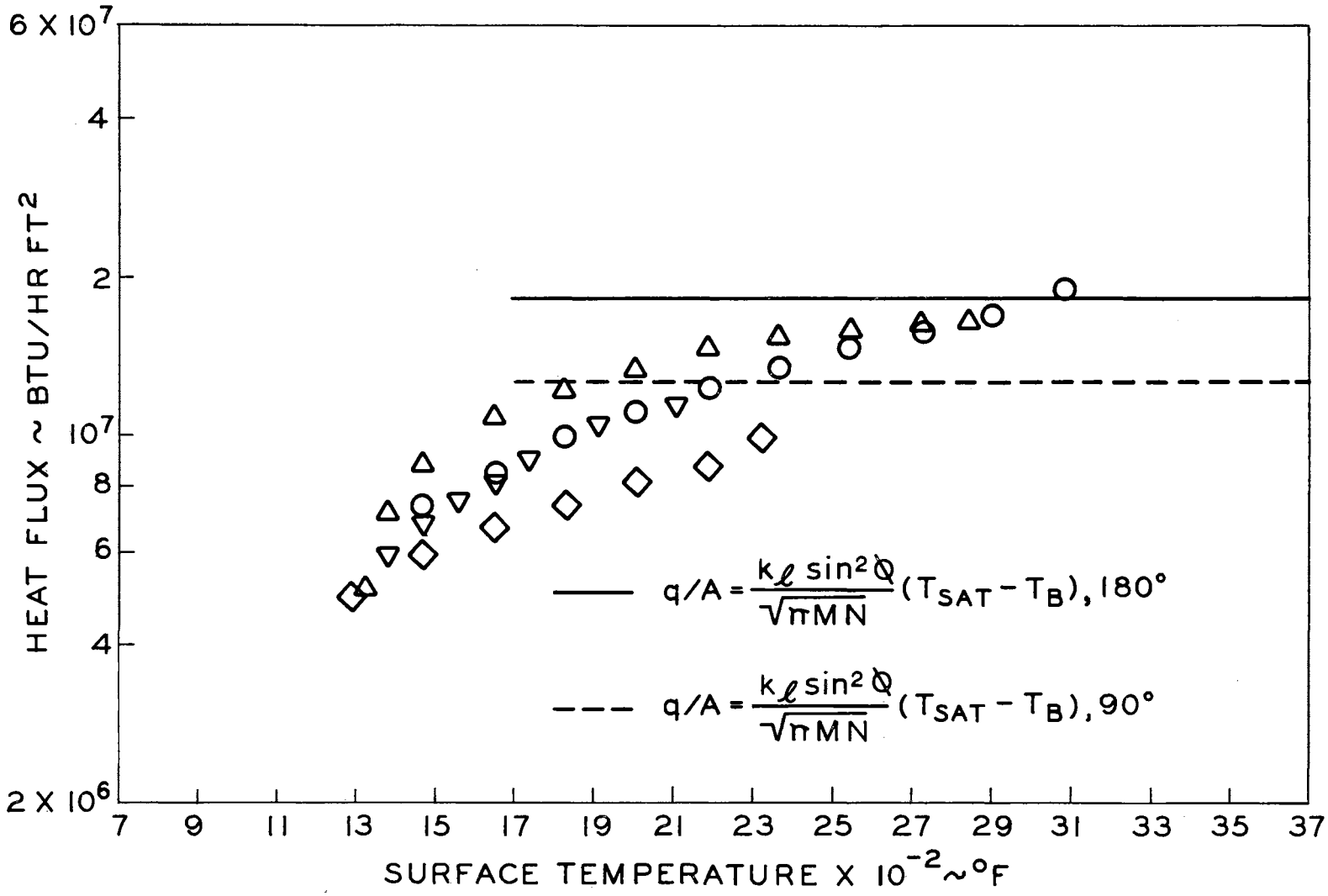

Figure 42. Comparison of Experimental Data and Film Boiling Theory: U_∞ = 10.0 ft/sec, T_{Na} = 842°F.

question of whether "separation" occurred while the sphere moved through the liquid sodium. The average heat flux for each run was obtained by the so-called equilibrium manner described in Chapter VI. Briefly, the sphere inlet and exit equilibrium temperatures are found and the relation,

$$(q/A)_{AVG.} = \frac{m\Delta H}{A\Delta t} \quad ,$$

is used to calculate the heat flux. The integrated mean heat flux was found by employing the relation,

$$(q/A)_{MEAN} = \frac{1}{\Delta t} \int_{o}^{\Delta t} q/A(t)dt \quad .$$

This technique was applied to the heat flux versus time plots such as Figure 30. If "separation" occurred during an experiment, the average heat flux for the experiment should be approximately 1/2 of the integrated mean heat flux. This is because the instantaneous heat flux is a local heat flux, and the assumption is made that the entire sphere behaves in a manner similar to the measured point. However, if the major portion of the heat transfer takes place on the front half of the sphere, where the temperature measurements were made, this method would predict an overall mean heat flux from the sphere surface approximately twice as high as actually occurred. Table II presents the results of this comparison. The two heat fluxes, which were computed by different methods, are in excellent agreement for all the data runs which were reduced. Con-

TABLE II

COMPARISON OF AVERAGE AND INTEGRATED HEAT FLUXES

Run	Average Heat Flux (BTU/HR FT^2 x 10^6)	Integrated Mean Heat Flux (BTU/HR FT^2 x 10^6)
59	10.48	14.00
60	9.17	8.91
61	(not calculated)	(not calculated)
62	6.28	7.52
63	12.00	13.32
64	10.93	10.65
65	(not calculated)	(not calculated)
66	8.16	8.76
67	8.50	8.26
68	11.88	9.43
69	(not calculated)	(not calculated)
70	11.15	12.18
71	12.60	11.80
72	8.69	(not calculated)
73	8.55	(not calculated)
74	10.95	9.25
75	9.75	9.54
76	5.71	6.06
77	5.48	5.51
78	(not calculated)	(not calculated)
79	6.52	8.34
80	6.39	5.33
81	6.56	6.76
82	5.23	5.02
83	4.60	3.97
84	8.17	8.97
85	6.55	4.99
86	5.33	4.37
87	10.65	7.95

sequently, in the remainder of this work, it was assumed that "separation" did not occur, and all theoretical work was performed using the entire surface of the sphere.

It is instructive to calculate the thickness of the vapor film, δ, required to accomodate the heat fluxes calculated from equation (38). Writing the expression for film thickness, one obtains from equation (35),

$$\delta = \frac{k_v}{k_\ell} \quad \frac{\Delta T}{\Delta T_B} \quad \frac{\sqrt{\pi\ Mn}}{\sin^2 \phi}$$

For the case considered in Figure 40, that is, U_∞ = 10.0 ft/sec and sodium temperature = 572°F, the film thickness at the 90-degree position on a 1/2-inch diameter sphere at 3472°F was calculated and is given by,

$$\delta = 7.65 \times 10^{-6} \text{ inch.}$$

Although the surface of the sphere was kept relatively smooth, it is anticipated that surface roughnesses much larger in magnitude than this calculated film thickness existed. Therefore, it is physically unrealistic that such a thin vapor film could exist adjacent to the sphere surface. This suggests that there is no vapor film present at all. The combination of a large amount of subcooling in the liquid sodium and velocity of the sphere could tend to prevent the formation of vapor at the sphere surface.

If no vapor film exists around the hot sphere, then the problem becomes one of single phase flow of liquid sodium around the

sphere with convective heat transfer. This also introduces the possibility of superheating the liquid sodium in small layers near the sphere surface. The liquid sodium will try to assume the temperature of the contacting wall. Since sphere surface temperatures much higher than the boiling temperature of sodium are encountered this would require superheating of the liquid sodium.

Comparison of Experimental Data to Superheating Theory

If superheating of liquid sodium does occur, very high temperature differences between the sodium-sphere interface and the bulk of the sodium could exist. Since the thermal conductivity of sodium is extremely high, tremendous quantities of energy could be transferred into the subcooled bulk of the sodium.

The theory developed in Chapter III for film boiling can be adapted for use in the superheating case. The vapor film need no longer be considered in an energy balance at the sphere surface. The net heat flux simply becomes the convective flux from the sphere surface into the bulk sodium. For this convective heat flux from the sphere surface into the bulk sodium, equation (38) will be used. However, the interface temperature can now assume values other than the saturation temperature. The equation becomes

$$q/A = \frac{k_\ell \sin^2 \phi}{\sqrt{\pi M \eta}} \quad (T_\ell - T_B) \qquad (39)$$

where T_ℓ is the temperature of the liquid sodium at the solid-liquid

interface. The assumption of potential flow of sodium around the sphere will be retained.

Equation (39) also is based on the assumption of laminar flow of liquid over the sphere. Transition to turbulence for flow around a sphere occurs near Re ≃ 300,000. The Reynolds number for these experiments varies from approximately 56,000 to 220,000. The corresponding Peclet number range is from 190 to 1600. The Reynolds number and Prandtl number were evaluated at the arithmetic mean of the sphere surface temperature and the bulk sodium temperature. The flow should remain laminar over this range of Reynolds numbers.

The maximum heat flux which could occur for the superheating case would be if the liquid sodium instantly assumed the temperature of the sphere surface as it contacted the sphere surface.

Figure 43 shows heat flux values calculated from equation (39) plotted versus surface temperature assuming that $T_\ell = T_W$. Also shown in Figure 43 are points which were taken from Figures 36 and 36 representing experimental data. Although somewhat higher than the experimental data, the superheating theory correctly predicts the trend of the experimental data. The superheating theory predicts an increasing heat flux with increasing sphere surface temperature which agrees with the experimental data trend.

The theory can be brought into better agreement with the data if it is assumed that the expression for heat flux can be written as,

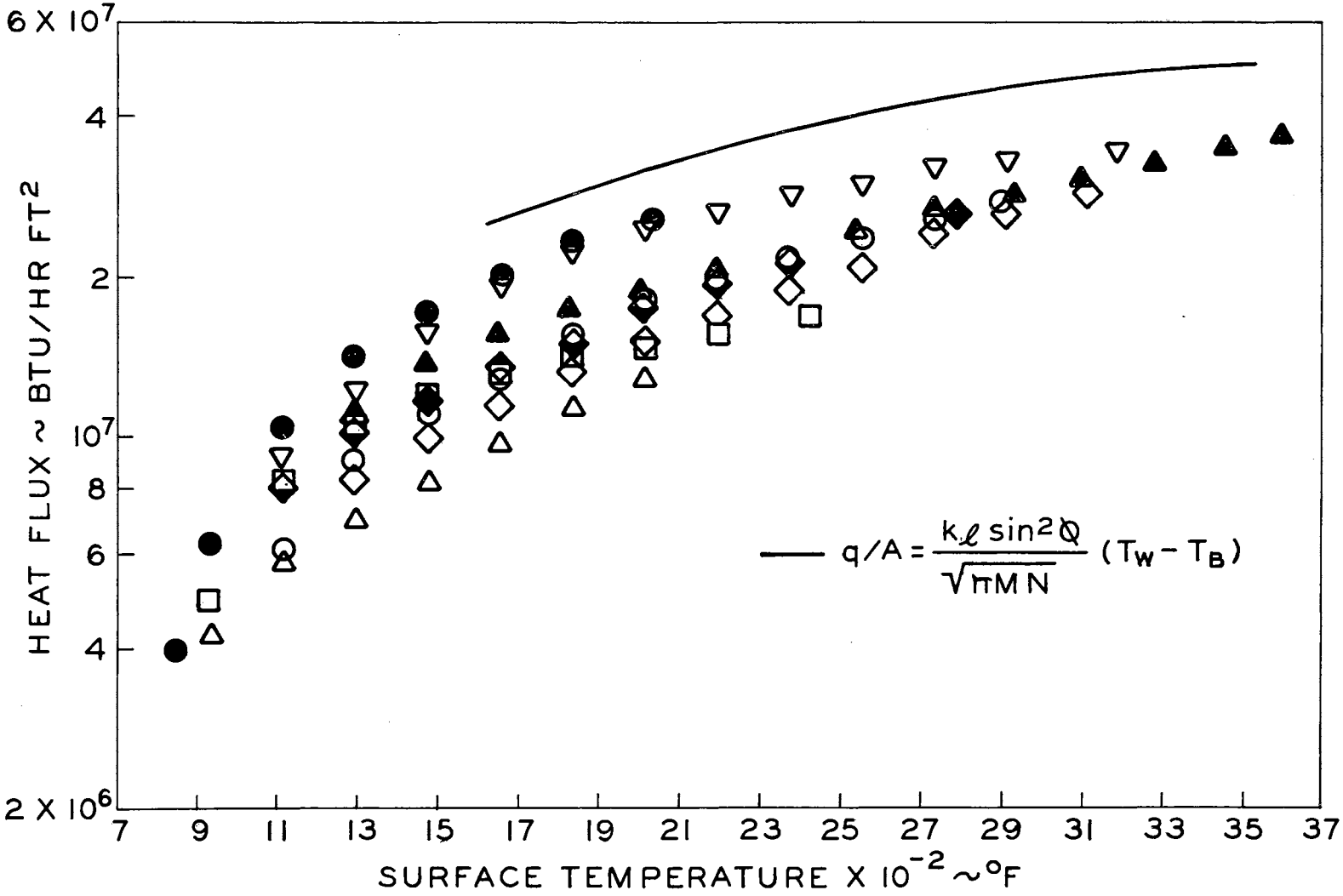

Figure 43. Comparison of Experimental Data and Superheating Theory: U_∞ = 10.0 ft/sec, T_{Na} = 572°F, T_ℓ=T_w.

$$q/A = K \frac{k_\ell \sin^2 \phi}{\sqrt{\Pi M \eta}} (T_W - T_B) \qquad (40)$$

The factor K could be thought of as a correction factor for the neglect of viscosity effects in the boundary layer, and for the situation where the liquid sodium near the wall does not immediately assume the wall temperature. Figure 44 shows equation (40) plotted for two values of K, K = 0.54 and K = 0.60. The plot for K = 0.54 agrees well with the lower temperature data whereas the plot for K = 0.60 agrees well with the higher temperature data. It is apparent that K is a function of surface temperature. This suggests that the data perhaps could be correlated by an expression of the form,

$$q/A = C(T_W - T_B)^n \quad .$$

Correlation of Data with Temperature Difference

The data were plotted on log-log coordinates to evaluate C and n. Figures 45, 46 and 47 show these plots. The data in Figure 45 represent data points which were taken from Figures 35 and 36. These data could be correlated by the expression,

$$q/A = 2.98 \times 10^4 (T_W - T_B)^{0.88}$$

where temperature is in °F and heat flux in BTU/HR FT^2. Figure 47 shows data points which were taken from Figure 39 obtained at U_∞ = 10.0 ft/sec and T_{Na} = 842 °F. These data could be correlated

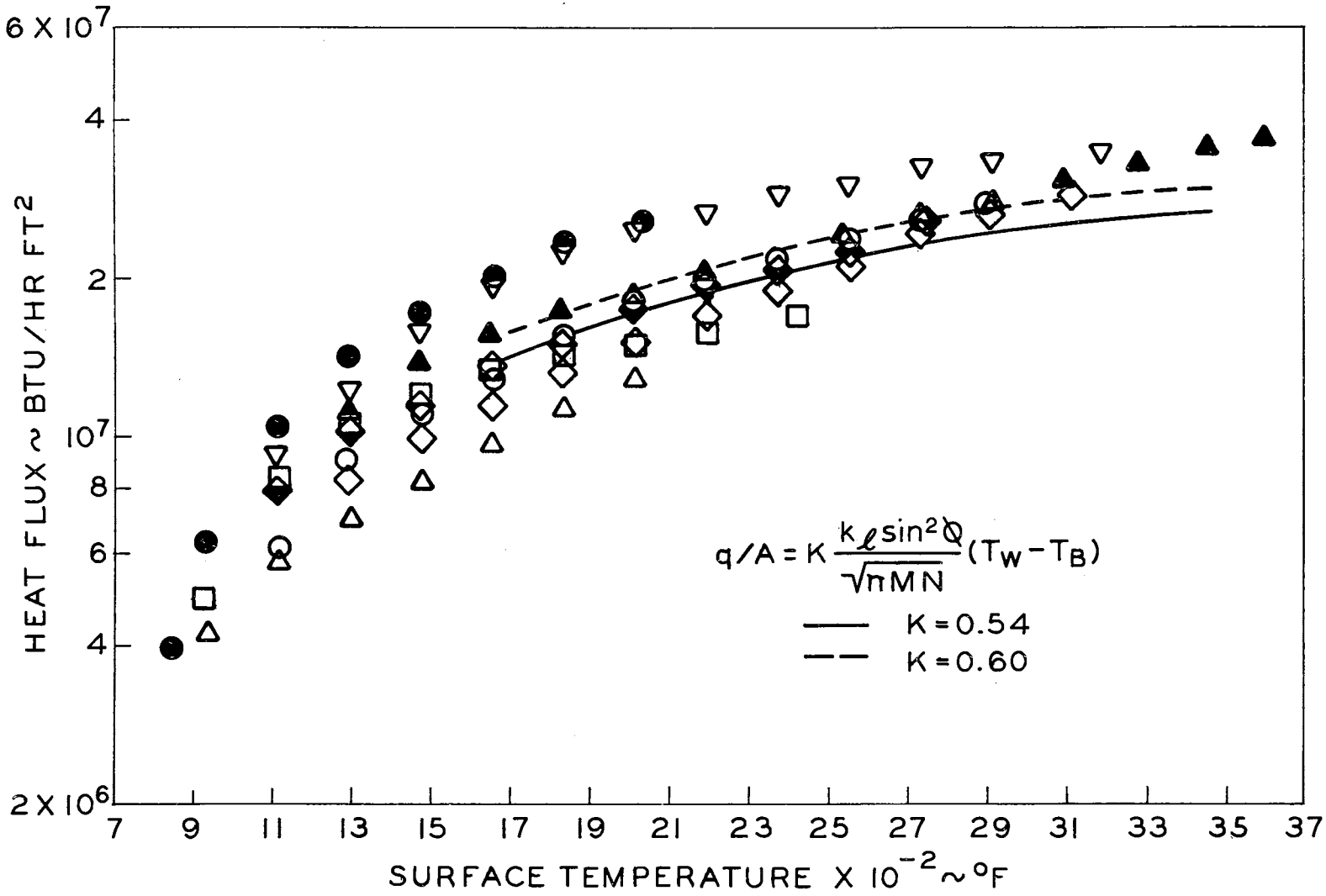

Figure 44. Comparison of Experimental Data and Superheating Theory: U_∞ = 10.0 ft/sec, T_{Na} = 572°F.

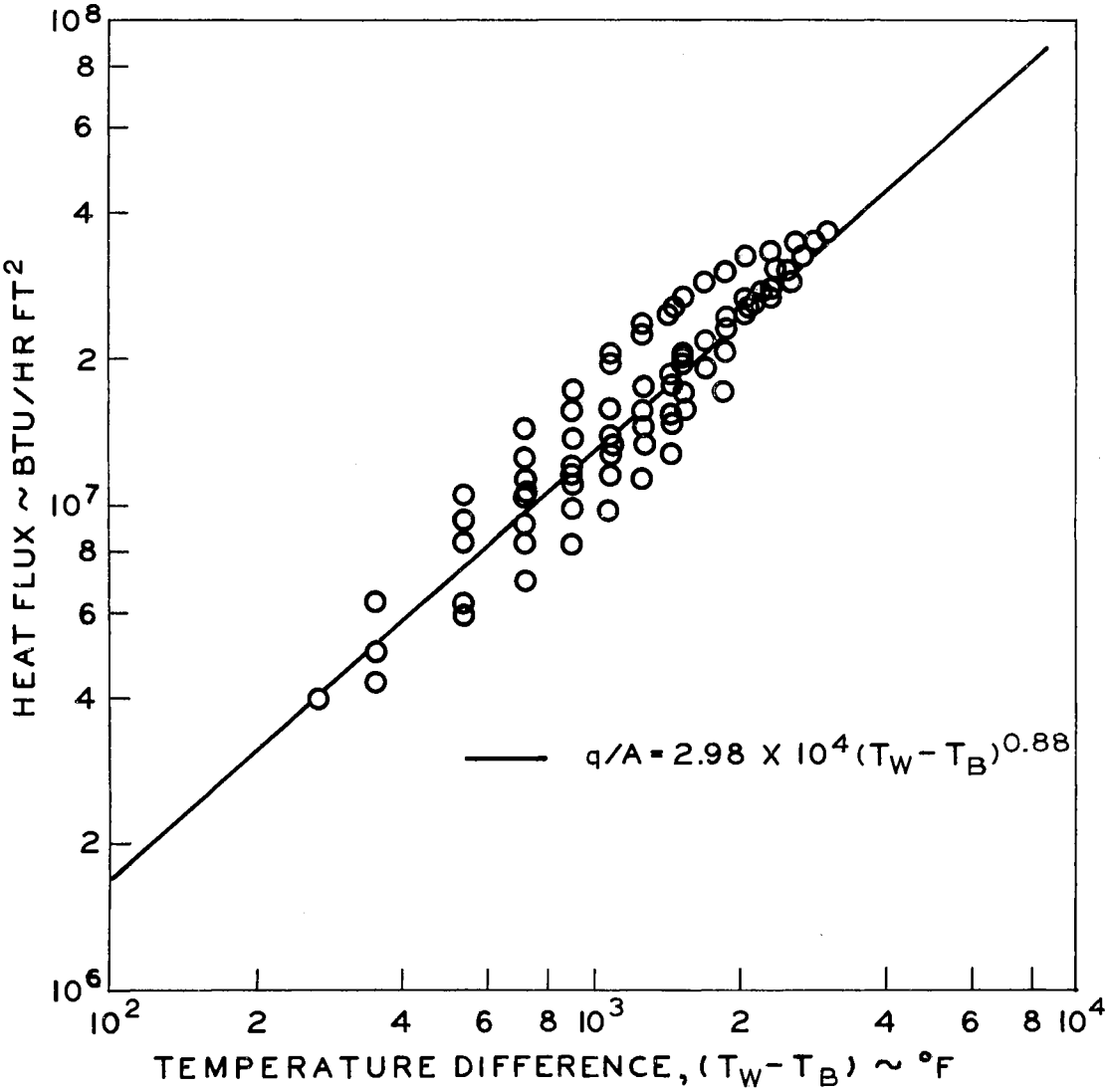

Figure 45. Heat Flux Versus Temperature Difference: U_∞ = 10.0 ft/sec, T_{Na} = 572°F.

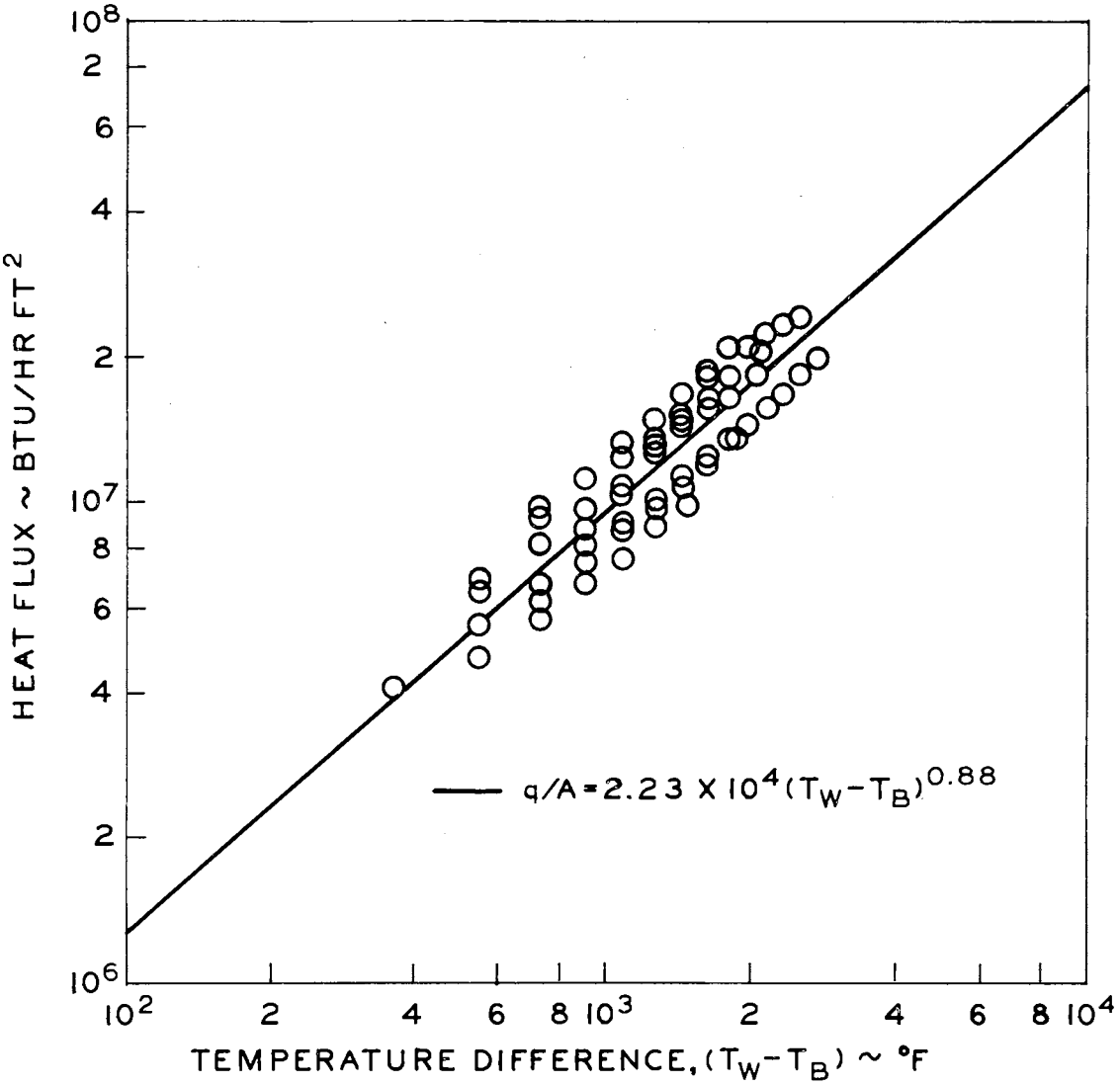

Figure 46. Heat Flux Versus Temperature Difference: U_∞ = 6.0 ft/sec, T_{Na} = 572°F.

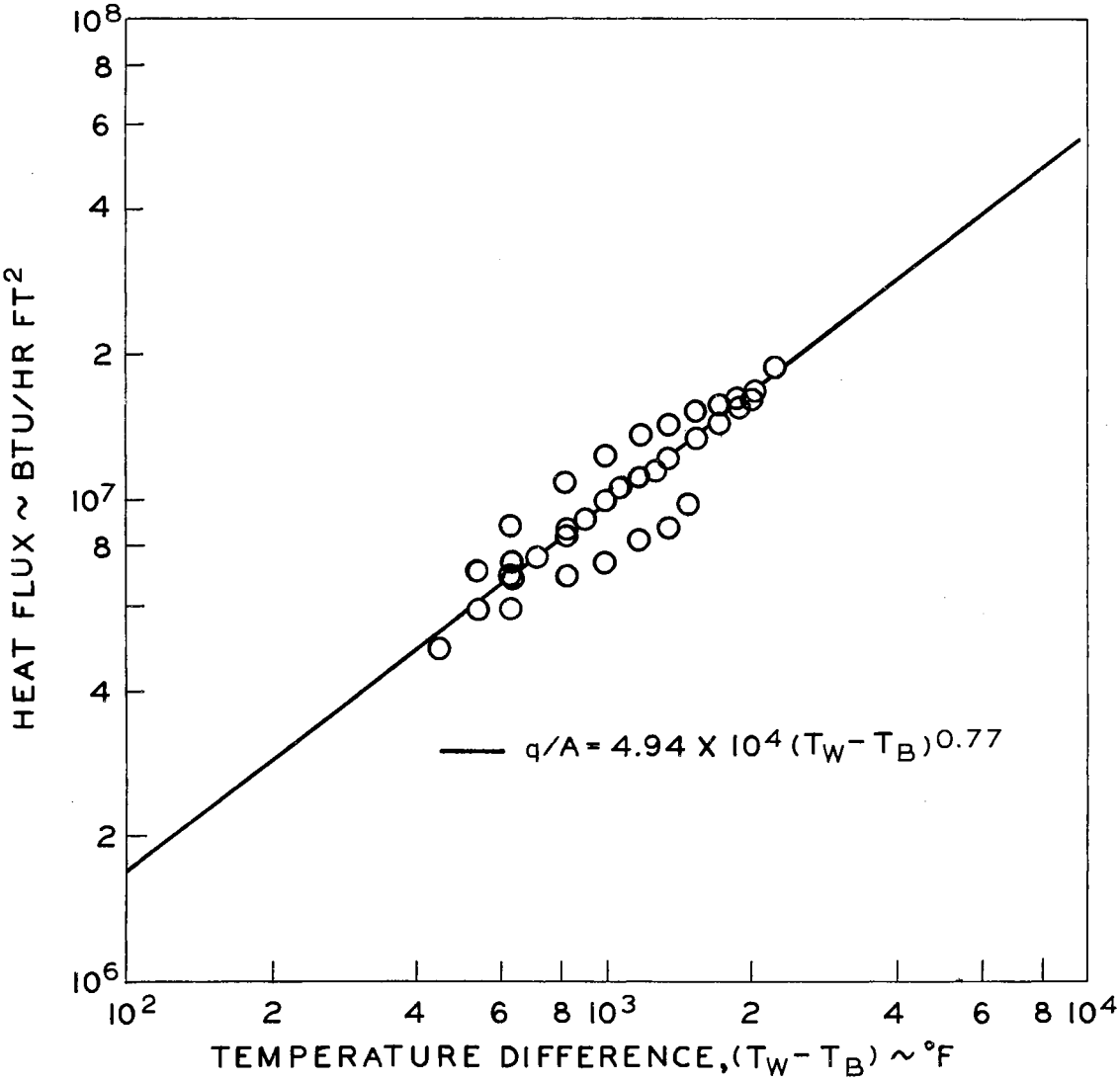

Figure 47. Heat Flux Versus Temperature Difference: U_∞ = 10.0 ft/sec, T_{Na} = 842°F.

by the relation,

$$q/A = 4.94 \times 10^4 \ (T_W - T_B)^{0.77}$$

The exponent, n, for heat flux measured in 842°F sodium differs considerably from that obtained from data taken in 572°F. Data at conditions other than those associated with Figures 45, 46, and 47 were sparse and were not plotted on log-log coordinates.

The reduction of the experimental data to an equation of the form

$$q/A = C(T_W - T_B)^n$$

provides a convenient tool for engineers and designers to calculate heat fluxes from spheres to liquid sodium with a minimum of effort. All that is required is the knowledge of the wall and bulk temperatures. It should be emphasized that these expressions are the result of curve fitting and not the result of theoretical considerations.

The variation of the exponent n with T_B suggests that the actual phenomena may be more complicated than was recognized in the development of the film theory and the superheat theory. However, the idealizations which were employed in the development of the theories were necessary in order to obtain solutions for this complicated problem.

Effect of Velocity

Figure 48 presents data which were obtained in 572°F sodium at various velocities. These measurements were made to obtain the effect of sphere velocity upon the heat flux. The lines representing data obtained at 3.48, 12.00, and 14.06 ft/sec were obtained by fairing curves through the data points representing the respective velocities in Figure 38. The lines representing data obtained at 6.00 ft/sec and 10.00 ft/sec are plots of the correlating equations (41) and (42) respectively.

Examination of Figure 48 shows the trend of increasing heat flux with increasing sphere velocity up to approximately 12.0 ft/sec. At high surface temperatures, the heat flux curve for U_∞ = 12.0 ft/sec falls lower than that for U_∞ = 10.0 ft/sec. The variation between these curves is within the limits of experimental error, however. The heat flux curve obtained at U_∞ = 14.06 ft/sec. falls lower than even the heat flux curve for U_∞ = 6.00 ft/sec. The 20 percent maximum experimental error which could be present fails to account for this result. Therefore the results at 14.06 ft/sec must be considered anomalous. It should be pointed out that the lines representing velocities of 6.0 and 10.0 ft/sec represent many individual data runs, whereas the lines for the other three velocities represent only single data runs. Consequently, the 6.0 and 10.0 ft/sec lines must be considered to represent statistically a much better indication of the effect of sphere velocity upon heat

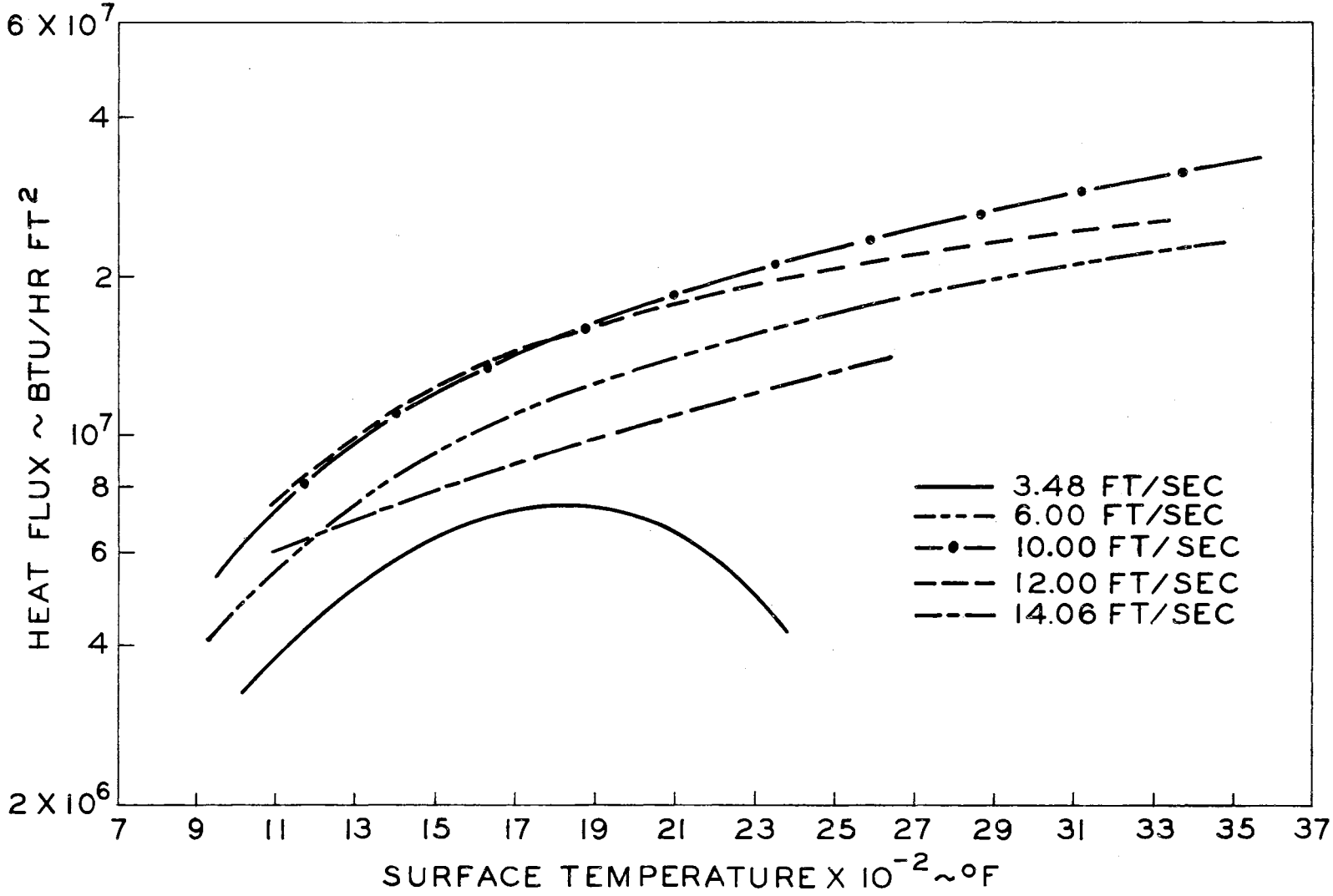

Figure 48. Heat Flux Versus Surface Temperature: T_{Na} = 572°F, Various Velocities.

flux. The measurements made at these two velocities indicate that the heat fluxes follow the square root of velocity dependence as predicted by both the film boiling and superheat theories.

The fact that the heat flux depends upon the square root of velocity in both theories is caused by the assumption of potential flow of the liquid around the sphere. Vliet and Leppert (63), have found that the heat flux from spheres to water varies with velocity to the 0.66 power. This value, 0.66, was found from experimental data where the effects of viscosity were present. A similar variation of velocity dependence was not observed in this study. It should be noted that the scatter of the experimental data could mask any such variation. However, the data trends indicate that the assumption of potential (frictionless) flow is valid for the range of experimental conditions investigated in this study.

Conclusions and Recomendations

The results of this investigation have provided a new insight into the basic mechanism of heat transfer from extremely hot spheres into highly subcooled liquids such as molten sodium. It was shown that the combined effects of large degrees of subcooling and of motion of the sphere tend to prevent the formation of vapor at the surface of the sphere. A theory was developed in this study by assumming that liquid sodium could be in contact with a surface that is much hotter than the boiling temperature of sodium. The

limiting case for maximum heat transfer from a sphere to liquid sodium can be calculated with this superheat theory by assuming that the sodium immediately assumes the sphere surface temperatures as it contacts the surface. The heat fluxes which were calculated from the experimental data were in every case less than this limiting heat flux. Even better agreement with the experimental data could be achieved with a slight modification of the superheat theory.

It was shown that the film boiling theory represents only a first-order approximation of the actual physical process for heat transfer from a sphere to liquid sodium. The many restrictive assumptions which were necessary in the formulation of the film theory contribute to its inability to describe the actual heat transfer mechanism. Furthermore, the extremely thin vapor film thicknesses calculated from this theory support the superheat theory.

The superheat theory provides a much simpler tool to calculate heat fluxes from heated surfaces into highly subcooled liquids such as sodium than the film boiling theory. The superheat theory is essentially one of non-boiling convective heat transfer from the heated surface to the flowing liquid. This case is much more amenable to analysis than the relatively complicated problem of solving two boundary layer systems which is necessary in the film boiling problem.

The heat fluxes calculated from the experimental data could be correlated by an expression of the form,

$$q/A = C(T_W - T_B)^n$$

The values of C and n were determined for three sets of experimental conditions:

U_∞	T_B	C	n
10.0 ft/sec	572 °F	2.98×10^4	0.88
6.0 ft/sec	572 °F	2.23×10^4	0.88
10.0 ft/sec	842 °F	4.94×10^4	0.77

An expression of this type represents a curve fit for the experimental data and is not the result of any theory. Consequently these values of C and n should be used only over the range of conditions established by the experiments.

The results of this study indicate that very large quantities of energy can be transferred from extremely hot particles to highly subcooled sodium without vapor formation. However, superheating of thin layers of liquid sodium near the sphere could occur. Many small particles in close proximity with each other, dispersed in liquid sodium, could provide a matrix of highly superheated sodium. Vapor nucleation could result in vapor formation of such magnitude to create damaging pressure pulses in a reactor core which is undergoing a destructive power excursion. Vapor nucleation would depend upon the number and spacing of particles, their total energy dissipation, and the energy storage capability of the sur-

rounding coolant. A study of these effects upon energy transfer and pressure generation would be of value in determining the consequences of a destructive nuclear excursion.

In conclusion it can be stated that:

1. A valuable set of experimentally obtained heat fluxes from spheres to liquid sodium has been obtained in this study. To the author's knowledge no other data of this type has been obtained. The demonstrated accuracy of the data is good.
2. The superheat theory which was developed in this study provides a new, simpler technique for the calculation of heat transfer from extremely hot particles moving through highly subcooled fluids of high thermal conductivity.
3. The results of the experimental and theoretical work which was performed in this study indicate that large amounts of energy can be transferred from a hot spherical particle to highly subcooled liquid sodium without vapor being formed at the sphere surface.
4. The film boiling theory which was developed in this study represents a first-order approximation of the experimental data.
5. The experimental data was put into the simple form,

$$q/A = C(T_W - T_B)^n \quad ,$$

for use by reactor safety analysts. Heat fluxes can be calculated by knowing only the sphere surface and bulk sodium temperatures and the sphere velocity.

The following recommendations for possible future investigations are suggested as a result of the present study.

1. Further experimental work will be required to verify the absence of vapor around a hot sphere passing through highly subcooled liquid sodium.
2. Further experimental work should be performed to obtain the effect of subcooling upon the heat flux by making measurements in sodium up to its saturation temperature.
3. The effect of velocity should be more thoroughly investigated by performing experiments over a wider range of velocities. The effect of sphere diameter upon heat flux should also be obtained.
4. More refined theoretical studies of the problem of heat transfer from an extremely hot sphere into liquid sodium are recommended. In particular an analysis relaxing the assumption of constant fluid properties is needed. In general better methods for treating flow around spheres are needed.

BIBLIOGRAPHY

1. Clark, J. A., and H. Merte, Jr. "Boiling Heat Transfer With Cryogenic Fluids at Standard, Fractional, and Near-Zero Gravity." Trans. ASME Series C Vol. 86 (1964) pp. 351-359.

2. Leidenfrost, J. G. "De Aquae Communis Nonnullis Qualitatibus Tractatus." Duisburg (1756). (Discussed in reference 18.)

3. Drew, T. B., and A. C. Mueller. "Boiling." AIChE Journ. Vol. 33, No. 1 (1937) p. 463.

4. Pilling, N. B., and T. D. Lynch. "Cooling Properties of Technical Quenching Liquids." Trans. Am. Inst. of Mining and Met. Eng. Vol. 62 (1920) pp. 665-688.

5. Mosciki, I., and J. Broder. "Spheroidal State of Liquids on Heated Metallic Surfaces." Roczniki Chem. Vol. 6 (1926) pp. 319-354.

6. Nukiyama, S. "Experiments on the Determination of the Maximum and Minimum Values of the Heat Transferred Between a Metal Surface and Boiling Water." AERE-trans. 854 (1960).

7. McAdams, W. H. et al. "Heat Transfer at High Rates to Water With Surface Boiling." Ind. and Eng. Chem. Vol. 41, No. 9 (1949) pp. 1945-1953.

8. Kreith, F., and M. Summerfield. "Heat Transfer to Water at High Flux Densities With and Without Surface Boiling." Trans. ASME Vol. 71 (1949) pp. 905-915.

9. Rohsenow, W. M., and J. A. Clark. "A Study of the Mechanism of Boiling Heat Transfer." Trans. ASME Vol. 73 (1951) pp. 609-620.

10. Forster, K. E., and R. Grief. "Heat Transfer to a Boiling Liquid-Mechanisms and Correlations." Trans. ASME Series C Vol. 81 (1959) pp. 43-53.

11. Moore, F. D., and R. B. Mesler. "The Measurement of Rapid Surface Temperature Fluctuations During Nucleate Boiling of Water." AIChE Journ. Vol. 7 (1961) pp. 620-624.

12. Rallis, C. J., and H. H. Jawurek. "The Mechanism of Nucleate Boiling." Paper A/CONF. 28/P/600 Presented at Third United Nations Int. Conference on the Peaceful Uses of Atomic Energy, Geneva (May 1964).

13. Hendricks, R. C., and R. Sharp. "Initiation of Cooling Due to Bubble Generation on a Heated Surface." NASA TN D-2290 (April 1964).

14. Vliet, G. C., and G. Leppert. "Critical Heat Flux for Nearly Saturated Water Flowing Normal to a Cylinder." Trans. ASME Series C Vol. 86 (1964) pp. 59-67.

15. Vliet, G. C., and G. Leppert. "Critical Heat Flux for Sub-Cooled Water Flowing Normal to a Cylinder." Trans. ASME Series C Vol. 86 (1964) pp. 68-74

16. Bromley, L. A. "Heat Transfer in Stable Film Boiling." Chem. Eng. Prog. Vol 46, No. 5 (1950) pp. 221-227.

17. Bromley, L. A. et al. "Heat Transfer in Stable Film Boiling." Ind. and Eng. Chem. Vol 45, No. 12 (1953) pp. 2639-2646.

18. Motte, E. I., and L. A. Bromley. "Film Boiling of Flowing Sub-cooled Liquids." Ind. and Eng. Chem. Vol 49, No. 11 (1957) pp. 1921-1928.

19. Westwater, J. W. "Boiling of Liquids." Advances in Chemical Engineering, Vol. II, ed. T. B. Drew and J. W. Hoopes, Jr. Academic Press, New York (1958) p. 10.

20. Grober, H., S. Erk, and U. Grigull. Fundamentals of Heat Transfer, McGraw-Hill, New York (1961) p. 328.

21. Branchero, J. T., G. E. Barker, and R. H. Boll. "Stable Film Boiling of Liquid Oxygen Outside Single Horizontal Tubes and Wires." Chem. Eng. Prog. Symp. Series Vol. 51, No. 17 (1955) pp. 21-31.

22. McAdams, W. H. et al. "Heat Transfer From Single Horizontal Wires to Boiling Water." Chem. Eng. Prog. Vol 44, No. 8 (1948) pp. 639-646.

23. Bromley, L. A. "Effect of Heat Capacity of Condensate." Ind. and Eng. Chem. Vol 44, No. 12 (1952) pp. 2966-2969.

24. Ellion, M. E. "A Study of the Mechanism of Boiling Heat Transfer." JPL Memo 20-99 (1954).

25. McFadden, P. W., and R. J. Grosh. "High-Flux Heat Transfer Studies: An Analytical Investigation of Laminar Film Boiling." ANL-6060 (1959).

26. Chang, Y. P. "Wave Theory of Heat Transfer in Film Boiling." Trans. ASME Series C Vol. 81 (1959) pp. 1-12.

27. Hsu, Y. Y., and J. W. Westwater. "Approximate Theory for Film Boiling on Vertical Surfaces." Chem. Eng. Prog. Symp. Series Vol. 56, No. 30 (1960) p. 15.

28. Bradfield, W. S. et al. "Film Boiling on Hydrodynamic Bodies." Convair Research Report 37 (1960).

29. Westwater, J. W. "Boiling of Liquids." Advances in Chemical Engineering, Vol. I ed. T. B. Drew and J. W. Hoopes, Jr., Academic Press, New York (1956) p. 44.

30. Bradfield, W. S. "Liquid-Solid Contact in Stable Film Boiling." Ind. and Eng. Chem. Fundamentals, Vol. 5 No. 2 (1966) pp. 201-204.

31. Berenson, P. J. "Film Boiling Heat Transfer From a Horizontal Surface." Trans. ASME Series C Vol. 83 (1961) pp. 351-358.

32. Sparrow, E. M., and R. D. Cess. "Film Boiling in a Forced Convection Boundary Layer Flow." Trans. ASME Series C Vol. 83 (1961) pp. 370-376.

33. Sparrow, E. M., and R. D. Cess. "Subcooled Forced Convection Film Boiling on a Flat Plate." Trans. ASME Series C Vol. 83 (1961) pp. 377-379.

34. Tachibana, F., and S. Fukui. "Heat Transfer in Film Boiling to Subcooled Liquids." Int. Dev. in Heat Transfer Part II (1961) pp. 219-233.

35. Koh, J. C. Y. "Analysis of Film Boiling on Vertical Surfaces." Trans. ASME Series C Vol. 84 (1962) pp. 55-62.

36. Sparrow, E. M., and R. D. Cess. "The Effect of Subcooled Liquid on Laminar Film Boiling." Trans. ASME Series C Vol. 84 (1962) pp. 149-156.

37. Frederking, T. H. K., and J. A. Clark. "Natural Convection Film Boiling on a Sphere." Advances in Cryogenic Engineering, ed. K. D. Timmerhaus, Plenum Press, New York (1963) pp. 501-506.

38. Sparrow, E. M. "The Effect of Radiation on Film Boiling Heat Transfer." Int. Journ. of Heat and Mass Transfer Vol. 7 (1964) pp. 229-237.

39. Kobayashi, K. "Film Boiling Heat Transfer Around a Sphere in Forced Convection." Journ. of Nuclear Science and Technology Vol. 2, No. 2 (1965) pp. 62-67.

40. Farmer, W. F., Ph.D. Thesis, University of Tennessee, reported by H. F. Poppendiek. "Liquid Metal Heat Transfer." Heat Transfer Symp. Univ. Mich. (1963).

41. Lyon, R. E., A. S. Foust, and D. L. Katz. "Boiling Heat Transfer with Liquid Metals." Chem. Eng. Prog. Symp. Series Vol. 51, No. 17 (1955) pp. 41-47.

42. Madsen, N., and C. F. Bonilla. "Heat Transfer to Sodium-Potassium Alloy in Pool Boiling." Chem. Eng. Prog. Symp. Series Vol. 56, No. 30 (1960) pp. 251-259.

43. Korneev, M. I. "Pool Boiling Heat Transfer With Mercury and Magnesium Amalgams." Teploenerg. Vol. 2, No. 4 (1955) p. 44.

44. Noyes, R. C. "An Experimental Study of Sodium Pool Boiling Heat Transfer." Trans. ASME Series C Vol. 85 (1963) pp. 125-131.

45. Noyes, R. C. "Summary of Sodium Boiling and Condensing Studies." Proceedings of 1962 High-Temperature Liquid-Metal Heat Transfer Technology Meeting, BNL 756 (C-35) Upton, New York, (1962) pp. 97-113.

46. Subbotin, V. I. et al. "Heat Removal From the Reactor Fuel Elements Cooled by Liquid Metals." Paper A/CONF 28/P/328 Presented at Third United Nations Int. Conference on the Peaceful Uses of Atomic Energy, Geneva (May 1964).

47. Marto, P. J., and W. M. Rohsenow. "Effect of Surface Conditions on Nucleate Pool Boiling of Sodium." Trans. ASME Series C Vol 88, (1966) pp. 196-204.

48. Marto, P. J., and W. M. Rohsenow. "Nucleate Boiling Instability of Alkali Metals." Trans. ASME Series C Vol. 88 (1966) pp. 183-195.

49. Wiener, M. M. "Heat Transfer to Pool Boiling Potassium." (unpub. M. S. Thesis, Columbia Univ., 1963).

50. Colver, C. P., and R. E. Balzhiser. "A Study of Saturated Pool Boiling Potassium up to Burnout Heat Fluxes." AIChE Preprint No. 27, Seventh National Heat Transfer Conference, Cleveland (1964).

51. Adams, J. M. "An Investigation of Heat Transfer to Pool-Boiling Magnesium." ASME Paper 65-WT-49 (1965).

52. Krakoviak, A. I. "Notes on the Liquid-Metal Boiling Phenomena." ORNL TM-618 (1963).

53. Holtz, R. E. "A Study of the Initiation of Nucleate Boiling in the Liquid Metals." ANL-6980 (1964).

54. Tang, Y. S. "Liquid-Metal Boiling Heat Transfer." Nuclear Applications Vol. 1 (1965) pp. 521-537.

55. Schlichting, H. Boundary Layer Theory, 4th ed. McGraw-Hill (New York, N. Y., 1960) p. 187.

56. Milne-Thomson, L. M. Theoretical Hydrodynamics, 4th ed. MacMillian Co. (New York, N.Y., 1960) p. 464.

57. Sideman, S. "The Equivalence of the Penetration Theory and Potential Flow Theories." Ind. and Eng. Chem. Vol 58, No. 2 (1966) pp. 54-58.

58. Dunn, S. T., National Bureau of Standards, Washington, D. C., Private Communications, November 15, 1965

59. Kutateladze, S. S. et al. "Heat Transfer During Transverse Flow Around Cylinders." Liquid-Metal Heat Transfer Media Consultants Bureau, Inc., New York (1959) pp. 77-81.

60. Hampel, C. A. Rare Metals Handbook, 2nd ed. Reinhold Co. (New York, N.Y., 1961).

61. Stolz, G. "Numerical Solutions to an Inverse Problem of Heat Conduction for Simple Shapes." Trans. ASME Series C Vol. 82 (1960) pp. 20-26.

62. Dunning, E. L. "Thermodynamic Properties of Sodium." ANL-6246, 1960.

63. Vliet, G. C., and G. Leppert. "Forced Convection Heat Transfer From an Isothermal Sphere to Water." Trans. ASME Series C Vol 85 (1963) pp. 163-171.

APPENDIX A

SOLUTION TO LIQUID AND VAPOR BOUNDARY LAYER EQUATIONS

The reduced energy equation for liquid flowing around a spherical vapor space can be written as

$$u_r \frac{\partial T}{\partial r} + u_\phi \frac{1}{r} \frac{\partial T}{\partial \phi} = \alpha \frac{\partial^2 T}{\partial r^2} \tag{A1}$$

Equation (A1) is written in spherical coordinates (r,ϕ,θ) by assuming axial symmetry and neglecting conduction in the ϕ-direction as compared to convection in that direction. It is also assumed that heat is transferred in a very thin liquid layer. The velocities, u_r and u_ϕ, represent velocity in the radial and angular directions respectively. T is temperature and α is the thermal diffusivity of the liquid.

The boundary conditions applicable to the case of liquid overriding a vapor film are given by,

$$\begin{aligned} T &= T_B & r &= \infty & \phi &\geq 0 \\ T &= T_{sat} & r &= R & \phi &> 0 \\ T &= T_B & \infty &\geq r \geq R & \phi &= 0 \end{aligned} \tag{A2}$$

where T_B represents the temperature in the bulk liquid flowing past the spherical region and T_{sat} is the saturation temperature of the liquid. R is the radius of the spherical region, and if the vapor film thickness is assumed thin, the radius of the solid sphere may be used for this quantity.

Defining y by y = r-R, one may write

$$u_r = -3U_\infty \frac{y}{R} \cos\phi;\ u_\phi = 3/2U_\infty \sin\phi \ .$$

Transformation variables can be defined as,

$$\begin{aligned} \Delta T &= T - T_{sat}, \\ \psi &= y \sin^2 \phi, \\ \eta &= \int_0^\phi \sin^3 \phi \, d\phi \ . \end{aligned} \tag{A3}$$

Equation (A1) can now be written as

$$\frac{\partial \Delta T}{\partial \eta} = M \frac{\partial^2 \Delta T}{\partial \psi^2} \ , \tag{A4}$$

where M is defined by

$$M = (2/3)\ R\ \alpha/U_\infty \ .$$

The boundary conditions (A2) transform into

$$\begin{aligned} &\Delta T = T_B - T_{sat} && \psi = \infty && \eta \geq 0 \\ &\Delta T = 0 && \psi = 0 && \eta > 0 \\ &\Delta T = T_B - T_{sat} && \infty \geq \psi \geq 0 && \eta = 0 \end{aligned} \tag{A5}$$

Equation (A4) and the associated boundary conditions constitute a system of equations identical to the heat conduction equation for which solutions are known. A solution is

$$\frac{T - T_B}{T_{sat} - T_B} = \operatorname{erfc}\left[\frac{\psi}{2\sqrt{M\eta}}\right] \ , \tag{A6}$$

where the complementary error function is defined by

$$\operatorname{erfc}(a) = 1 - \operatorname{erf}(a) = 1 - \frac{2}{\sqrt{\pi}} \int_0^a e^{-\lambda^2} \, d\lambda \ .$$

The heat flux into the liquid from the liquid-vapor interface can be found by differentiating equation (A6). The heat flux can be written as

$$q/A = -k\left(\frac{\partial T}{\partial y}\right)_{y=0} \ . \tag{A7}$$

The temperature gradient $\frac{\partial T}{\partial y}$ can be written as

$$\frac{\partial T}{\partial y} = \frac{\partial T}{\partial \psi} \frac{\partial \psi}{\partial y} + \frac{\partial T}{\partial \eta} \frac{\partial \eta}{\partial y} .$$

However, $\frac{\partial \eta}{\partial y}$ is zero, and the gradient becomes

$$\frac{\partial T}{\partial y} = \frac{\partial T}{\partial \psi} \frac{\partial \psi}{\partial y} ,$$

or alternately

$$\frac{\partial T}{\partial y} = \frac{\partial \Delta T}{\partial y} = \frac{\partial \Delta T}{\partial \psi} \frac{\partial \psi}{\partial y}$$

The term $\frac{\partial \Delta T}{\partial \psi}$ is evaluated as

$$\frac{\partial \Delta T}{\partial \psi} = - \frac{\Delta T_B}{\sqrt{\pi} \sqrt{M \eta}} ,$$

where $\Delta T_B = T_{sat} - T_B$ and

$$\frac{\partial \psi}{\partial y} = \sin^2 \phi .$$

Therefore the heat flux into the bulk liquid from the liquid-vapor interface becomes

$$q/A = \frac{k \Delta T_B \sin^2 \phi}{(\pi M \eta)^{1/2}} \qquad \text{(A8)}$$

Vapor Boundary Layer

The momentum and energy conservation equations for a vapor film flowing around a sphere can be written as

$$u \frac{\partial u}{\partial x} + v \frac{\partial u}{\partial y} = - \frac{1}{\rho} \frac{\partial p}{\partial x} + \frac{\mu}{\rho} \frac{\partial^2 u}{\partial y^2} \qquad \text{(A9)}$$

$$u \frac{\partial T}{\partial x} + v \frac{\partial T}{\partial y} = \alpha \frac{\partial^2 T}{\partial y^2} , \qquad \text{(A10)}$$

where u and v are the components of vapor velocity in the x-direction (along the sphere surface) and the y-direction (normal to the sphere surface) respectively. The pressure at any point in the vapor film is

represented by p. The boundary conditions applicable to this case are

$$\begin{aligned} &y = 0, \quad u = 0 \quad T = T_w \ , \\ &y = \delta \quad u = U(x) \quad T = T_{sat} \ , \end{aligned} \tag{A11}$$

where δ is the film thickness and $U(x) = 3/2\ U_\infty \sin \phi$. By assuming that inertia effects and energy convection in the vapor boundary layer are negligible equations (A9) and (A10) can be written as

$$\frac{\partial p}{\partial x} = \mu \frac{\partial^2 u}{\partial y^2} \tag{A12}$$

$$\frac{\partial^2 T}{\partial y^2} = 0 \tag{A13}$$

The solution to equation (A13) can be immediately written as

$$T = C_1\, y + C_2 \ .$$

Evaluations of the constants C_1 and C_2 from the boundary conditions give

$$T = T_w + (T_{sat} - T_w)\ y/\delta \ .$$

The following result is obtained by rearranging

$$\frac{T - T_{sat}}{T_w - T_{sat}} = 1 - y/\delta \ . \tag{A14}$$

The temperature distribution in the vapor film simply turns out to be linear.

The solution to equation (A12) can be written as

$$u = \frac{1}{2\mu} \frac{\partial p}{\partial x} y^2 + C_3\, y + C_4 \ .$$

C_4 is zero from the condition that $u = 0$ at $y = 0$. Evaluation of the constant C_3 gives

$$u = 3/2\ U_\infty(\sin\phi)y/\delta + \frac{1}{2\mu}\frac{\partial p}{\partial x}(y^2 - y\delta) . \qquad (A15)$$

If it is assumed that the pressure in the liquid layer is "impressed" upon the vapor layer, the pressure gradient term $\frac{\partial p}{\partial x}$ can be replaced by a velocity gradient term. Bernoulli's equation for the liquid neglecting height changes is

$$p_o = p + 1/2\ \rho\ U^2 = \text{constant} .$$

By taking the derivative with respect to x, the following is obtained

$$\frac{\partial p}{\partial x} = -\rho\ U\frac{\partial U}{\partial x}$$

U is the velocity of the liquid at the liquid-vapor interface. Therefore $\frac{\partial p}{\partial x}$ can be written as

$$\frac{\partial p}{\partial x} = -(3/2)^2\ \frac{\rho U_\infty^2}{R}\ \cos\phi\ \sin\phi .$$

Substitution of this result into equation (A15) gives

$$u = 3/2\ U_\infty\ \sin\phi\left[y/\delta + 3/4\ \frac{\rho U_\infty}{\mu\ R}\cos\phi)\ (y\delta - y^2)\right]. \qquad (A16)$$

Equation (A16) represents the velocity at any point in the vapor film.

APPENDIX B

EXPERIMENTAL TECHNIQUE

The sequence of events which were followed when the heat transfer apparatus was used to obtain data is given in this appendix.

1. Turn on all electrical equipment to allow for warmup.
2. Check the water and oxygen content of the argon atmosphere. Normally these should be approximately 5 ppm.
3. Check for water in the oil reservoir for the sodium tank cooling system.
4. Turn sodium tank cooling oil recirculating system on.
5. Check thermocouples monitoring the sodium temperature and the sodium tank heat exchanger temperature to see that they are in place and connected.
6. Check pressure in box.
7. Turn electrical heaters on and begin heating the sodium.
8. As the sodium is being heated, continually check the pressure in the box. (A good indication of a sudden pressure rise in the box is the manner in which the gloves hang. If they stand out rigidly, the pressure is high.) Also, monitor the temperature of the sodium tank heat exchanger. If this temperature exceeds 100°C, turn on the cooling water to the oil-water heat exchanger.

9. Remove any oxide film from the top of the sodium pool.
10. Allow sodium to reach desired steady state conditions.
11. Check data recording system for readiness.
12. Turn on oil recirculating system for the induction heating coil.
13. Check induction heating system flow meter for oil flow and also for any indication of oil-water mixing.
14. Position sphere in induction heating coil.
15. Heat sphere to desired temperature. (Observed visually on the Visicorder galvanometer system.)
16. Actuate motor, take data run.
17. Check pressure in glovebox.
18. Repeat steps 9, 10, 11, 14, 15, 16, 17 until required data range is covered.
19. When data taking is complete, turn electrical sodium tank heaters off. Increase cooling water rate to the sodium tank oil cooling system so that maximum cooling can occur.
20. When induction coil oil system has reached approximately room temperature, turn off pump.
21. After 5 minutes, shut down induction generator.
22. Monitor sodium temperature until sodium has solidified.
23. Turn off sodium tank oil recirculating system and cooling water.

APPENDIX C

EXPERIMENTAL TEMPERATURE-TIME DATA

Run	Vel. f.p.s.	Sodium Temp. °F	T. C. No.	Temp. In °F	Temp. Out °F	Time Sec.
28	10.36	577	TCP #1	3434		
29	9.83	572	"	3020		
30	6.82	572	"	3326		
31	6.04	572	"	3317		
32	11.50	572	TCP #3	3317		
33	10.70	568	"	3542	2174	0.0729
34	11.30	572	TCP #5	3427	2290	0.0655
35	11.30	572	"	3308	2201	0.0655
36	10.15	577	"	3056	2035	0.0729
37	10.60	568	TCP #3	3398	2183	0.0770
38	10.25	577	"	2967	1931	0.0785
39	10.00	572	"	2957	2021	0.0778
40	10.00	570	"	2732	1832	0.0778
41	10.00	572	"	2264	1616	0.0778
42	9.80	574	TCP #5	3416	2048	0.0793
43	9.92	572	"	2480	1654	0.0783
44	10.70	574	"	2111	1544	0.0726
45	10.10	574	TCP #3	3389	2237	0.0770
46	10.26	572	"	2948	1976	0.0758
47	10.45	572	"	2597	1841	0.0744
48	10.45	576	"	2228	1652	0.0744
49	10.69	570	TCP #5	3384	2336	0.0735
50	10.10	572	"	2660	1814	0.0770

51	10.30	577	TCP #5	3074	2062	0.0755
52	10.45	577	TCP #3	3074	2147	0.0665
53	9.60	572	"	2786	1895	0.0724
54	10.45	572	"	2417	1787	0.0665
55	9.50	576	TCP #5	3155	2120	0.0732
56	10.80	570	"	2750	1934	0.0644
57	10.45	572	"	2426	1792	0.0664

Run 59 Date 7/19/66 Velocity 9.60 ft/sec Temp. Na 572°F

Thermocouple No. 93 Time in Sodium .115 sec T.C. Shape Straight

Thermocouple Position 0.828 Sphere Diameter 0.500 in.

Time (sec)	0.00	0.01	0.02	0.03	0.04	0.05	0.06	0.07	0.08
Temp (°F)	3182	3083	2804	2534	2318	2138	2174	1877	1778

Time (sec)	0.09	0.10	0.11	0.12	0.13	0.14	0.15	0.16	0.17
Temp (°F)	1688	1616	1548	1486	1450				

Time (sec)	0.18	0.19	0.20	0.21	0.22	0.23	Min .136	Equil. .7
Temp (°F)							1450	2183

Run 60 Date 7-19-66 Velocity 9.60 ft/sec Temp. Na 577°F

Thermocouple No. 93 Time in Sodium .115 sec T.C. Shape Straight

Thermocouple Position 0.828 Sphere Diameter 0.500 in.

Time (sec)	0.00	0.01	0.02	0.03	0.04	0.05	0.06	0.07	0.08
Temp (°F)	2759	2678	2444	2196	2030	1900	1787	1674	1587

Time (sec)	0.09	0.10	0.11	0.12	0.13	0.14	0.15	0.16	0.17
Temp (°F)	1515	1472	1427	1400	1368				

Time (sec)	0.18	0.19	0.20	0.21	0.22	0.23	Min .135	Equil. .7
Temp (°F)							1368	1742

Run 61 Date 7/19/66 Velocity 10.26ft/sec Temp. Na 572°F

Thermocouple No. 93 Time in Sodium .1077 sec T.C. Shape Straight

Thermocouple Position 0.828 Sphere Diameter 0.500 in.

Time (sec)	0.00	0.01	0.02	0.03	0.04	0.05	0.06	0.07	0.08
Temp (°F)	2678	2579	2345	2120	1967	1832	1728	1634	1571

Time (sec)	0.09	0.10	0.11	0.12	0.13	0.14	0.15	0.16	0.17
Temp (°F)	1499	1445	1404	1369	1360				

Time (sec)	0.18	0.19	0.20	0.21	0.22	0.23	Min .13	Equil. .7
Temp (°F)							1360	1720

Run 62 Date 7/19/66 Velocity 9.76 Temp. Na 570°F

Thermocouple No. 93 Time in Sodium .1131 sec. T.C. Shape Straight

Thermocouple Position 0.828 Sphere Diameter 0.500 in.

Time (sec)	0.00	0.01	0.02	0.03	0.04	0.05	0.06	0.07	0.08
Temp (°F)	2030	1958	1787	1625	1540	1436	1368	1310	1256

Time (sec)	0.09	0.10	0.11	0.12	0.13	0.14	0.15	0.16	0.17
Temp (°F)	1211	1175	1144	1126	1112				

Time (sec)	0.18	0.19	0.20	0.21	0.22	0.23	Min .13	Equil. .7
Temp (°F)							1112	1301

Run 63 Date 7/20/66 Velocity 9.60ft/sec Temp. Na 572°F

Thermocouple No. 93 Time in Sodium .115 sec T.C. Shape Straight

Thermocouple Position 0.828 Sphere Diameter 0.500 in.

Time (sec)	0.00	0.01	0.02	0.03	0.04	0.05	0.06	0.07	0.08
Temp (°F)	3600	3497	3232	2912	2669	2471	2314	2174	2048

Time (sec)	0.09	0.10	0.11	0.12	0.13	0.14	0.15	0.16	0.17
Temp (°F)	1967	1882	1823	1769					

Time (sec)	0.18	0.19	0.20	0.21	0.22	0.23	Min .132	Equil. .7
Temp (°F)							1724	2354

Run 64 Date 7/20/66 Velocity 5.5 ft/sec Temp. Na 572°F

Thermocouple No. 93 Time in Sodium .127 sec T.C. Shape Straight

Thermocouple Position 0.828 Sphere Diameter 0.500 in.

Time (sec)	0.00	0.01	0.02	0.03	0.04	0.05	0.06	0.07	0.08
Temp (°F)	3101	3029	2813	2570	2381	2201	2066	1962	1877

Time (sec)	0.09	0.10	0.11	0.12	0.13	0.14	0.15	0.16	0.17
Temp (°F)	1787	1706	1652	1598					

Time (sec)	0.18	0.19	0.20	0.21	0.22	0.23	Min .142	Equil. 1.20
Temp (°F)							1535	1760

Run 66 Date 7/21/66 Velocity 5.98 ft/sec Temp. Na 570°F

Thermocouple No. 93 Time in Sodium .116 sec T.C. Shape Straight

Thermocouple Position 0.828 Sphere Diameter 0.500 in.

Time (sec)	0.00	0.01	0.02	0.03	0.04	0.05	0.06	0.07	0.08
Temp (°F)	2624	2570	2408	2210	2048	1904	1796	1724	1652

Time (sec)	0.09	0.10	0.11	0.12	0.13	0.14	0.15	0.16	0.17
Temp (°F)	1580	1526	1436	1418					

Time (sec)	0.18	0.19	0.20	0.21	0.22	0.23	Min .13	Equil. .18
Temp (°F)							1382	1706

Run 67 Date 7/21/66 Velocity 6.03 ft/sec Temp. Na 572°F

Thermocouple No. 93 Time in Sodium .115 sec T.C. Shape Straight

Thermocouple Position 0.828 Sphere Diameter 0.500 in.

Time (sec)	0.00	0.01	0.02	0.03	0.04	0.05	0.06	0.07	0.08
Temp (°F)	2687	2624	2462	2264	2084	1985	1895	1814	1742

Time (sec)	0.09	0.10	0.11	0.12	0.13	0.14	0.15	0.16	0.17
Temp (°F)	1688	1616	1580	1544					

Time (sec)	0.18	0.19	0.20	0.21	0.22	0.23	Min .125	Equil. ~ .7
Temp (°F)							1526	1769

Run 68 Date 7/21/66 Velocity 5.48ft/sec Temp. Na 572°F

Thermocouple No. 93 Time in Sodium .127 sec T.C. Shape Straight

Thermocouple Position 0.828 Sphere Diameter 0.500 in.

Time (sec)	0.00	0.01	0.02	0.03	0.04	0.05	0.06	0.07	0.08
Temp (°F)	3299	3254	3056	2813	2615	2422	2255	2129	2048

Time (sec)	0.09	0.10	0.11	0.12	0.13	0.14	0.15	0.16	0.17
Temp (°F)	1958	1879	1814	1576					

Time (sec)	0.18	0.19	0.20	0.21	0.22	0.23	Min .146	Equil. 1.5
Temp (°F)							1661	1877

Run 70 Date 7/26/66 Velocity 10.1ft/sec Temp. Na 570°F

Thermocouple No. 91 Time in Sodium .1092 sec T.C. Shape Bent

Thermocouple Position 0.828 Sphere Diameter 0.500 in.

Time (sec)	0.00	0.01	0.02	0.03	0.04	0.05	0.06	0.07	0.08
Temp (°F)	2894	2811	2649	2471	2332	2174	2057	1944	1850

Time (sec)	0.09	0.10	0.11	0.12	0.13	0.14	0.15	0.16	0.17
Temp (°F)	1769	1679	1625	1571	1551	1548	1519	1519	

Time (sec)	0.18	0.19	0.20	0.21	0.22	0.23	Min .16	Equil. .6
Temp (°F)							1519	1679

Run 71 Date 7/28/66 Velocity 10.45 ft/sec Temp. Na 570°F

Thermocouple No. 91 Time in Sodium 0.11 sec T.C. Shape Bent

Thermocouple Position 0.828 Sphere Diameter 0.500 in.

Time (sec)	0.00	0.01	0.02	0.03	0.04	0.05	0.06	0.07	0.08
Temp (°F)	3141	3092	2876	2660	2516	2354	2228	2107	1994

Time (sec)	0.09	0.10	0.11	0.12	0.13	0.14	0.15	0.16	0.17
Temp (°F)	2084	1814	1733	1688	1643	1634	1620		

Time (sec)	0.18	0.19	0.20	0.21	0.22	0.23	Min .15	Equil. ∿.7
Temp (°F)							1620	1778

Run 72 Date 7/28/66 Velocity 10.1ft/sec Temp. Na 572°F

Thermocouple No. 91 Time in Sodium 0.116 sec T.C. Shape Bent

Thermocouple Position 0.828 Sphere Diameter 0.500 in.

Time (sec)	0.00	0.01	0.02	0.03	0.04	0.05	0.06	0.07	0.08
Temp (°F)	2678	2674	2570	2219	2075	1931	1832	1724	1634

Time (sec)	0.09	0.10	0.11	0.12	0.13	0.14	0.15	0.16	0.17
Temp (°F)	1562	1481	1418	1364	1328	1310	1292	1283	

Time (sec)	0.18	0.19	0.20	0.21	0.22	0.23	Min .162	Equil. 1.90
Temp (°F)							1283	1670

Run 73 Date 7/29/66 Velocity 9.98 ft/sec Temp. Na 572°F

Thermocouple No. 93 Time in Sodium .114 sec T.C. Shape Straight

Thermocouple Position 0.828 Sphere Diameter 0.500 in.

Time (sec)	0.00	0.01	0.02	0.03	0.04	0.05	0.06	0.07	0.08
Temp (°F)	2795	2768	2561	2345	2156	2021	1904	1836	1769

Time (sec)	0.09	0.10	0.11	0.12	0.13	0.14	0.15	0.16	0.17
Temp (°F)	1679	1625	1571	1526	1499				

Time (sec)	0.18	0.19	0.20	0.21	0.22	0.23	Min .135	Equil. ~ .90
Temp (°F)							1497	1823

Run 74 Date 8/1/66 Velocity 9.90 ft/sec Temp. Na 842°F

Thermocouple No. 91 Time in Sodium .120 sec T.C. Shape Bent

Thermocouple Position 0.828 Sphere Diameter 0.500 in.

Time (sec)	0.00	0.01	0.02	0.03	0.04	0.05	0.06	0.07	0.08
Temp (°F)	3155	3092	2984	2777	2624	2462	2354	2246	2156

Time (sec)	0.09	0.10	0.11	0.12	0.13	0.14	0.15	0.16	0.17
Temp (°F)	2066	1985	1904	1859	1805	1796	1778		

Time (sec)	0.18	0.19	0.20	0.21	0.22	0.23	Min .15	Equil. ~1.05
Temp (°F)							1778	1868

Run 75 Date 8-1-66 Velocity 10.9 ft/sec Temp. Na 842°F

Thermocouple No. 91 Time in Sodium .108 sec T.C. Shape Bent

Thermocouple Position 0.828 Sphere Diameter 0.500 in.

Time (sec)	0.00	0.01	0.02	0.03	0.04	0.05	0.06	0.07	0.08
Temp (°F)	2849	2804	2714	2606	2408	2300	2219	2102	1994

Time (sec)	0.09	0.10	0.11	0.12	0.13	0.14	0.15	0.16	0.17
Temp (°F)	1904	1841	1778	1742	1706	1697	1688		

Time (sec)	0.18	0.19	0.20	0.21	0.22	0.23	Min .15	Equil. ∿.87
Temp (°F)							1688	1796

Run 76 Date 8/1/66 Velocity 11.35 ft/sec Temp. Na 838°F

Thermocouple No. 91 Time in Sodium .104 sec T.C. Shape Bent

Thermocouple Position 0.828 Sphere Diameter 0.500 in.

Time (sec)	0.00	0.01	0.02	0.03	0.04	0.05	0.06	0.07	0.08
Temp (°F)	2327	2300	2201	2120	2012	1922	1895	1769	1706

Time (sec)	0.09	0.10	0.11	0.12	0.13	0.14	0.15	0.16	0.17
Temp (°F)	1652	1598	1553	1526	1508	1499			

Time (sec)	0.18	0.19	0.20	0.21	0.22	0.23	Min .14	Equil. 1.13
Temp (°F)							1499	1724

Run 77 Date 8/1/66 Velocity 10.7 ft/sec Temp. Na 842°F

Thermocouple No. 91 Time in Sodium .110 sec T.C. Shape Bent

Thermocouple Position 0.828 Sphere Diameter 0.500 in.

Time (sec)	0.00	0.01	0.02	0.03	0.04	0.05	0.06	0.07	0.08
Temp (°F)	2120	2084	2048	1904	1814	1751	1679	1625	1571

Time (sec)	0.09	0.10	0.11	0.12	0.13	0.14	0.15	0.16	0.17
Temp (°F)	1526	1481	1436	1418	1400	1391			

Time (sec)	0.18	0.19	0.20	0.21	0.22	0.23	Min .14	Equil. .77
Temp (°F)							1391	1499

Run 79 Date 8/22/66 Velocity 10.20 ft/sec Temp. Na 577°F

Thermocouple No. 91 Time in Sodium .114 sec T.C. Shape Bent

Thermocouple Position 0.828 Sphere Diameter 0.500 in.

Time (sec)	0.00	0.01	0.02	0.03	0.04	0.05	0.06	0.07	0.08
Temp (°F)	2435	2345	2210	2030	1868	1733	1625	1553	1481

Time (sec)	0.09	0.10	0.11	0.12	0.13	0.14	0.15	0.16	0.17
Temp (°F)	1418	1373	1319	1292	1283				

Time (sec)	0.18	0.19	0.20	0.21	0.22	0.23	Min .13	Equil. ~.2
Temp (°F)							1283	1679

Run 80 Date 8/22/66 Velocity 10.2 ft/sec Temp. Na 577°F

Thermocouple No. 91 Time in Sodium .114 sec T.C. Shape Bent

Thermocouple Position 0.828 Sphere Diameter 0.500 in.

Time (sec)	0.00	0.01	0.02	0.03	0.04	0.05	0.06	0.07	0.08
Temp (°F)	2016	1980	1868	1724	1607	1508	1414	1350	1292

Time (sec)	0.09	0.10	0.11	0.12	0.13	0.14	0.15	0.16	0.17
Temp (°F)	1247	1202	1166	1139	1126				

Time (sec)	0.18	0.19	0.20	0.21	0.22	0.23	Min .13	Equil. 2.0
Temp (°F)							1126	1256

Run 81 Date 8/22/66 Velocity 6.38 ft/sec Temp. Na 570°F

Thermocouple No. 91 Time in Sodium .192 sec T.C. Shape Bent

Thermocouple Position 0.828 Sphere Diameter 0.500 in.

Time (sec)	0.00	0.01	0.02	0.03	0.04	0.05	0.06	0.07	0.08
Temp (°F)	2669	2588	2457	2318	2156	2074	1863	1742	1652

Time (sec)	0.09	0.10	0.11	0.12	0.13	0.14	0.15	0.16	0.17
Temp (°F)	1580	1517	1454	1400	1355	1319	1292	1256	1220

Time (sec)	0.18	0.19	0.20	0.21	0.22	0.23	Min .20	Equil. 2.0
Temp (°F)	1202	1184	1166				1166	1382

Run 82 Date 8-22-66 Velocity 5.45 ft/sec Temp. Na 572°F

Thermocouple No. 91 Time in Sodium 219 sec T.C. Shape Bent

Thermocouple Position 0.828 Sphere Diameter 0.500 in.

Time (sec)	0.00	0.01	0.02	0.03	0.04	0.05	0.06	0.07	0.08
Temp (°F)	2426	2390	2300	2152	1980	1832	1706	1616	1544

Time (sec)	0.09	0.10	0.11	0.12	0.13	0.14	0.15	0.16	0.17
Temp (°F)	1454	1418	1364	1328	1292	1243	1220	1202	1166

Time (sec)	0.18	0.19	0.20	0.21	0.22	0.23	Min .23	Equil. ∿ 2.01
Temp (°F)	1148	1112	1094	1076	1067	1058	1058	1238

Run 83 Date 8/22/66 Velocity 5.99 ft/sec Temp. Na 572°F

Thermocouple No. 91 Time in Sodium .194 sec T.C. Shape Bent

Thermocouple Position 0.828 Sphere Diameter 0.500 in.

Time (sec)	0.00	0.01	0.02	0.03	0.04	0.05	0.06	0.07	0.08
Temp (°F)	2057	2030	1922	1809	1652	1562	1418	1382	1328

Time (sec)	0.09	0.10	0.11	0.12	0.13	0.14	0.15	0.16	0.17
Temp (°F)	1274	1238	1202	1166	1148	1112	1085	1067	1049

Time (sec)	0.18	0.19	0.20	0.21	0.22	0.23	Min .21	Equil. ∿ 2.0
Temp (°F)	1031	1013	1004	991			991	1134

Run 84 Date 8/24/66 Velocity 6.20ft/sec Temp. Na 842°F

Thermocouple No. 91 Time in Sodium .122 sec T.C. Shape Bent

Thermocouple Position 0.828 Sphere Diameter 0.500 in.

Time (sec)	0.00	0.01	0.02	0.03	0.04	0.05	0.06	0.07	0.08
Temp (°F)	2795	2782	2732	2597	2471	2349	2246	2129	2003

Time (sec)	0.09	0.10	0.11	0.12	0.13	0.14	0.15	0.16	0.17
Temp (°F)	1904	1796	1724	1679	1634	1616	1607		

Time (sec)	0.18	0.19	0.20	0.21	0.22	0.23	Min .15	Equil.
Temp (°F)							1607	1787

Run 85 Date 8/25/66 Velocity 4.28 ft/sec Temp. Na 572°F

Thermocouple No. 91 Time in Sodium .152 sec T.C. Shape Bent

Thermocouple Position 0.828 Sphere Diameter 0.500 in.

Time (sec)	0.00	0.01	0.02	0.03	0.04	0.05	0.06	0.07	0.08
Temp (°F)	2458	2440	2354	2237	2102	1940	1796	1688	1634

Time (sec)	0.09	0.10	0.11	0.12	0.13	0.14	0.15	0.16	0.17
Temp (°F)	1517	1454	1400	1346	1310	1265	1247	1229	

Time (sec)	0.18	0.19	0.20	0.21	0.22	0.23	Min .16	Equil.
Temp (°F)							1229	1445

Run 86 Date 8/25/66 Velocity 3.48 ft/sec Temp. Na 577°F

Thermocouple No. 91 Time in Sodium .187 sec T.C. Shape Bent

Thermocouple Position 0.828 Sphere Diameter 0.500 in.

Time (sec)	0.00	0.01	0.02	0.03	0.04	0.05	0.06	0.07	0.08
Temp (°F)	2363	2350	2264	2152	2012	1868	1733	1638	1562

Time (sec)	0.09	0.10	0.11	0.12	0.13	0.14	0.15	0.16	0.17
Temp (°F)	1499	1436	1373	1337	1292	1265	1238		

Time (sec)	0.18	0.19	0.20	0.21	0.22	0.23	Min	Equil.
Temp (°F)								1346

Run 87 Date 8/31/66 Velocity 14.06 ft/sec Temp. Na 572°F

Thermocouple No. 91 Time in Sodium .080 sec T.C. Shape Bent

Thermocouple Position 0.828 Sphere Diameter 0.500 in.

Time (sec)	0.00	0.01	0.02	0.03	0.04	0.05	0.06	0.07	0.08
Temp (°F)	2534	2498	2386	2237	2066	1904	1760	1661	1580

Time (sec)	0.09	0.10	0.11	0.12	0.13	0.14	0.15	0.16	0.17
Temp (°F)	1517								

Time (sec)	0.18	0.19	0.20	0.21	0.22	0.23	Min .10	Equil.
Temp (°F)							1454	1670

APPENDIX D

FORTRAN COMPUTER PROGRAMS FOR DATA REDUCTION METHODS

```
      PROGRAM SP TR CL
C     SPHERE TRANSIENT COOLING
      DIMENSION X(20),F(100),G(100),DELQ(100),THETA(100),Q(100)
      DIMENSION TEMP(100)
C     READ IN PARAMETERS
    5 READ 1, ALPHA,RHO,CP,R,RHOST,EXPNO
      IF(EOF,60)999,17
    1 FORMAT (5F12.6,I4)
   17 READ 2,(X(I),I=1,15)
    2 FORMAT (5F12.6)
      READ 3,TEMPI,TIME,DELTM,NUM
    3 FORMAT (3F12.6,I6)
      READ4,(TEMP(I),I=1,NUM)
    4 FORMAT (6F12.6)
      Z = RHO * CP * R / 3.0
      P =(R*R/ALPHA) *(RHOST * RHOST/6.0 *.10)
      S =(R*R/ALPHA) * 0.06667
C     CALCULATE RESPONSE FUNCTION F
      F(1)=0.0
      A = DELTM
      DO 11 I=1,NUM
      K=I+1
      SUM = 0.0
      DO 10 J=1,15
      B =0.0
      W =SIN(X(J)*RHOST)/(RHOST *SIN(X(J)))
      Y =EXP(-X(J)*X(J)*ALPHA/(R*R) *A)/(X(J)*X(J)*ALPHA/(R*R))
      B = W*Y
      SUM = SUM +B
   10 CONTINUE
      H=A+P*.667*SUM
   15 F(K)=H
      A=A+DELTM
   11 CONTINUE
C     CALCULATE RESPONSE FUNCTION  G
      G(1)=0.0
      A1=DELTM
      DO 20 I=1,NUM
      L=I+1
      SUM1 = 0.0
      DO 21 J=1,15
      B1=0.0
      B1 =EXP(-X(J)*X(J) *ALPHA/(R*R) *A1)/(X(J)*X(J) *ALPHA/(R*R))
      SUM1 = SUM1 +B1
   21 CONTINUE
      V=A1+S*.667*SUM1
   24 G(L)=V
      A1 =A1 + DELTM
   20 CONTINUE
C     CALCULATE DELQ(I)
      U=Z*(TEMPI-TEMP(1))/F(2)
      DELQ(1)=U
      DO 30 I=2,NUM
      A2=Z * (TEMPI -TEMP(I))
      M=I-1
      L1=I+2
```

```
      SUM2 = 0.0
      DO 31 J=1,M
      B2=DELQ(J)*F(L1+J)
   31 SUM2 = SUM2 + B2
      V1=(A2-SUM2)/F(2)
   30 DELQ(I)=V1
C     CALCULATE  Q(I)
      SUM4 = 0.0
      DO 50  I=1,NUM
      B4=DELQ(I)
      SUM4 = SUM4 + B4
   50 Q(I)=SUM4
C     CALCULATE  SURFACE TEMPERATURE
      DO 40 I=1,NUM
      SUM3=0.0
      I3=I+2
      DO 41 J=1,I
      B3=DELQ(J)*G(I3-J)
   41 SUM3 =SUM3 + B3
      V2=SUM3/Z
   40 THETA(I)=V2
      CONTINUE
C     PRINT  OUT  PARAMETERS
      NUM1=NUM+1
      PRINT 60 ,EXPNO
   60 FORMAT (45H SPHERE TRANSIENT COOLING   EXPERIMENT NUMBER, I4 )
      PRINT 61,ALPHA,CP,R,RHOST
   61 FORMAT (7H ALPHA=,F8.4,10X,4H CP=,F8.4,10X,3H R=,F8.4,10X,7H RHOST
     1=,F8.4)
      PRINT 62 ,TEMPI,DELTM,NUM
   62 FORMAT (7H TEMPI=,F10.4,5X,7H DELTM=,F10.6,5X,5H NUM=,I5,//)
      PRINT 73, Z
   73 FORMAT (10X,*Z=*,F12.6)
      PRINT 63
   63 FORMAT(10X,*RESPONSE FUNCTION*)
      PRINT 64,(F(I),I=1,NUM1)
   64 FORMAT (10X,6F12.6)
      PRINT 69
   69 FORMAT (10X,*RESPONSE FUNCTION G*)
      PRINT 70, (G(I),I=1,NUM1)
   70 FORMAT (10X,6F12.6)
      PRINT 65
   65 FORMAT(10X,*SURFACE HEAT FLUX*)
      PRINT 66,(Q(I),I=1,NUM)
   66 FORMAT (10X,6F12.6)
      PRINT  67
   67 FORMAT(10X,*SURFACE TEMPERATURE DIFFERENCE*)
      PRINT 68, (THETA(J),J=1,NUM)
   68 FORMAT (10X,6F12.6 )
      GO TO 5
  999 STOP
      END
```

```
      PROGRAM SP TR CL
C     TRANSIENT COOLING OF SPHERE WITH KNOWN COEFFCIENT
      DIMENSION B(100),SUM(100),THETA(20),C1(100),C2(100),C3(200)
      DIMENSION C4(100),C5(200)
      READ 1,ALPHA,RHO,H,R,THCON,DELTM
    1 FORMAT (6F12.6)
      READ 2,M,N
    2 FORMAT (2I6)
      READ 3,(B(I),I=1,M)
    3 FORMAT (12F6.3)
      READ 4,(C1(I),I=1,M)
    4 FORMAT (6F12.6)
      READ 5,(C2(I),I=1,M)
    5 FORMAT (6F12.6)
      READ 6,(C3(I),I=1,M)
    6 FORMAT (6F12.6)
      READ 7,(C4(I),I=1,M)
    7 FORMAT (6F12.6)
      READ 8, (C5(I),I=1,M)
    8 FORMAT (6F12.6)
      DO 31 L=1,4
      THT = ALPHA*DELTM/(R*R)
      S=THT
      B1 = H*R/THCON
      IF (B1-0.1) 999,100,100
  100 CONTINUE
      IF (B1-31.0) 101,101,999
  101 CONTINUE
      PRINT 102
  102 FORMAT (10X,*SPHERE COOLING WITH KNOWN COEFFICIENT*,/)
      PRINT 103,H
  103 FORMAT (10X,*H=*,F12.6)
      PRINT 104,ALPHA,THCON,DELTM
  104 FORMAT (10X,*ALPHA=*,F12.6,* THCON=*,F12.6,* DELTM=*,F12.6)
      PRINT 105,R,RHO,M,N
  105 FORMAT (10X,*R=*,F12.6,* RHO=*,F12.6,* M=*,I4,* N=*,I4,/)
      DO 10 J=1,M
      A=B(J)
      IF (B1-A) 11,11,10
   10 CONTINUE
   11 CA =C1(J)-(B(J)-B1)*(C1(J)-C1(J-1))/(B(J)-B(J-1))
      CB = C2(J)-(B(J)-B1)*(C2(J)-C2(J-1))/(B(J)-B(J-1))
      CC =C3(J)-(B(J)-B1)*(C3(J)-C3(J-1))/(B(J)-B(J-1))
      CD = C4(J) -(B(J)-B1)*(C4(J)-C4(J-1))/(B(J)-B(J-1))
      CE = C5(J)-(B(J) -B1)*(C5(J)-C5(J-1))/(B(J)-B(J-1))
      DO 30 I=1,N
      G=RHO/R
C     CALCULATE REDUCED TEMPERATURE
      DO 20 K=1,2
      A1=(SINF(CA)-CA*COSF(CA))*EXPF(-CA*CA*THT)*SINF(CA*G)/
     1(CA*(CA-SINF(CA)*COSF(CA)))
      A2 = (SINF(CB)-CB*COSF(CB))*EXPF(-CB*CB*THT)*SINF(CB*G)/
     1(CB*(CB-SINF(CB)*COSF(CB)))
      A3=(SINF(CC)-CC*COSF(CC))*EXPF(-CC*CC*THT)*SINF(CC*G)/
     1(CC*(CC-SINF(CC)*COSF(CC)))
      A4=(SINF(CD)-CD*COSF(CD))*EXPF(-CD*CD*THT)*SINF(CD*G)/
```

```
     1(CD*(CD-SINF(CD)*COSF(CD)))
      A5=(SINF(CE)*CE*COSF(CE))*EXPF(-CE*CE*THT)*SINF(CE*G)/
     1(CE*(CE-SINF(CE)*COSF(CE)))
      SUM(K)=A1+A2+A3+A4+A5
      THETA(K) =2,0*SUM(K)/G
      G=1,0
  20  CONTINUE
      PRINT 21,I,THETA(1)
  21  FORMAT (10X,*THETA(1) AFTER*,I4,*TIME INCREMENTS*,F12.6)
      PRINT 22,I,THETA(2)
  22  FORMAT (10X,*THETA(2) AFTER*,I4,*TIME INCREMENTS =*,F12.6)
      D=I
  30  THT =THT+D*S
  31  H=H+0,1
 999  STOP
      END
```

VITA

Larry Claude Witte

Candidate for the Degree of

Doctor of Philosophy

Thesis: HEAT TRANSFER FROM A SPHERE TO LIQUID SODIUM DURING FORCED CONVECTION

Major Field: Mechanical Engineering

Biographical:

Personal Data: Born in Hamilton County, Texas, April 27, 1939, the son of Clarence and Mildred Witte.

Education: Received the Bachelor of Science degree from Arlington State College, Arlington, Texas, with a major in Mechanical Engineering, in May, 1963; received the Master of Science degree from Oklahoma State University, Stillwater, Oklahoma, with a major in Mechanical Engineering, in January, 1965; completed the requirements for the Doctor of Philosophy degree in December, 1966.

Professional experience: Alternated work and study sessions between Ling-Temco-Vaught, Inc. and Arlington State College from February, 1962 to June, 1963; Associate Aerodynamics Engineer, L-T-V, Inc., June, 1963 to September, 1963 and June, 1964 to September, 1964.

Professional organizations: The author is a member of the following honorary, educational and professional organizations: Pi Tau Sigma, Epsilon Nu Gamma, Phi Kappa Theta, and American Society of Mechanical Engineers.